PONTIFICIA UNIVERSIDAD CATOLICA DE CHILE
FACULTAD DE CIENCIAS BIOLOGICAS
DEPARTAMENTO ECOLOGÍA

The Spatial Ecology of Microbes

by

Miles T. Wetherington

Thesis submitted to the Department of Ecology
of Pontificia Universidad Católica de Chile, as one of the requirements
to qualify for the Doctoral of Philosophy degree in Biological Sciences: Ecology.

Supervisor	:	Dr. Juan E. Keymer (Universidad de Asyén, Chile)
Co-supervisor	:	Dr. Peter Galajda (Biological Research Center, Hungary)
Coordinador	:	Dr. Mauricio Lima (PUC, Chile)
Committee	:	Dr. Fernan Federici (PUC, Chile)
Committee	:	Dr. María Luisa Cordero (Universidad de Chile, Chile)

April, 2021
Santiago, Chile

Dedicated to my parents, Maria and Chuck.

Thank you for a lifetime of guidance and support.

Summary

Guided by cell biophysics experimentation and equipped with toolsets from theoretical ecology, the aim of my thesis is to explore the ways in which spatial structure influences the dynamics and distributions of microbial cells, populations and communities.

In my first project, we highlighted range expansion experiments of a colicin producing-colicin sensitive E.coli community on solid agar; The process of colony formation is driven by colicin production, cell lysis and division all driving the dynamical structure and ecological composition of the colony. Making analogies to percolation theory from statistical physics, we were able to develop a spatial model to quantify regimes of strain coexistence, competitive exclusion and extinction.

Next we aimed to understand the spatial conditions under which microbial common goods games could persist. A particular bacterial system motivating this study was Pseudomonas aeruginosa, which excretes a costly 'iron-scavenging' compound (siderophore) in order to bind and transport iron across the cell membrane. This compound represents a common-pool resource, susceptible to exploitation by nearby bacteria free from producing this metabolically costly resource. With this system in mind we asked the following question: what spatial conditions permit these common-pool resources to be monopolized by a cooperator strategy in competition with an exploiter strategy? By developing a stochastic spatial model, we quantified the phase transition from monopolized to exploited and predicted which circumstances to expect coexistence between niche constructing and exploiter strategies as a result of differences in niche monopolization and colonization rates, respectively, and when to expect a collapse of the niche and a 'tragedy of the commons'.

Following this work, I began to apply newly acquired expertise in microfluidics, microfabrication techniques, microscopy and experimental cell biophysics in order to observe and study the spatial colonization dynamics of E.coli and P.aeruginosa in structured microfabricated landscapes. We

showed how these two bacterial species enact a competition-colonization tradeoff where the faster colonizing E.coli can be overwhelmed locally by the slower but superior competitor, P.aeruginosa. This work constituted the first evidence of an abstract ecological theory in a spatial bacterial community. Furthermore, these results showed the importance of spatial structure in leading to coexistence as E.coli is able to effectively localize P.aeruginosa populations when competing in a patchy landscape via priority-effects. Conversely, in well-mixed 'mean-field' conditions the superior competitor always wins. In order to address the priority effects observed by E.coli, we made analogies to the Kronig-Penny model of solid state physics to our patchy landscape. To help understand the role habitat structure plays in the process of ecological colonization via invading wave populations, we represented our patchy landscapes as a periodic potential. An interesting result of such interpretation is the opening for the possibility of Anderson localization phenomena to take place; whereby species modulate each other's dynamic habitat landscape. In this scenario E. coli cells modulate the potential seen by P.aeruginosa and introduce randomness to ecological corridors. In this way E. coli can induce strong localization in the spatial distribution of the P.aeruginosa metapopulation. This work highlights the importance of invisible corridor interactions and their potential to determine patterns of patch occupancy.

Building on these results we next made an explicit connection between the topological properties of spatially structured microbial landscapes and Taylor's Law, which asserts that the fluctuations within a metapopulation is a power law function of the mean. This statistical phenomena of populations, while well-documented in both the macro- and microscopic world, has yet to be connected to processes shaping spatially structured microbial populations and communities. Pursuing this analogy from solid state physics further we generated different degrees of randomness in the patch-connecting ecological corridor widths within a microfabricated microfluidics landscape, we found that a critical level of randomness leads to a qualitative transition in the fluctuation scaling of an Escherichia coli metapopulation. That induced randomness leads to such a result is neither expected experimentally nor completely understood theoretically. Nevertheless, these results bring a landscape perspective to Taylor's law and the desire to connect this phenomena to ecological processes. Furthermore, bridging Taylor's Law with other ecological scaling laws is an ongoing effort in the field of macroecology and one which we think would benefit from collaborations between theoreticians and experimental cell biophysics techniques like the one implemented here.

Finally, given the unique perspective of this collaborative effort between cell biophysics and theoretical ecology, we conclude this thesis with a review of the literature in the field. Primarily, we focus on the necessary theoretical ecology needed for cell biophysicists to interpret their experimental results. In particular, we review landmark experimental cell biophysics discoveries from the past 15 years ranging from single-cell, population and community/biofilm studies, as well as following-up with newer findings all of which we discuss from an ecological viewpoint.

Resumen

Guiado por la experimentación de biofísica celular y equipado con conjuntos de herramientas de ecología teórica, el objetivo de mi tesis es explorar las formas en que la estructura espacial influye en la dinámica y distribución de células, poblaciones y comunidades microbianas.

En mi primer proyecto, destacamos los experimentos de expansión del rango de una comunidad de E. coli productora de colicina frente a la sensible a la colicina en agar sólido; El proceso de formación de colonias está impulsado por la producción de colicina, la lisis celular y la división, todo lo cual impulsa la estructura dinámica y la composición ecológica de la colonia. Al hacer analogías con la "Teoría de la Percolación" de la física estadística, pudimos desarrollar un modelo espacial para cuantificar los regímenes de coexistencia, exclusión competitiva y extinción.

Siguiente, nuestro objetivo era comprender las condiciones espaciales en las que los juegos microbianos comunes podían persistir. Un sistema bacteriano particular que motivó este estudio era Pseudomonas aeruginosa, que excreta un compuesto químico costoso "eliminador de hierro" (sideróforo) para unir y transportar el hierro a través de la membrana celular. Este compuesto representa un recurso común, susceptible de ser explotado por bacterias cercanas aliviadas del costo de producción de este recurso metabólicamente caro. Con este sistema en foco, nos hacemos la siguiente pregunta: ¿qué condiciones espaciales permiten que estos recursos de uso común sean monopolizados por una estrategia cooperativa en competencia con una explotadora? Al desarrollar un modelo espacial estocástico, cuantificamos la fase de transición de monopolizado a explotado y predijimos qué circunstancias esperarían la coexistencia entre la construcción de nichos y las estrategias de explotación como resultado de las diferencias en las tasas de colonización y monopolización de nichos respectivamente, y cuándo esperar un colapso de nicho y una "tragedia de los comunes".

Después de este trabajo, comencé a aplicar la experiencia recién adquirida en microfluídica,

técnicas de microfabricación, microscopía y biofísica celular experimental para observar y estudiar la dinámica de colonización espacial de *E. coli* y *P. aeruginosa* en paisajes estructurados microfabricados. Mostramos cómo estas dos especies bacterianas promulgan una compensación de competencia-colonización donde la *E. coli* de colonización más rápida puede ser abrumada localmente por el competidor más lento pero superior, *P. aeruginosa*. Este trabajo constituyó la primera evidencia de una teoría ecológica abstracta en una comunidad bacteriana espacial. Además, estos resultados mostraron la importancia de la estructura espacial para conducir a la coexistencia, ya que *E. coli* puede localizar de manera efectiva las poblaciones de *P. aeruginosa* cuando compite en un paisaje irregular a través de efectos de prioridad. Por el contrario, en condiciones de "campo medio" bien mezcladas, el competidor superior siempre gana. Para abordar los efectos prioritarios observados por *E. coli*, hicimos analogías con el modelo Kronig-Penny de la física del estado sólido con nuestro paisaje irregular. Para ayudar a comprender el papel que juega la estructura del hábitat en el proceso de colonización ecológica a través de las poblaciones de olas invasoras, representamos nuestros paisajes irregulares como un potencial periódico. Un resultado interesante de tal interpretación es la apertura a la posibilidad de que ocurran los fenómenos de localización de Anderson; mediante el cual las especies modulan el paisaje de hábitat dinámico de las demás. En este escenario, las células de *E. coli* modulan el potencial visto por *P. aeruginosa* e introducen aleatoriedad en los corredores ecológicos. De esta manera, *E. coli* puede inducir una fuerte localización en la distribución espacial de la metapoblación de *P. aeruginosa*. Este trabajo destaca la importancia de las interacciones de los corredores invisibles y su potencial para determinar patrones de ocupación de parches.

A continuación, hicimos una conexión explícita entre las propiedades topológicas de los paisajes microbianos estructurados espacialmente y 'Taylor's Law', que afirma que las fluctuaciones dentro de una metapoblación es una función de ley de potencia de la media. Este fenómeno estadístico de las poblaciones, aunque está bien documentado tanto en el mundo 'macro' como en el microscópico, aún no se ha relacionado con los procesos que configuran las poblaciones y comunidades microbianas estructuradas espacialmente. Siguiendo esta analogía de la física del estado sólido, generamos diferentes grados de aleatoriedad en los anchos de los corredores ecológicos de conexión de parches dentro de un paisaje de microfluidos microfabricados, encontramos que un nivel crítico de aleatoriedad conduce a una transición cualitativa en la escala de fluctuación de una metapoblación de

E. coli. Que la aleatoriedad inducida lleve a tal resultado no se espera experimentalmente ni se comprende completamente teóricamente. Sin embargo, estos resultados aportan una perspectiva de paisaje a la Taylor's Law y el deseo de conectar este fenómeno con los procesos ecológicos. Además, unir la Taylor's Law con otras leyes de escala ecológica es un esfuerzo continuo en el campo de la macroecología y creemos que se beneficiaría de la colaboración entre teóricos y técnicas de biofísica celular experimental como la que se implementó aquí.

Finalmente, dada la perspectiva única de este trabajo colaborativo entre la biofísica celular y la ecología teórica, concluimos esta tesis con una revisión de la literatura en el campo. En primer lugar, nos centramos en la ecología teórica necesaria para que los biofísicos celulares interpreten sus resultados experimentales. En particular, revisamos los descubrimientos de biofísica de células experimentales históricas de los últimos 15 años que van desde estudios unicelulares, de población y de comunidad / biopelícula, así como el seguimiento con hallazgos más nuevos, todos los cuales discutimos desde un punto de vista ecológico.

Publications & to be submitted

- **Wetherington, Miles T.** and Juan E. Keymer. Expansion, Exploitation and Extinction: Niche Construction in Ephemeral Landscapes. Sci Rep 10, 10067 (2020).
- **Wetherington, Miles T.**, and Juan E. Keymer. "What Does Not Kill You Makes You Stronger." Trends in Microbiology 25.8 (2017): 605-607.
- **Wetherington, Miles T.**, Dér, László, Nagy, Krisztina, Noorlag, Janneke, Galajda, Péter, Keymer, Juan E. "Competition Colonization trade-off in Spatial Microbial Meta-communities on-chip". To be submitted.
- **Wetherington, Miles T.**, Dér, László, Nagy, Krisztina, Galajda, Péter, Keymer, Juan E. "One Slope Doesn't Fit All: Landscape Structure Changes Taylor's Law in Microbial Metapopulations". To be submitted.
- Juan E. Keymer and **Wetherington, Miles T.** "Ecology for physicists: the dynamics of cells in spatially structured habitats." *Invited review, Reports on Progress in Physics.* To be submitted.

'The constructionist hypothesis breaks down when confronted with the twin difficulties of scale and complexity. The behavior of large and complex aggregates of elementary particles, it turns out, is not to be understood in terms of a simple extrapolation of the properties of a few particles. Instead, at each level of complexity entirely new properties appear, and the understanding of the new behaviors requires research which I think is as fundamental in its nature as any other.'

- Philip Warren Anderson, More Is Different

Contents

Introduction

Microbial ecosystems display unparalleled ecological complexity on earth. Consider a single gram of soil; containing billions of organisms and thousands of species [1] each with their own evolutionary paths and life-histories struggling for existence in a physico-chemical environment which is in turn changing in response to their structural modifications, metabolic excretions and uptakes. The fluctuation of populations and communities of microbes resonating with their constructed abiotic landscape has transpired at multiple scales of space and time over the 4.5 billion years of earths evolution and even provided the engine for the planetary biogeochmical cycles all living organisms rely on [2]. Hierarchically constructed by selection at the level of the cell, population and community, microbial ecosystems have displayed robustness to the perturbations that have decimated multicellular life, time and again [3, 4] allowing this self-organized microbial dance to sustain itself far from equilibrium eventually leading to emergent properties at the planetary scale. Darwin's entangled bank can be re-purposed in this light, now, however, entanglement occurs at multiple scales of biological organization and space.

The importance of scale in space, time and organization has not escaped the attention of ecologists [5]. It could be stated that the main objective of the field of ecology over the past half-century has been to unify mechanistic principles at one scale to observed patterns at another [6, 7, 8]: How do local interactions lead to population level fluctuations [9, 10]? Shape foraging strategies [11]? Permit coexistence between different life-histories [12, 13] and scale up to patterns of biodiversity [14]? Finally, can these local interactions lead to critical transitions in ecosystems [15], and, if so, can we predict them in time to reverse course?

In order to synthesize such grandiose and far-flung questions, ecological theory has become integrated with concepts from statistical physics [16] which, within its own field helped to derive the

macroscopic properties of thermodynamics through microscopic mechanisms. The patch-dynamics framework [17] is one such perspective that considers the heterogeneous, mosaic landscape of real ecosystems to be an emergent property arising from a composition of discrete homogeneous individual patches [12]. This approach lends itself to being scale-invariant such that the spatial grain *sensu* Wiens [18], i.e., the scale of such patches, defines the scale of the observer [6]; Whether that observer is an individual organism, population or localized ecological community therefore depends on the question at hand. This first approximation to real-world landscapes is equivalent to interacting particle systems such as the Ising Model, capable of faithfully approximating the behavior of ferromagnetic systems where individual 'patches' are occupied by differing spin states [19]. Returning to an ecological perspective, the local dynamics occurring at the level of patches (particle interactions) can lead to landscape level transitions. Therefore, the patch-dynamics framework is a general topological perspective, linking local and regional spatial scales whose organizational scale – organism, population, community – depends on spatial granularity. It is this integrated synthesis which leads to foundational concepts of ecological systems such as the metapopulation [20], the metacommunity [21] and the approach to understanding critical transitions in such systems [22, 15].

Given the scale-invariance of the patch-dynamics framework, its application to microbial ecosystems is evident. Yet, early hypothesis concerning the ecology of microbial systems did not emphasize the importance of space, nor scale, instead, asserting "Everything is everywhere and the environment selects" [23]; therefore suggesting a strict niche theory – perfect ecological selection – where the regional species pool is at the scale of the planet. This consesus held on until landmark studies during the genomics revolution showed that the bio-geographical patterns first observed in macroscopic ecosystems were in fact universal and well represented in microbial landscapes [24]. Emerging from this, a well-rounded theoretical ecology approach including concepts from island biogeography [8], metapopulation theory [20] and later, metacommunity theory [21] began to percolate into the field [25]. Interestingly, this early conceptual assertion paralleled the techniques implemented by experimentalists aimed at studying microbial systems in the laboratory. To overcome this perception, scientific revolutions in optics and nano/micro-fabrication techniques were necessary.

Returning to the single gram of soil, any hope to find patterns and understand processes underlying this complex system requires simplifications. For most of the history of microbiology, this

included dismissing spatial structure and instead, relying on well-mixed experimentation. More recently, thanks to a revolution in microfluidics and micro-fabrication techniques [26], we are able to study how spatial structure effects microbial ecosystems with micron and nanometer precision in laboratory settings [27]. This framework has been an ideal setting for testing ecological and evolutionary theory, for example; detailing the importance of space in maintaining diversity in non-transitive communities [28]; connecting replicator dynamics and the social dilemmas associated with evolutionary game theory [29] to spatially extended microbial communities exhibiting the prisoners dilemma [30, 31]; and establishing connections with the classical spatial predator-prey experiments of C.B. Huffaker [32], now using *Bdellovibrio bacteriovorus* - *Escherichia coli* predator-prey systems [33].

Aside from antagonistic interactions, microfluidic studies have revealed the ways in which microbes can solve problems collectively. *Bacillus subtilus* have been observed time-sharing nutrients during biofilm expansion. Through the coupling of cell metabolic state and membrane potential [34], starving cells in the core of a biofilm send a long range electrical signaling to the periphery. This causes a halt in growth and allows for nutrients to diffuse to the core before expansion can commence, leading to oscillating growth dynamics [35]. This complex form of communication, reminiscent of how neurons fire in the brain, has only begun to be investigated [36] and highlights the fundamental discoveries that lie ahead when studying the microbial world in its spatial context.

While these examples of microfluidics based research exemplify the potential for studying microbes in a spatial context, many questions still remain. The aim of this thesis is to implement a perspective grounded in theoretical ecology, such as the patch-dynamic framework, and apply it to the spatial ecology of microbes:

Chapter 1 I aim to understand the spatial conditions under which microbial common goods games can persist. A particular bacterial system motivating this study is *Pseudomonas aeruginosa*, which excretes a costly 'iron-scavenging' compound (siderophore) in order to bind and transport iron across the cell membrane. This compound represents a common-pool resource, susceptible to exploitation by nearby bacteria free from producing this metabolically costly resource [37]. Clinical studies have provided first evidence that this social dilemma can lead to complex eco-evolutionary dynamics which have an impact on the virulence of lung colonization and pneumonia in patients [38]. With this system in mind I asked the following question: what spatial conditions permit common-

pool resources to be monopolized by a cooperator strategy in competition with an exploiter strategy? By developing a stochastic spatial model, I quantified the phase transition from monopolized to exploited and predict in which circumstances to expect a 'tragedy of the commons' [39].

Chapter 2 We scale down to the interactions of single cells. In this chapter we highlight experimental work by Von bronk and collaborators [40] who studied the range expansion of 2 strains of *E. coli*, one colicin producing and the other colicin susceptible. The process of colony formation is driven by colicin production, cell lysis and division, all driving the dynamical structure and ecological composition of the colony. We focus on the importance of initial conditions in leading to long-term community outcomes. Furthermore we make connections to percolation theory [41] and develop a spatial model to quantify regimes of strain coexistence, competitive exclusion and extinction.

Chapter 3 We zoom back out to the scale of microbial metacommunities. In this investigation we detail, for the first time, a clear example of an otherwise abstract theory of classical ecology towards the competition-colonization dynamics of a spatially structured microbial metacommunity. By implementing this 2 species – *E. coli* & *P. aeruginosa* – microbial metacommunity in a micro-fabricated spatially structured 'patchy landscape' microfluidic device and following via time-lapse microscopy, we are able to observe as the competition and colonization dynamics unfold over 48hrs with high spatial and temporal precision. Repeating this procedure N=72 times, we acquire a detailed statistical ensemble of patch-level and landscape-level dynamics. Next, to address these quantitative results, which guides our intuition, we extend the classical ecological theory of the competition-colonization trade-off [42, 43, 44] using a spatially explicit model. Furthermore, when we compare such 'patchy landscape' experimental results with a simpler 'flat (non-patchy) landscape' and well-mixed system, we find qualitatively different outcomes. While the latter is a non-trivial result, it has been documented and led to an understanding of the importance of space [45]. However, to address the more intricate differences between 'patchy' and 'flat' landscapes, we introduce concepts from solid-state physics [46] which provide a conceptual framework for understanding our findings. We expect this framework to transcend beyond these significant findings, and to play a broader role when considering the importance of spatial structure in the landscape ecology of microbes; from the emergence and maintenance of microbial biodiversity and ecosystem function to the rise and proliferation of antibiotic resistance.

Chapter 4 Motivated by our findings from our metacommunity experiments, we make an explicit connection between the topological properties of spatially structured microbial landscapes and Taylor's Law, which asserts that the fluctuations within a metapopulation is a power law function of the mean. This statistical phenomena of populations, while well-documented in both the macro- and microscopic world, has yet to be connected to processes shaping spatially structured microbial populations and communities. By inducing different degrees of randomness in the patch-connecting ecological corridor widths within a microfabricated microfluidics landscape, we find that a critical level of randomness leads to a qualitative transition in the fluctuation scaling of an *Escherichia coli* metapopulation. That induced randomness leads to such a result is neither expected experimentally nor completely understood theoretically. Nevertheless, these results advance the discussion of Taylor's law and the desire to connect this phenomena to ecological processes. Furthermore, we discuss the potential of bridging Taylor's Law with other ecological scaling laws.

Chapter 5 we highlighting the importance of theoretical ecology to the field of cell biophysics and in particular the study of microbes in spatially structured, microfluidic, environments. For this review we target physicists entering this nascent field, likely unaware of the theoretical ecology relevant to such microscopic systems. In particular we start from the dynamics of single cells, their growth and the phenomena of aging, which we relate to a population level adaptive dynamic process [47], all the way up to the consideration of the ecological community (biocenosis), introduced almost 150 years ago [48] as a concept for understanding microbial consortia and communities we are reliant on.

Chapter 1

Expansion, Exploitation and Extinction: Niche Construction in Ephemeral Landscapes

> The organism cannot be regarded as simply the passive object of autonomous internal and external forces; it is also the subject of its own evolution.
>
> - Richard Levins

We aim to understand general consequences of niche construction on metapopulation dynamics in ephemeral landscapes. To this effect, a contact process-like stochastic spatial model is introduced where local populations colonize and go extinct on a dynamic landscape of habitable and destroyed patches. In contrast to previous models, where the extinction threshold is a consequence of available niche rendered by global rates of patch destruction/renewal, here we investigate how the metapopulation persists when they are the sole generators of their own niche. Niche construction is full-filled by localized populations through the transformation of destroyed patches in their neighborhood to viable habitat for future colonization. With this theoretical framework we are able to address the dual nature of niche construction by investigating the ephemerality of the landscape (destruction rate) and the continuum of population level strategies, where construction comes at a cost to colonization. Using mean field theory and Monte Carlo simulations of the model, we are able to quantify optimal population level strategies in a wide range of ephemeral landscapes. Interestingly, we observe qualitative differences at the extinction threshold between analytic and numeric results. Investigating this discrepancy further, we find that increasing niche construction neighborhood in the spatial model leads to two interrelated effects *i*) an increased rate in range expansion *ii*) a loss in resiliency and return of the discontinuous transition at the extinction threshold. Furthermore, in the discontinuous regime of the model, spatial clustering prior to a critical transition disappears. This is a significant finding as spatial clustering has been considered to be an early warning signal before ecosystems reach their 'tipping point'. In addition to maintaining stability, we find local niche construction strategies have an advantage when in scramble competition with an exploiter strategy because of their ability to monopolize the constructed niche due to spatial adjacency. As the niche construction neighborhood expands this advantage disappears and the exploiter strategy out-competes the niche constructor. In some cases the exploiter pushes the niche constructor to extinction, thus a tragedy of the commons ensues leading to 'ecological suicide' and a collapse of the niche.

1.1 Introduction

Understanding the co-regulatory feedback between living systems and their environment is a primary goal driving ecological research [49, 50, 51]. Over the past quarter-century, research has primarily focused on studying the differences between ecological and evolutionary dynamics [52, 51], most notable of these are the closely related concepts, ecosystem engineering and niche construction. Ecosystem engineering occurs within the lifetime of an individual in a population, and is defined as its modification of the microenvironment within which it makes a living. In turn, the consequences of these actions have an impact on the coupled physical environment and ecological community (i.e. the ecotope [53]). Ecosystem engineers play an important role in the restoration and maintenance of the landscape [54], the resilience of ecosystems [55] and are often regarded as keystone species due to their role in stabilizing communities [52, 56].

An ecological interpretation of niche construction includes the mechanisms of ecosystem engineering along with all byproducts comprising the life-history of the organism (behavior, nutrient uptake, and excretion for example detritus [57], etc.) which may be considered more indirect forms of modification [58].

The microbial world is typified by such feedback processes; for example, the exchange of metabolic byproducts plays an important role in creating and maintaining interdependent or 'syntrophic' relationships where two or more microbial groups live symbiotically via nutrient cross-feeding [59] or the transaction of other resources [60]. Such microbial consortia act as their own ecological units, often coexisting in harmony [61] and expanding beyond the niche of any one strategy. Furthermore, such niche construction has a tighter feedback to the ecological unit in question and can play an important role in influencing their evolutionary trajectory even playing a vital role in biogeochemical cycles [62]. In this way niche construction is a life history trait which has the potential to expand or maintain the ecological niche, including the trans-generational inheritance of improved local conditions (ecological inheritance). Alternatively, once this strategy emerges, it becomes vulnerable to exploitation, either from within the population or nearby strategies in competition for similar resources. If exploitation does not eliminate niche construction and this new exploiter-victim interaction becomes tightly coupled, exploiters will continue to profit by expanding into otherwise inaccessible regions [63].

The landmark work of Krakauer et al. addressed ecological and evolutionary consequences of niche construction in a Lotka-Voterra competition framework [64]. By shifting the focus from population genetics to an emphasis on ecological dynamics and the mechanisms for niche control, this approach differed from earlier theoretical investigations [65, 66]. We will briefly describe their system and summarize some of their findings as their work has inspired the model considered in this investigation. They introduce the constructed niche directly as an additional state variable in the dynamical system. If the niche is invested in by the developing population it acts as a public good, increasing the potential carrying capacity. In this way the abiotic environment feeds back into the ecological dynamics influencing the state-space over which a single strategy can persist in solitude i.e. its fundamental niche. There is a trade off to investing in the niche, notably, by allocating resources (energy/time/proportion of the local population) towards its construction and maintenance (c), one is inherently appropriating them away from immediate colonization of territory or resources ($1 - c$). In the case where the niche must be constantly invested in, due to external perturbations or dissipation for example, a balance between colonization and construction must be found.

This dilemma can be resolved via specialization within the population giving rise to a division of labor. Classic examples being the specialization of tasks between germ-line and somatic cells [67, 68] or the caste system in insect societies [69]. Alternatively, the costs of construction can be spread throughout the population evenly. This is common in microbial systems, for example in budding yeast *Saccharomyces cerevisiae* which, in order to metabolize sucrose, secretes a digestive enzyme (invertase) into the environment [70]. A similar mechanism has been well documented with *Pseudomonas aeruginosa* which, in iron-limited conditions, will begin to excrete an 'iron scavenging' extracellular compound (siderophore) to bind and transport iron across the cell membrane [71].

In single strategy ecosystems like these aforementioned microbial systems the niche is maximized by strategies which allocate resources evenly between niche construction and reproduction (where $c \approx 0.5$). However, when placed in competition with other strategies the niche acts as a common-pool resource, in other words it is nonexcludable and limited. Therefore, if 2 strategies compete and extract from this common-pool resource, the one with the lowest allocation towards niche construction (the exploiter strategy) dominates, eventually pushing the other to extinction [72]. This has been shown to be the case explicitly in well-mixed versions of the aforementioned microbial

systems; when wild-type strategies are in resource competition with exploiter strategies that do not excrete the costly enzymes/compounds they go extinct [73, 37].

Notice, however, in driving the other strategy to extinction the exploiter loses access to the portion of the niche that was constructed, which was also verified experimentally (See figure 3C in [73]). Logically this leaves us with the dilemma that ecological dynamics should push niche construction as a strategy to extinction. Herein lies the tragedy of the commons, where the resource in question has been manifested by niche construction [39]. In an environment where habitat renewal is not free and the fundamental niche is not inherent to the environment, for example cases where disturbances are frequent [12], local facilitation is necessary for establishment (see [74] for a review) or the ecosystem is susceptible to critical transitions [75], this scenario can lead to a form of evolutionary suicide ([76] and see [77] for a review).

With this dilemma laid out before us, and with these microbial systems in mind, how is niche construction maintained?

One universal yet often overlooked feature of niche construction is its relative spatial structure and scale compared to other ecological interactions at play, for example colonization. For laboratory settings of the microbial systems mentioned, well-mixed conditions ensure that niche construction is global. Whereas outside these simplified laboratory scenarios, real populations are spatially distributed generating a population of populations, i.e. metapopulation [20]. In this natural scenario the scale of niche construction is limited by the rate of diffusion [78], i.e. it is relatively localized to subpopulations within the metapopulation. Therefore, accessibility of the constructed niche can range from a completely privatized good to a common pool resource. Studying this transition within the excludability spectrum from monopolized to exploited is the goal of this work. Since it is a broad concept, we narrow our view of niche construction to the mechanism by which an ecological unit (population, microbial consortia, etc.) renews the necessary and sufficient conditions for persistence in its surrounding environment. Opposing this effort is the dissipation of order from the external environment, for example disturbances observed in ecosystems which are a characteristic found at all scales of biological organization (meteorite impacts, forest fires, antibiotic injections etc.).

In the next section we introduce the contact process, a general model of spatial colonization and extinction dynamics. Giving some background, we then develop our niche construction model. For those not interested in the specific mathematical details of the model, the main features can be

found in figure 1 with the models Markov diagram and the colonization-construction trade-off.

Equipped with this model, we ask the following questions; how does the spatial structure of niche construction effect *i)* metapopulation resilience and qualitative behavior at the extinction threshold in the face of disturbances, *ii)* spatial range expansion at the scale of the metapopulation and, *iii)* the overall carrying capacity with respect to disturbance, and finally, *iv)* when in direct competition with an exploiter strategy, in what scenarios should we expect to see constructor dominance? exploiter dominance? and coexistence?

1.2 The Model

1.2.1 The Contact Process

As a point of departure for our model, we begin by introducing the contact process (CP) [79], an interacting particle system [80] which follows colonization and extinction dynamics of particles on a countable set of spatial locations ($\mathcal{L}$). For our landscape we will consider a 2D lattice consisting of 256 by 256 sites with periodic boundary conditions $\mathcal{L} = \mathbb{Z}_{256} \times \mathbb{Z}_{256} \cong \mathbb{Z}^2_{256}$. On the landscape $\mathcal{L}$ populations (occupied patches) go extinct (at rate δ) and recruit adjacent habitable patches (at rate 1) stochastically and in continuous time. When we say some event happens at rate q this signifies that given parameter q the time between occurrences has an exponential distribution $P(t_i \leq t) = 1 - exp(-qt)$ and a mean of $1/q$. Patches in the landscape ($x, y \in \mathcal{L}$) can be in one of two states $S = \{\varnothing, 1\}$ which correspond to vacant habitat and occupied habitat, respectively. Consequently, we can describe the state of site x at time t as $\xi_t(x)$. Hence, ξ_t assigns a state S to all sites in the landscape: $\xi_t : \mathcal{L} \to S$. Considering the colonization and extinction dynamics of individual patches, we are left with the defining reactions of the contact process:

$$1_x \xrightarrow{\delta} \varnothing_x$$

$$\varnothing_x + 1_y \xrightarrow{1/Z_*} 1_x + 1_y,$$

Where the colonization neighborhood Z_* for site x is defined by the interaction range r_* using the Hamming coordinate system:

$$Z_*(x, r_*) = \{y \in \mathcal{L} : ||x - y|| \leq r_*\}$$

As an example, if $r_* = 1$, each patch has four neighbors (North, East, South and West). In this scenario, if our focal patch is vacant we pick a neighbor randomly, if the neighbor is occupied it colonizes with probability 1. Thus colonization dynamics are dependent on the conditional probability of neighboring patches being occupied, which in turn are dependent on their neighbors, and so on. Following this it is easy to understand that an exact analytic solution to the CP is not feasible due to its spatial structure. That being said, several important features of the model have been proven rigorously and its significance in the study of absorbing state phase transitions is well documented [81]. A first attempt to understanding the dynamics of the model requires an investigation into the mean field approximation (MFA). This approach assumes the system to be 'well-mixed', in other words, the spatial structure is disregarded and the effect of all other sites (p) is approximated and by an averaged effect, thus reducing the many-bodied problem to a one-bodied problem:

$$\dot{p} = p(1 - p) - \delta p \tag{1.1}$$

Incidentally, this also happens to be Levins equation of metapopulation dynamics [20]. Setting $\dot{p} = 0$ and solving for p we arrive at the steady state equilibrium:

$$\widehat{p} = 1 - \mathcal{R}_0^{-1} \tag{1.2}$$

We have introduced a new term, the 'basic reproductive number', $\mathcal{R}_0 = 1/\delta$ [82] which contains all the information about the life history necessary to determine the long-term outcome in the mean field limit:

$$\widehat{p} = \begin{cases} 1 - {\mathcal{R}_0}^{-1}, & \text{if } \mathcal{R}_0 > 1 \\ 0, & \text{otherwise} \end{cases} \tag{1.3}$$

This approximation has its limitations which we see when comparing the critical extinction of the mean field limit ($\delta_c = 1$) with the CP ($\delta_c \approx 0.6065$) for $r_* = 1$. The diminished δ_c in the CP is due to crowding of populations which leads to some portion of colonization events to fall on already occupied patches. Spatial structure adds limitations to the efficacy of colonization, this is emphasized as we approach δ_c.

1.2.2 Ephemeral Landscapes

Next, we consider a landscape where patch lifetime is ephemeral (*sensu* Keymer et al. [83]), therefore, aside from the landscape being occupied or vacant we add a third possible state, destroyed. This signifies a degradation in the local habitat thus leaving it unavailable for immediate colonization. All patches, regardless of state, are destroyed at rate e, if no mechanism for habitat renewal exists, the entire lattice converges to completely destroyed $\bar{s} = 0$ where $\bar{s}$ stands for long term suitable habitat. Keymer et al. investigated the extinction threshold of the contact process on a dynamic landscape defined by global rates of habitat destruction (e) and renewal (λ) where they envisioned λ as an ecosystem service independent of the metapopulation dynamics. Aside from the necessary conditions for the life-history of the population (i.e. $\mathcal{R}_0 > 1$), the extinction threshold is dependent on two aspects of the landscape;

i) patch lifetime, $\tau \equiv \frac{1}{e}$

ii) and long term suitable habitat, $\bar{s} = \frac{\lambda}{\lambda+e}$

If patch lifetime is shorter than some critical time span ($\tau < \tau_{min}$), the dynamic corridors generated by habitat renewal are too short lived for populations to navigate through via colonization of vacant patches, likewise, below a minimum amount of suitable habitat ($\bar{s} < \bar{s}_{min}$), a spanning cluster of destroyed patches percolates the landscape leaving clusters of populations fragmented from suitable habitat [84]. In both cases the metapopulation enters the absorbing state (global extinction).

1.2.3 Coupling Niche Construction to Metapopulations in Ephemeral Landscapes

In order to connect metapopulation dynamics to the generation of the landscape, we introduce a niche constructor strategy (NC) ($\xi_t(x) = 1$) which, along with having the capacity to recruit local vacant sites ($\xi_t(y) = \varnothing$) via immediate colonization, is also capable of converting local destroyed sites ($\xi_t(y') = -1$) to vacant and available for future colonization events. Thus, we are left with the following set of reactions (Figure 1 for schematic):

$$1_x \xrightarrow{\delta} \varnothing_x$$

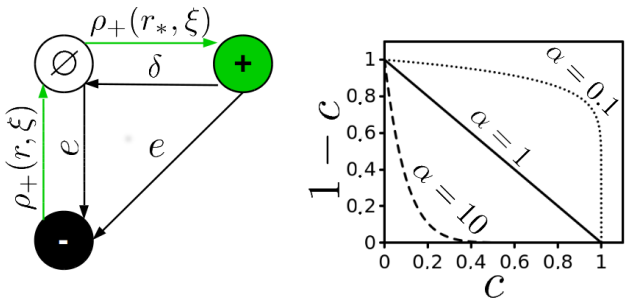

Figure 1.1: NC Reactions and the Colonization-Construction Trade-off. Left: Schematic showing the reactions for the NC model. The probability of colonization $(1 - c)$ and construction c events occurring are dependent on the density (ρ) of occupied sites within the colonization (r_*) and construction range (r) of the stochastic process (ξ). Sites in the lattice acquire one of 3 possible states, $S = \{-, \varnothing, +\}$ so the state of the system at time t is $\xi_t : \mathcal{L} \to S$. Right: Trade-off between construction (x-axis) and colonization (y-axis) with respect to 3 different values of α.

$$\varnothing_x, 1_x \xrightarrow{e} -1_x$$

$$-1_x + 1_y \xrightarrow{c/Z} \varnothing_x + 1_y$$

$$\varnothing_x + 1_y \xrightarrow{(1-c)^\alpha/Z_*} 1_x + 1_y,$$

Notice that neighborhood sizes for colonization Z_* and construction Z are not necessarily the same. Furthermore, the capacity for construction c comes at an energetic cost to colonization: $(1 - c)^\alpha$ where the value of α determines the efficacy of niche construction.

Replacing the global ecosystem service rate λ with one dependent on the state of local populations we can study the coupling between the metapopulation and landscape.

The model described above has 6 parameters; population extinction δ, patch destruction e, patch construction c, construction efficacy α and the two neighborhood sizes for colonization Z_* and construction Z. The mean field approximation for this version of the model will be introduced next, followed by a comparison to the interacting particle system (IPS). After presenting these results we make an addition to the model where we add a second strategy (exploiter, where $c = 0$) which competes for colonizable space (scramble competition). We then discuss results in the context of landscape dynamics and competition.

1.2.4 Mean Field Approximation

Here we consider the mean field approximation for the model with NC in an ephemeral landscape. Since global densities sum to unity we substitute for one of the states. For our purposes, we chose the global density of vacant patches $p_\varnothing = 1 - p_+ - p_-$. Now we can write down the mean field approximation just considering the dynamics of destroyed p_- and occupied patches p_+:

$$\dot{p}_- = e(1 - p_-) - cp_+p_- \tag{1.4}$$

$$\dot{p}_+ = (1 - c)^\alpha p_+(1 - p_+ - p_-) - p_+(\delta + e) \tag{1.5}$$

Besides the absorbing state $\widehat{p}_- = 1$ there exists a steady state equilibrium $\widehat{p}_+ > 0$. Although the exact solution is not particularly insightful, some observations are in order: we can determine the long-term suitable habitat

$$\bar{s} = 1 - \widehat{p}_- = \frac{c\widehat{p}_+}{c\widehat{p}_+ + e} \tag{1.6}$$

Note, $c\widehat{p}_+$ can be defined as the total effort towards niche construction by the metapopulation. Substituting in the following $\Lambda \equiv c\widehat{p}_+$ we have returned to the expression for suitable habitat [83] which is now coupled to the state of the metapopulation:

$$\bar{s} = \frac{\Lambda}{\Lambda + e} \tag{1.7}$$

For our model this expression is equivalent to the fundamental niche for the specific life history-landscape mapping in question and, like Levins expression for metapopulation occupancy, we can describe the abundance or realized niche as:

$$\widehat{p}_+ = \bar{s} - \frac{\tilde{\delta}}{(1 - c)^\alpha} \tag{1.8}$$

Where, $\tilde{\delta} = \delta + e$. In the case where $e = 0$ and $c = 0$ we return to the canonical equation for metapopulation occupancy (eq. 2).

In the next section we compare the analytic results of the mean field with numerical simulations of the IPS. We use a von Neumann neighborhood for colonization and construction. Colonization

neighborhood is fixed to the nearest neighborhood ($||Z_*|| = 4$). Unless specified otherwise, the construction neighborhood ($||Z||$) is identical. However, in order to study the transition from monopolized to exploited niche we will consider other interaction ranges for construction (r) in which case the construction neighborhood can be computed accordingly:

$$||Z|| = 2r(r+1) \tag{1.9}$$

We explored the 2D parameter space generated by the landscape dynamics e and population strategy c with respect to mean occupancy $\langle p_+ \rangle$ through Monte Carlo methods. To study long-term behavior, the lattice was completely occupied to start all simulations.

1.3 Results: Niche Construction Model

1.3.1 Mean Field Approximation and Interacting Particle System Comparison

From figure 2, it is clear that the steady state equilibrium of the MFA overestimates the region of parameter space where the metapopulation can persist. Comparing the plots in figure 2 we see the curve $e(c)$ defines the population extinction threshold. MFA and IPS alike, the optimal trade-off between colonization and construction is landscape dependent. Tracing along the edge of the x-axis (where the landscape is almost static) we see the highest occupancy where little investment is made towards construction. This is due to the limited impact of destruction on the outcome of the metapopulation. As the rate of habitat destruction increases (i.e. as habitat lifetime decreases, $\tau \to 0$), strategies with conservative efforts towards construction (small c) cannot persist and an increased investment towards the maintenance of the niche is necessary for metapopulation survival. Notably, the vertex of the extinction threshold curve (construction strategy c_{**} which persists in the broadest range of landscapes) is around $c_{**} = 0.4$ for both IPS and MFA, qualitatively similar to the conclusion made by Krakauer et. al for the single strategy system.

Figure 3 shows a simulation where the metapopulation is able to persist in an ephemeral landscape even when confined to small clusters. These clusters are able to sustain themselves and create the corridors within the landscape (See 1D spatial transects on R.H.S of figure 3), thus escaping extinction. Although individual patches are fleeting, the metapopulation persists. It should be noted

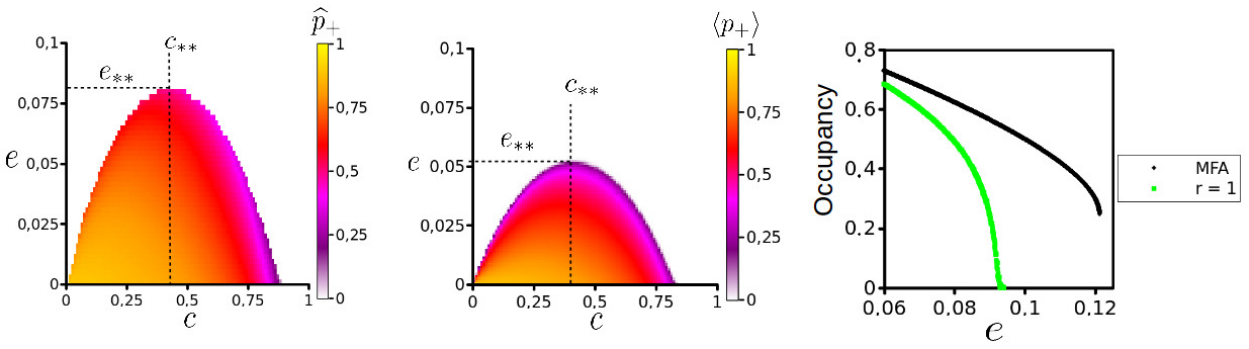

Figure 1.2: Long-term behavior of the NC Model. Results from the MFA (Left) and the IPS (Center) parameter spaces, with the life-history strategy adopted (c) along the x-axis and dynamics of the landscape (e) in the y-axis. For both $\delta = 0.1$ and $\alpha = 1$. For IPS, simulations ran for 5000 times steps, where, upon reaching the steady state, a mean occupancy $\langle p_+ \rangle$ was calculated from the following 250 time steps. In total, 10,000 simulations were run by sweeping the parameter space $\{c, e\}$ creating a 100x100 matrix. Right: Divergence in the qualitative behavior of the niche construction model. For the MFA a discontinuous transition exists for the order parameter $\widehat{p}_+$, whereas the discontinuity disappears in the IPS for $r = 1$ and we are left with a continuous transition, similar to the CP. Other parameters for MFA and IPS $\{\alpha, \delta, c\} = \{1, 0, 0.4\}$.

that near the extinction threshold, as shown in figure 3, the occupied patches always self-organize into these clusters for $r = 1$. This landscape level spatial organization has been recognized as an early warning signal for arid ecosystems about to transition to a desert state [85].

While the quantitative difference in the MFA and IPS extinction threshold is expected, the qualitative differences observed between MFA and IPS were not anticipated. Following the behavior of the deterministic MFA a sudden transition occurs at $e(c)_{crit}$, discontinuously jumping to extinction. Considering this result, one would expect the IPS to transition similarly (i.e. discontinuously) to the absorbing state. Instead we are left with a continuous phase transition, much like the one documented for the contact process. This observation suggests that our model falls in a larger group of mathematical models whose properties are universal and independent of the dynamical details, specifically, the Directed Percolation Universality Class [81]. To confirm this, one would need to perform finite size scaling analysis in order to derive the critical exponents of this model [86].

Typical of continuous phase transitions there exists a scaling regime; where the order parameter $\langle p_+ \rangle$ behaves as a power law as it approaches the critical value for extinction/habitat destruction (δ_c, e_c) in both CP and NC particle systems (L.H.S., Figure 4). Furthermore, both display similar critical slowing-down divergence of the relaxation time as shown by 3 simulations run for values below, at and above the critical point. This is suggested by the linear decrease in population size

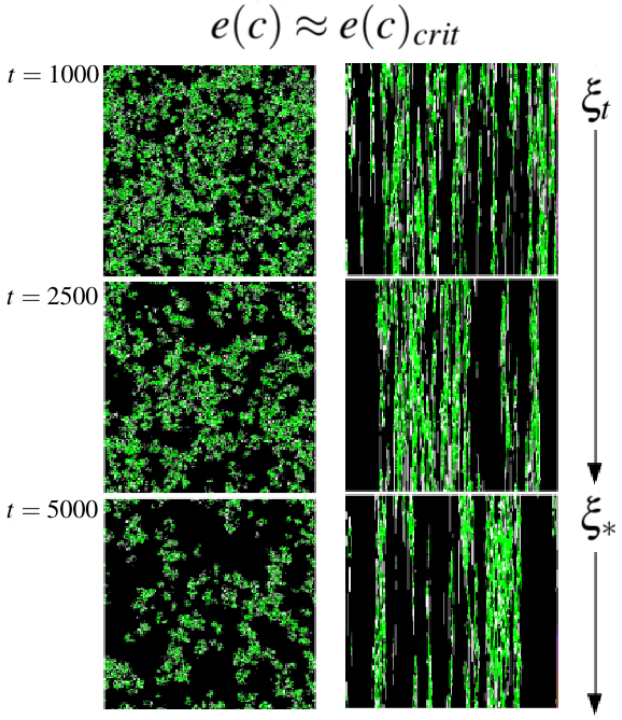

Figure 1.3: Left: Snapshots of the particle system at $t = 1000, 2500, 5000$. Occupied (green), Vacant (white) & Destroyed (black) sites. Right: A 1D spatial transect of the particle system for 256 time steps. After a transient period (ξ_t) the final snapshot/transect shows the system after it has reached the steady state (ξ_*). Parameter values used for this simulation were at the edge near the extinction threshold (See IPS in Figure 2); $\{\alpha, \delta, c, e\} = \{1, 0.1, 0.25, 0.045\}$

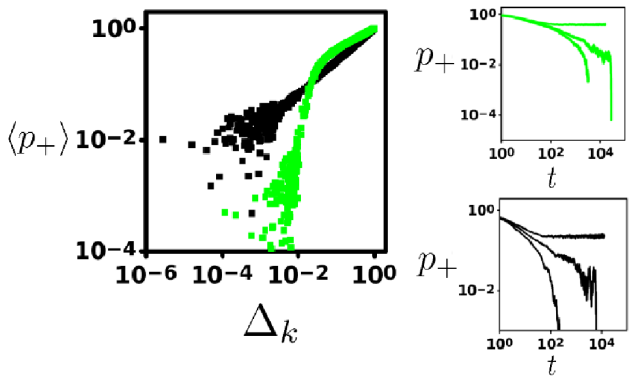

Figure 1.4: Left: Log-log plot showing critical behavior of the order parameter (long-term occupancy, $\langle p_+ \rangle$) as we approach the critical point δ_{crit} and e_{crit} for the contact process (black) and NC model (green), respectively. As these systems near the critical point ($\Delta_k \equiv |k - k_{crit}|$ for $k = \delta, e$), the order parameters display power law behavior with unique critical exponents (indicated by the unique slope for each). The critical exponent for the contact process determined from this slope (≈ 0.6116) holds up well against previous estimates [81]. Parameters for the niche construction model $\{\alpha, \delta, c\} = \{1, 0, 0.4\}$. Right: Dynamical behavior for the Niche Construction model (Top) and Contact process (Bottom) for $k < k_{crit}$ (subcritical), $k = k_{crit}$ (critical) and $k > k_{crit}$ (supercritical), from top to bottom in each plot. Divergence of relaxation time to extinction at the critical point ($k = k_{crit}$) is indicative of continuous phase transitions.

shown on the log-log plots on the R.H.S. of figure 4 at the critical points for the NC (top) and CP (bottom) models. Due to finite size constraints, fluctuations in this linear decrease emerge as $p_+ \to 0$.

1.3.2 Effect of Niche Construction Neighborhood on Range Expansion and Resiliency

In light of these striking discrepancies between spatial model and MFA prediction, we investigated the effect of construction range (r) on range expansion by the metapopulation starting from a single occupied site. During the initial expansion (ξ_t) the metapopulation is both colonizing vacant sites and renewing destroyed sites for future colonization. The landscape quickly becomes divided into two distinct spatial regions, *i*) A pattern of occupied, vacant and destroyed sites which maintains its heterogeneity via the extinction (δ), destruction (e) and construction (c) dynamics [87] and which we refer to as a 'mosaic' *sensu* [88] and *ii*) A homogeneous vacuum of destroyed sites where no local populations are nearby to combat the global destruction rate (e). While the exact configuration within the mosaic is constantly changing stochastically, a dynamical internal homeorhesis allows the metapopulation to not only persist, but expand as long as the landscape/population

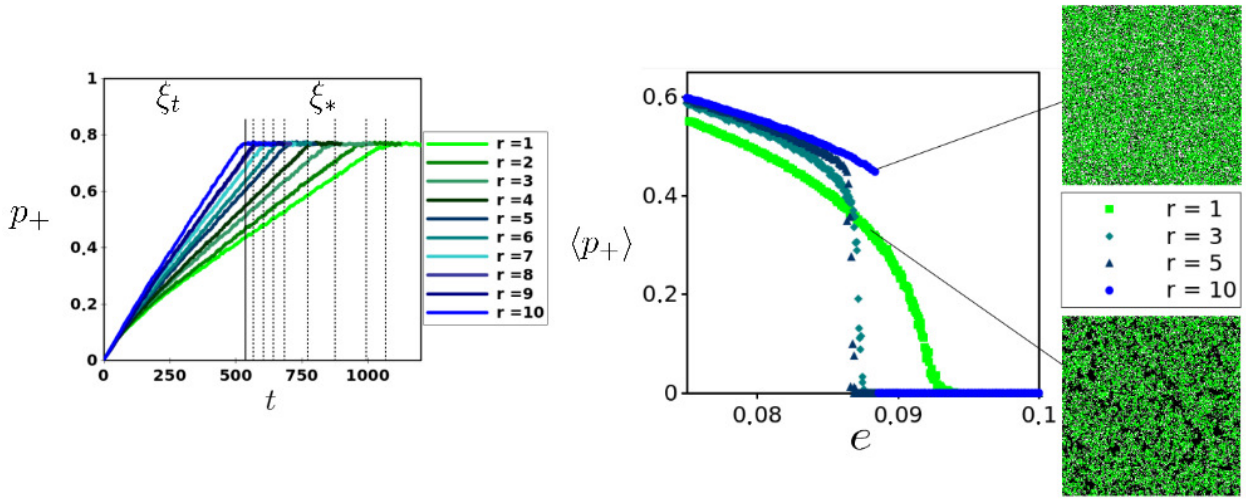

Figure 1.5: Left: Range expansion for niche constructor strategies with different r. After a transient period of expansion (ξ_t) which decreased as r increased, identical $\langle p_+ \rangle$ were reached for $e \ll e_{crit}$. The solid and consequent dotted vertical lines indicate the times (ξ_*) when each strategy ($r = 10, 9, ..., 1$) reached $\langle p_+ \rangle$. Simulations were run with the following parameter values $\{\alpha, \delta, c, e\} = \{1, 0.1, 0.4, 0.01\}$. Right: Long-term behavior for different r around e_{crit}. Parameters used for simulations were $\{\alpha, \delta, c\} = \{1, 0, 0.4\}$. Snapshots showing differences in spatial clustering taken from simulations at $e = 0.088$ for $r = 10$ and $r = 1$.

strategy mapping falls within the $e(c)_{crit}$ curve. Interestingly, at the boundary of these two spatial regions (mosaic and vacuum) we observe an edge effect: It is here, at the expansion front, where populations along the periphery of the mosaic can access the nearest sites of the vacuum, allowing them to convert destroyed sites into vacant sites, facilitating future expansion. As r becomes larger we observe a steady increase in the rate of range expansion (therefore a shorter transient period, ξ_t) eventually leading to the same long-term average occupancy $\widehat{p}_+$ at which point the vacuum vanishes (Figure 5). Intuitively, a larger r means a greater portion of occupied patches are able to convert destroyed patches into vacant niche at the mosaic-vacuum interface. Furthermore, periphery populations are able to renew destroyed sites beyond adjacency, therefore widening the gap between mosaic and vacuum which in turn increases the chance for propagules to land on vacant sites. Interestingly, the spatial texture of the edge changes as niche construction neighborhood, r, increases. A gap emerges between mosaic and vacuum because metapopulation expansion is no longer tightly coupled to niche expansion like in the adjacent niche construction strategy ($r = 1$). This subtle change at the mosaic-vacuum interface creates ecological opportunities which we address in the next section.

While this decoupling between the constructed niche and the local NC population (where $Z > Z_*$) does not come at an explicit additional cost since we consider the cost fixed for construction $(1-c)^\alpha$, it has surprising implications for the resiliency of the metapopulation. As we approach $e(c)_{crit}$ from below, $\langle p_+ \rangle$ begins to increase steadily with larger r. However, we observe a qualitative change in the behavior of the model at $e(c)_{crit}$ for $r > 1$; as r increases the transition to the absorbing state becomes steeper, eventually displaying a discontinuity, as shown for $r = 10$, and similar to the MFA. Additionally, the spatial clustering exhibited for $r = 1$ near $e(c)_{crit}$ disappears. This last observation happens to be the key to understanding why the extinction threshold changes qualitatively as r increases. To do so, it is useful to return to the mosaic-vacuum spatial paradigm. Now consider starting with a fully occupied lattice $p_+ = 1$. For small r as $e \to e_{crit}$ the metapopulation structure becomes fragmented, but clusters continue to persist (Figure 3). These clusters of occupied patches (mosaic) drift through the sea of uninhabitable patches (vacuum) occasionally fusing with other clusters and occasionally going extinct. Since this drift depends on their ability to renew the niche at the expansion front, they benefit from the highly condensed internal structure of the mosaic and the tight coupling with recent niche construction events. Internally, they maintain homeorhesis while capitalizing most effectively on renewed niche at the edge because any renewal events are likely to be adjacent to at least one viable population. If $e = e_{crit}$ then the relaxation time to extinction behaves as a power law as expected for continuous absorbing state phase transitions [81]. As r increases, clustering is lost for the same reason it aids in range expansion; instead of the decoupling between vacant niche and mosaic being generated at the expansion front of the metapopulation it exists over the entire landscape. Therefore, when $e = e_{crit}$, given enough time an area of the landscape will return to the vacuum. In contrast to the sub-critical regime, the vacuum now expands and the mosaic compresses, thus fragmenting the metapopulation. Since the niche construction neighborhood is large, no clustering occurs and the system experiences a rapid relaxation time to the absorbing state. While a larger neighborhood of niche construction increases range expansion it also makes the metapopulation more vulnerable to global extinction by changing the coupling between niche and population. At the larger scale this is observed by the disappearance of spatial clustering.

1.4 Addition to the Model

1.4.1 Competitive Scramble for Ephemeral Patches

To further explore the colonization-niche construction trade-off, we introduce an additional strategy to see how competition between two life-history strategies affects the long-term outcome of metacommunity persistence in this ephemeral landscape.

We introduce the basic contact process (See *Section 2.1.*) into the model as an exploiter strategy. Since the exploiter does not partition effort to construction it has a higher $\mathcal{R}_0$ than NC. Given a static landscape without destruction, the larger $\mathcal{R}_0$ will always push the smaller $\mathcal{R}_0$ strategy to eventual extinction. This example of the competitive exclusion principle [89] has been proven rigorously [90] in the context of competing contact processes. However, any non-zero destruction rate requires some investment in construction in order to persist in the landscape. Therefore, we would expect the exploiter to behave as a fugitive species [91], more capable of colonizing vacant niche, but unable to maintain a spatially connected metapopulation through time. For this model we do not assume any competitive hierarchy between the two strategies. An updated schematic of the complete model is provided (Figure 6).

1.5 Results: Scramble Competition Model

We first compare the dynamics of the model when construction is completely uncoupled to the NC (i.e. $||Z|| = \mathcal{L}$), versus when it is tightly coupled to the NC strategy ($||Z|| = ||Z_*||$) in Figure 6. We see that for the global case, exploiter out-competes the NC strategy globally, leading to its extinction. Once this occurs, nothing prevents the lattice from becoming completely destroyed. For future reference, we refer to this outcome as 'ecological suicide' since we do not consider evolving populations. In the tightly coupled case, where $r = 1$, we see a drastically different outcome in which the two strategies coexist.

Coexistence is possible because NC has the advantage in adjacency to the constructed niche, while exploiter has a colonization advantage (larger $\mathcal{R}_0$), this adjacency advantage diminishes for increased r. In the landscape, exploiter populations chase clusters of NC leading to the oscillations observed in Figure 6. With increased r, the fluctuations of the metacommunity occupancy increase

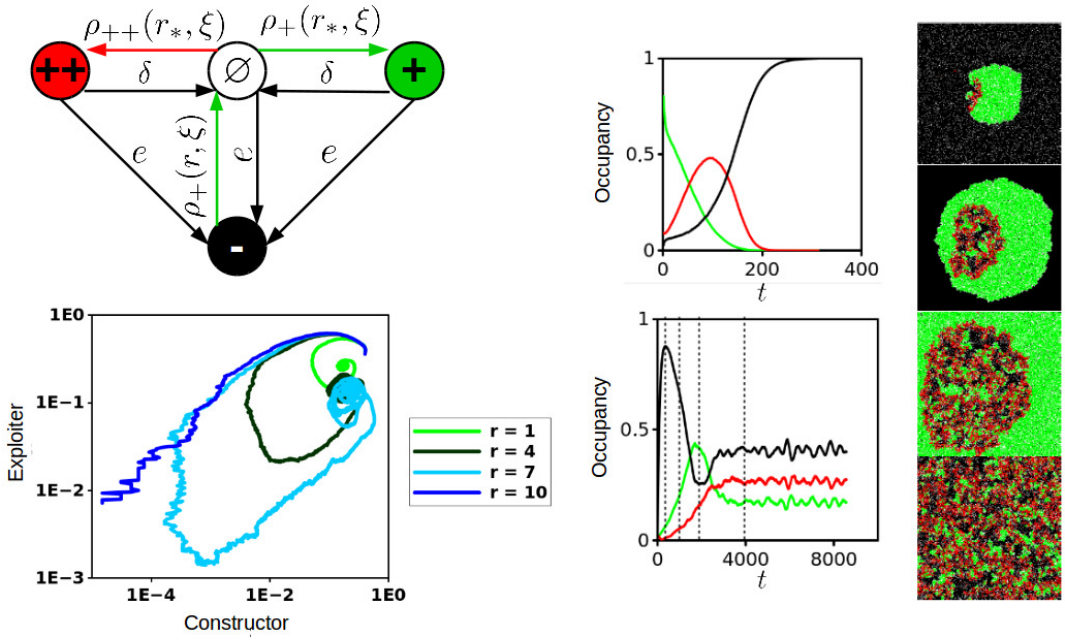

Figure 1.6: Top Left: Updated schematic of model with NC (green) and exploiter (red) competing for space. Bottom Left: Trajectories of the constructor-exploiter phase space for different r values. Larger values of r increase the likelihood of ecological suicide during the transient period. Oscillations are caused by range expansion/exploitation of the NC/ES populations. If the NC metapopulation can escape the first wave of exploitation from the exploiter strategy then coexistence is likely. Center: Population dynamics for global (top) and $r = 1$ (bottom) niche construction neighborhood following niche constructor (green) contact process (red) strategies along with destroyed habitat (black) in the coexistence regime: $\{\alpha, \delta, c, e\} = \{1, 0.1, 0.4, 0.01\}$. Right: Four snapshots taken at $t = 250, 1000, 2000, 4000$ from top to bottom, temporal locations of snapshots are indicated with vertical dashed lines. Frame 1 shows the exploiter population being fragmented from vacant sites due to habitat destruction, but rescued by the NC population expanding via the construction of viable habitat. Once the exploiter population establishes itself within the confines of the surrounding NC particles (frame 2 and 3) they can begin exploiting this renewed habitat and freshly vacated sites (generated by c and δ, respectively) due to their superior colonization rate. Eventually, the system equilibrates, although small fluctuations continue due to the local oscillations and the finite size of the landscape, see [92] for a discussion on this with respect to lattice models.

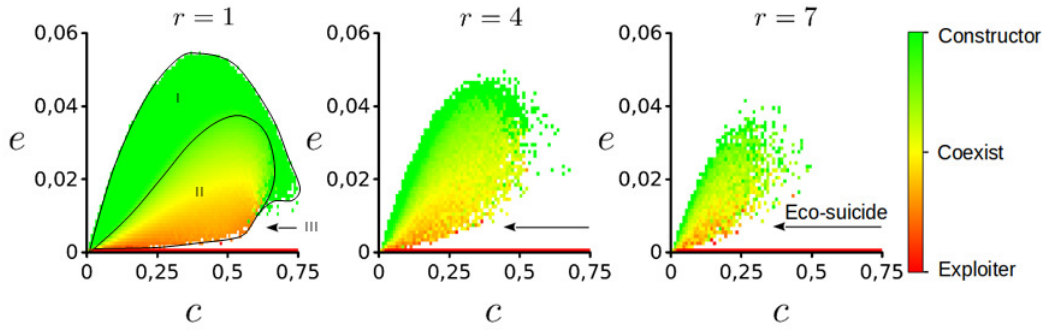

Figure 1.7: Parameter spaces $\{c, e\}$ for the model with scramble competition given three different niche construction neighborhoods, $r = 1, 4$ & 7 from left to right. Relative occupancy is measured as $\frac{\langle p_+ \rangle}{\langle p_+ \rangle + \langle p_{++} \rangle} \in [0, 1]$. Additional parameter values $\{\alpha, \delta\} = \{1, 0.1\}$.

in intensity because exploiters more effectively exploit renewed niche generated by NC populations both at the mosaic-vacuum interface and within the mosaic. While increased r leads to a faster rate of range expansion for the constructor in isolation, this benefit is lost when in scramble competition against exploiters.

If NC populations become surrounded by the exploiter they are likely to go extinct, unless a gap in the perimeter is created by either extinction or destruction events. Therefore, the NC strategy is only able to persist if they can access the interface with the vacuum.

Along with the previously observed instances where the landscape - population strategy mapping pushes the NC metapopulation to extinction (the trivial case) in the single strategy model, there exist 4 phases of the parameter space (Figure 7), described as follows:

i) High disturbance regime; Where constructor metapopulations can successfully monopolize the constructed niche due to the short life-span τ of patches leading to exploiter fragmentation and extinction. By escaping exploitation, the NC strategy is able to persist at the same global occupancy $\widehat{p}_+$ as in the single strategy scenario.

ii) Intermediate disturbance regime; Coexistence between NC and exploiter. Here a dynamic equilibrium is achieved due to a balance in the construction-colonization trade-off. In this regime exploiters are faster at colonizing constructed niche without completely exploiting the constructor population, which maintains itself through range expansion. Within this regime we see an overall decrease in patch occupancy ($\langle p \rangle$) but increase in total diversity reminiscent of the intermediate disturbance hypothesis [93].

iii) Low Disturbance regime causing ecological suicide; Exploiter forces constructor to extinction by effectively over-exploiting the constructed niche to the point of enclosing small clusters of constructor populations. If the constructor strategy cannot escape this confinement, they eventually go globally extinct resulting in the subsequent collapse of the niche and remaining exploiter metapopulation.

And, finally the iv) No disturbance regime, where competitive exclusion pushes the constructor to extinction collapsing the exploiter metapopulation. This regime is limited to the red horizontal line at the bottom of the parameter space where $e = 0$.

From these results we are interested in the transitions from one regime to the next when considering e and r. One striking discovery is the onset of ecological suicide from above $ii \rightarrow iii$ and below $iv \rightarrow iii$ which is enhanced with an increased effort towards niche construction ($c \rightarrow 1$), and expands in parameter space with increasing r. In contrast and counter-intuitive to expectations, we see an increase in constructor strategy occupancy as a response to increasing ephemerality of patches as we transition from $ii \rightarrow i$. This transition becomes noisier as r increases.

Interestingly, for $r > 1$, stochastic events on the lattice can determine the long-term outcome of the metacommunity. When a simulation starts, exploiter patches quickly colonize territory around NC patches which self organize into clusters. For $c \gg 0$ clusters of NC become encircled by exploiter patches, which eventually choke-out NC populations leading to ecological suicide. If however, they are able to slip past exploiter patches and reach the vacuum, they can continue to expand their range, at which point exploiter patches connected by vacancy will continue to follow their expansion. Alternatively, if exploiter patches become separated entirely from the NC metapopulation, exploiter populations will stay fragmented from vacant niche and eventually be vanquished by this self-inflicted fragmentation and the NC metapopulation will return to the long-term behavior of phase i). It is these mechanisms which lead to the noisy behavior of the model at the edge of the extinction threshold, and consequently, this noisiness is enhanced as the difference in size between colonization and construction neighborhoods increases from a relatively monopolized good ($Z_* = Z$) tightly coupled to the NS, to a public good ($Z_* < Z$), easily exploited by the ES.

1.6 Discussion

Our goal here has been to implement a spatial extension of the constructed niche as defined by Krakauer et al. [64], through the interacting particle system framework, in order to determine if a spatial perspective would reveal new and interesting insights into the ecological consequences of niche construction in ephemeral landscapes. While some observations made by Krakauer et al. were reconfirmed here in the spatial model, for example the optimal trade-off between construction and colonization in the single strategy system, new significant findings were also uncovered; for instance, in cases where niche construction is localized ($r = 1$) leading to the emergence of clustering. This clustering in turn allowed the metapopulation to maintain itself where larger r could not. This outcome was reminiscent of the bi-stability predicted by the MFA. In contrast to these mean field predictions, no such behavior was observed for the spatial model when r was limited to adjacent sites. Monte Carlo simulations revealed a continuous phase transition which was steeper than, but qualitatively similar to the contact process. As we increased r for the IPS this transition became more drastic, until it eventually vanished and the discontinuity predicted in the MFA was recovered.

Continuing our study of the single strategy model, we investigated the impact of r on range expansion. As expected, increased niche construction neighborhoods led to an increased rate of range expansion. Therefore, before implementing a second strategy into the model an unanticipated trade-off existed for the niche construction strategy between the rate of range expansion and susceptibility of the metapopulation to critical transitions.

Next, we studied the two strategy model, where the regular contact process behaved as an exploiter strategy to the niche constructor. As expected, increased niche construction neighborhood allowed for greater exploitation. For phases of the parameter space, the system experienced what we referred to as ecological suicide, where exploiter pushed NC to extinction, thus sowing the seeds to their own demise. Unexpectedly, extinction due to ecological suicide was not as clearly defined in our parameter space as the single strategy phase transitions. For example, unlike in the single strategy model where we located e_{crit} with extensive Monte Carlo simulations, we are unable to define critical neighborhood size where ecological suicide begins. This is possibly due to the stochastic nature of its mechanisms; wherein, clusters of NC sites capable of escaping local extinction via scramble competition are freed from the exploiter strategy allowing them to reach

equilibrium values equivalent to the single strategy model. For $r = 1$, ecological suicide is most probable when e is small and c large because the NC reproductive ratio ($\mathcal{R}_0$) is compromised by a high investment in niche construction. This allows the exploiter to quickly out-compete and surround NC before being fragmented by patches of destruction. As r increases the speed with which the exploiter is able to surround NC increases. The expanding area of the parameter space where ecological suicide occurs as r increases exemplifies the tragedy of the commons described by Krakauer et al. [64].

This result emphasizes the importance of spatial structure on the long-term and global outcome of niche constructor/exploiter metacommunity dynamics. Notably, how a few stochastic events changing the connectivity of patches between populations of niche constructing and exploiting strategies lead to drastically different outcomes. Specifically, the initial conditions of these founder populations (clusters of occupied sites surrounded by destroyed sites) can exhibit both stochastic (dominated by random chance events) and deterministic phases (predicted by the proportion of NC vs. CP sites in a cluster) [40, 94]. In this case, the transition between these two phases is determined by r.

Experimental results studying the spatial dynamics of a pair of engineered cross-feeding (niche constructor) *S. cerevisiae* and one non-reciprocating (exploiter) strategy also observed the spatial clustering in our models results of figure 6 [95]. The authors emphasize the self-organizational clustering as an effective assortment mechanism for individual cells to gain cooperative partners and exclude defectors.

Furthermore, clinical research following the colonization dynamics of *P. aeruginosa* in the lungs of mechanically ventilated patients show similar dynamics as our constructor-exploiter model [38]. The *P. aeruginosa* populations of patients monitored over a period of 3 weeks showed a rapid decline in quorum sensing diversity, emphasized by an increase of the lasR mutant (lasR) which likely evolved from the wild-type (wt) strain. The lasR mutant is considered an exploiter as it does not respond to the quorum signal but is able to benefit from the catabolic enzymes produced by wild-type strains and in this way creating a selective advantage [96]. The authors note that this advantage was only found whilst in the presence of the wild-type leading to fluctuations in occupancy between the exploiter (lasR) and constructor (wt) and reminiscent of the temporal dynamics of our model (see figure 6) and the long-term equilibrium of the coexistence regime (ii). In addition, in

patients where lasR did not successfully invade the population (i.e. only wt strategy), ventilator associated pneumonia occurred significantly faster suggesting, as our model does, that the release of exploitation increases the carrying capacity of the metapopulation in regime i.

Inspired by the earlier studies documenting this tragedy of the commons in *P.aeruginosa*, Jin et al. laid out how the production and excretion of these exploitable siderophores is modified in the presence of environmental stress (e in our model and [] tobramycin here) [97]. Using *in vivo* observational experiments, they discovered wt cells are capable of tuning the efflux pump responsible for the excretion of pyoverdine (siderophore) based off the stress level of the environment, in this way being able to monopolize the constructed niche in stressful environments. Using a well-mixed competition experiment, they were able to show that while moderately stressful environments (small e) reproduced the observations of [37] i.e. exploitation by mutant strain leading to wt extinction, more stressful environments (large e) counter-intuitively led to wt dominance characterized by this 'conditional privatization' (See figure 4 in [97]). While these experimental observations verify the qualitative behavior of our model results defined by regimes i-iv, yet verified is the effect r has on the shape of these regimes as in figure 7. We think range expansion experiments would be an ideal experimental set-up to study the role of space in constructor-exploiter dynamics [98].

While an extensive literature exists for studying spatial games in ecology and evolution [99, 100, 101], much of this is built on a strategy-strategy payoff matrix. Theoretical advances aimed at considering environmentally mediated resources, in our case the constructed niche, are still in their infancy [102, 103].

1.7 Conclusion

We envision the trade-off between colonization and construction to be a generalized predicament faced by populations and whose solutions to this dilemma mark the most significant transitions in the evolution of life on earth [104]. Of particular interest is the origins of multicellularity, which was most likely achieved through the division of labor between maintenance (construction) and replication (colonization) [68, 105]. Here we developed a 'toy ecology' within the interacting particle system framework [99] which we believe reproduces some of the conceptual dilemmas faced at this transition from population to individual. Furthermore, these findings have implications for the

study of ecosystems stability and susceptibility to critical transitions. Understanding which real world ecosystems are likely to behave as continuous vs. discontinuous phase transitions is crucial for their conservation and management.

sample

Chapter 2

What doesn't kill you makes you stronger

It is the system and its fragility, not events, that must be studied.

- Nassim Nicholas Taleb

Abstract

Colicin production is an extreme form of labor division; cells lyse after making the toxin! Stochastic phenotype switching allows producers to outcompete sensitive strains since colicin release frees up vacancy. If patch dynamics does not kill you, it stimulates adaptation to a dynamic habitat landscape which selects for rapid dispersal.

Introduction

During range expansion experiments [106], bacteria expand their occupancy by a space-colonization process initialized by depositing a single droplet of culture on hard agar. The struggle for existence in such ecological conditions provides a useful framework for testing theoretical predictions on the long-term outcome of spatially-driven community assembly. Until now, exploring the role of phenotypic heterogeneity plays on the colonization strategy of competing populations in these experiments has been missing. Combining experimental and theoretical efforts, von Bronk et al. [40] elegantly approach this question using a bacterial community consisting of colicin producer(C)and colicin sensitive(S)strains of *Escherichia coli*. Producer cells can stochastically switch their reproductively active(C+)phenotype into a non-dividing (C-) phenotype that is reproductively inactive but metabolically busy producing toxin, ultimately undergoing cell lysis and releasing colicin to the extracellular environment. The sacrifice of these individuals directly impacts the fitness of the sensitive strain which is in direct space competition with the producer. Although these suicidal cells do not enjoy a direct benefit, through inclusive fitness, the producer strain wins the war for territory provided the fraction of cells producing colicin is moderate. Experimentally manipulating the rate of switching, the authors observe several interesting phenomena which we discuss here from a landscape ecology perspective. In all experiments two temporal phases can be distinguished. The earlier phase is dominated by stochastic effects (Phase I) and the later phase is dominated by deterministic properties (Phase II). In both, results from percolation theory [41] can provide some insights into the underlying spatial ecology.

The stochasticity of Phase I is highly dependent on the initial conditions: Experiments were started with droplets, obtained from low-density cultures, contrary to other range expansion experiments [106] where initial conditions consisted of droplets at high cell density. By inoculating

with a high cell density droplet, both strains establish multiple clusters at the colony edge during the initial stage of growth. After adsorption of the droplet on to the surface, the spatial pattern of microcolonies is super-critical from the percolation theory standpoint, thus, the initial spatial distribution is dominated by occupancy. Alternatively, [40] begin with a low density droplet (sub-critical) with a mixed culture heavily in favor of the sensitive strain (1:100). Such a *biased* and *low density* droplet increases the chances that the spatial distribution of the less abundant population of colcin-producing cells is fragmented [84], therefore decreasing their chances of ending up at the edge of the colony at the end of phase I. Due to its low density, the initial spatial distribution after adsorption is dominated by vacancy. Stochasticity in Phase I is an effect caused by the heavy bias on the strain composition combined with the low density of the inoculating droplet.

The outcome of phase II is deterministic and dependent upon the degree of labor division (reproduction vs toxin), therefore two regimes are immediately distinguished depending on the presence or absence of colicin production and release. When switching is absent, a neutral ecology emerges since no toxin production means no real differences between strains. This is clearly shown in Figure 2C in [40] as a linear relationship between the number of colicin-producing clusters at the edge of the colony after Phase I ($N_{C,Edge}$) and the fraction of colicin producers persisting until the end of Phase II (F_C). At intermediate switching, producers dominate as long as one or more clusters are present at the colony edge after Phase I, highlighting the benefit of the colicin-producing strategy. Why do higher switching rates not lead to a similar domination? Guided by Figure 2B in [40], again we can make intuitive comparison, borrowing results from percolation theory. Intermediate switching generates enough cell clusters making colicin and freeing up vacancy for the dividing sub-population to spread. However, if switching is too high, the sub-population of dividing producers is too small to effectively compete for space with the sensitive population, as shown in Figure 2F in von Bronk *et al.* [40]. Notice that, while producer cells $C-$ are making colicin, they occupy space until lysis, which could otherwise be occupied by the actively dividing sub-population $C+$. The rate at which $C-$ subpopulations lyse corresponds to the rate of vacancy release thus generating patches of habitat which become available for recolonization. This promotes a dynamic habitat landscape for dividing sub-population $C+$ where extinction thresholds are expected [83]. If patch turnover is fast enough, dynamic corridors connect patches of vacancy and producers persist, otherwise, their habitat landscape fragments and they eventually go extinct (Figure 1).

To understand the significance of toxin effectivity S_s (rate at which sensitive cells stop growing in the presence of colicin) and switching rates S_c, von Bronk *et al.* [40] conducted numerical studies [80] describing sensitive and producer populations (Fig 4B in [40]).

Their theoretical framework a community model, exhibits behavior which is remarkably similar to their empirical observations. Here, we develop a simple but otherwise similar model, shifting our attention to some landscape ecology issues affecting the spatial dynamics of producers (C). In the absence of death and induction, the range expansion can be understood in the context of Richardson's model of spatial growth [107]. As shown in our Figure 1A, we incorporate induction with the probability α and lysis with probability δ to this model and use it to interpret the results of [40]. Our main point, shown in Figure 1B-D, is that extinction of producers at critical induction probabilities $\alpha_{crit}(\delta)$ is to be expected due to self-induced, dynamic-landscape-associated extinction thresholds [83]. An important observation made by von Bronk *et al.* [40] is that even when the sensitive population wins in the long term, experiencing such a dynamic habitat landscape during transient competition selects for faster spreaders. Enduring the damage from colicin exposure while competing transiently with producers makes the winning sensitive cells stronger at the expansion front when compared with a competition free scenario. This can be clearly appreciated in Figure 3B-C in [40], by comparing the area expansion rate with and without interaction at intermediate inducer concentrations. Here we have highlighted how dynamic landscapes of colicin production are characterized by a critical curve $\alpha_{crit}(\delta)$ defining persistence and extinction.

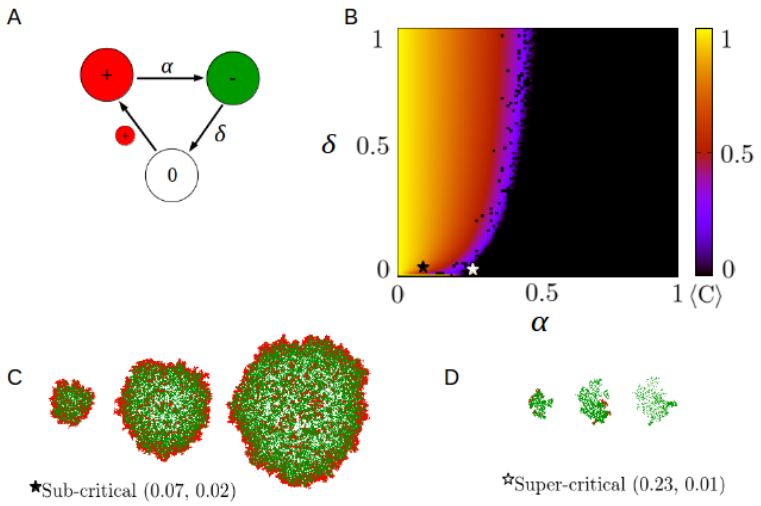

Figure 2.1: Extinction Thresholds in Dynamic Landscapes of Colicin Production (A) Spatial stochastic process xi_t, an interacting particle system, mapping a 2D lattice $mathcalL$ of 256^2 sites to three states: *state* 0 (white) represents vacancy, *state* + (red) active replicating particles which conquer nearby vacant sites, and *state* - (green) inactive particles committed to colicin production and not to replication. An empty site (0, white), completely surrounded with replicating particles (+, red) switch into non-replicating colicin-producing particles (-,green) dying out with probability δ. (B) Parameter space showing the long-term average (over $2.5 * 10^2$ generations) occupancy $/langleC/rangle = /langleC_+/rangle + /langleC_-/rangle$ after 10^3 generations. The scale bar represents $/langleC/rangle$ as a heat map. Notice the critical curve $\alpha_{crit}(\delta)$ defining zones of persistence and extinction (blue-black interface). Symbols represent values for two simulations starting from a small cluster of replicating particles (+, red) at the center of an otherwise empty lattice. Three snapshots of the lattice configuration $\xi_t : \mathcal{L} \to \{0, +, -\}$ at times $t_1 = 60$, $t_2 = 120$, and $t_3 = 180$ are shown in C and D, respectively. (C) Parameters shown in B correspond to $\alpha = 0.07$ and $\delta = 0.02$ in the persistence zone, that is, $\alpha < \alpha_{crit}(\delta)$. (D) Parameters shown in B correspond to $\alpha = 0.23$ and $\delta = 0.01$ in the extinction zone, that is, $\alpha > \alpha_{crit}(\delta)$.

Chapter 3

Competition-Colonization trade-off in Spatial Microbial Meta-communities *on-chip*

To do science is to search for repeated patterns, not simply to accumulate facts.

-Robert MacArthur

Far better an approximate answer to the right question, which is often vague, than the exact answer to the wrong question, which can always be made precise.

-John Tukey

To exploit locations or explore the landscape? This is the core of the competition-colonization trade-off; a dichotomy structuring ecological communities at large. By using microfluidic devices as structured bacterial habitats we show that *E. coli* is a fast colonizer but poor competitor while *P. aeruginosa* is a slow colonizer but superior competitor. We provide experimental evidence highlighting the relevance of this trade-off in structuring metacommunities of bacteria in spatially distributed habitats.

3.1 Introduction

With an estimated one trillion (10^{12}) microbial species on Earth [108], a primary goal of microbial ecology is to understand the mechanisms which maintain such vast biodiversity [109] and lead to the patterns of species distributions observed [110, 111]. The urgency for a basic understanding is only increased as we continue to learn more about the spatial subtleties of the microscopic world and the important roles microbes play for our own well-being, working as functional microbiomes present in both our bodies and the ecosystems we rely on [112, 113, 114]. To improve our current knowledge of the spatial biology of microbes, significant research efforts have been directed towards understanding how the spatial structure of habitats determines ecological processes. For example, how does structure affect colonization-extinction dynamics? How do these processes shape local communities coupled via dispersal? Does habitat patchiness at one scale permit coexistence and influence biodiversity patterns at larger scales? A myriad of potential theoretical frameworks, both niche [115] and neutral [116], detailing specific mechanistic processes permitting coexistence between species can be used to address these questions. One of the lessons learned from theoretical community ecology has been the understanding that there is not one silver bullet for maintaining biodiversity, but rather many potential causes for coexistence [21]. These can depend on specific details of the system being studied, for example, regional species pools [117], ephemerality [118] and physical structure of the landscape [119]. However, for bacteria, the spatially explicit nature of habitat landscapes is of paramount importance as their habitats are typically porous and patchy at the microscopic scale.

In a spatially distributed habitat, the physical structure of the landscape as well as how ephemeral are the species inhabiting it are understood to play an important role in community composition by changing colonization, extinction and dispersal rates, yet they are rarely considered experimentally [120, 121]. Additionally, the implementation of ecological theory, developed through the study of macroscopic systems such as metacommunity theory [21] and ecological succession [122], is welcome and necessary for addressing this overarching question of microbiology. It is, however, important to understand the vast differences in both the physical and biological nature of microbial landscapes and its living constituents compared to their macroscopic counterparts. One of the primary reasons for this discrepancy has to do with the separation of time scales between evolutionary and ecological

dynamics traditionally assumed to be inherent to macroscopic systems, though see [123] for a fresh synthesis. Microbes are constantly regulating and responding to their environment physically and chemically, through biofilm formation [124], collective migration [125], consumption of nutrients, and excretion of metabolites in ways that have an immediate effect on habitat quality (ecological inheritance) and thus ecological selection [126, 127]. For example, niche construction of this kind may play a role in regards to ecological succession in microbial landscapes where the stochastic nature of primary colonization events can dictate the trajectory of local community development (priority effects) [128]. This is particularly important in environments where succession occurs rapidly and dispersal capabilities play an important role in determining the order of species arrival [129]. A variety of microbial ecosystems fall into this category, including the phyllosphere (leaf surfaces) [122], human skin [130], and the rhizosphere (soil-root interface), where periodic inputs of labile organics by plants such as sugar, amino acids and mucilage lead to fierce and frequent microbial colonization/competition events for optimal access [131, 132]. Predicting how this microbe-environment coupling shapes patch (community) and landscape (metacommunity) composition is still an open ended question. To progress in this endeavor, we need to understand the spatial scaling laws linking the structure of the habitat with the biology of populations and the ecology of communities [18].

In this work, we studied the colonization by *Escherichia coli* and *Pseudomonas aeruginosa* bacteria competing in a spatially distributed habitat landscape structured at the micron-scale constituting a bacteria meta-community *on-chip* (see Fig. 1). Building upon previous work in similar patchy landscapes [133, 31, 134], we focus on the following questions: (*i*) in what order do the species colonize the landscape? (*ii*) how does this impact transient dynamics and long-term metacommunity composition? and (*iii*) how reproducible are these metacommunity dynamics?

We found that the order of colonization is reproducible, where *E. coli* and *P. aeruginosa* demonstrate a life-history competition colonization trade-off as *E. coli* always colonizes first (fast colonizer) followed by succession by the superior competitor, *P. aeruginosa* (slow colonizer). In habitats with patchiness, landscape and patch level coexistence is possible due to local habitat modification by the inferior competitor *E. coli*. These habitat modifications are most pronounced within ecological corridors where micro-colony formation effectively limits dispersal and sometimes leads to fragmentation events disconnecting the landscape and preventing the superior competitor from dominating the entire landscape (priority effects). In habitats with no patchiness, we found coexistence based

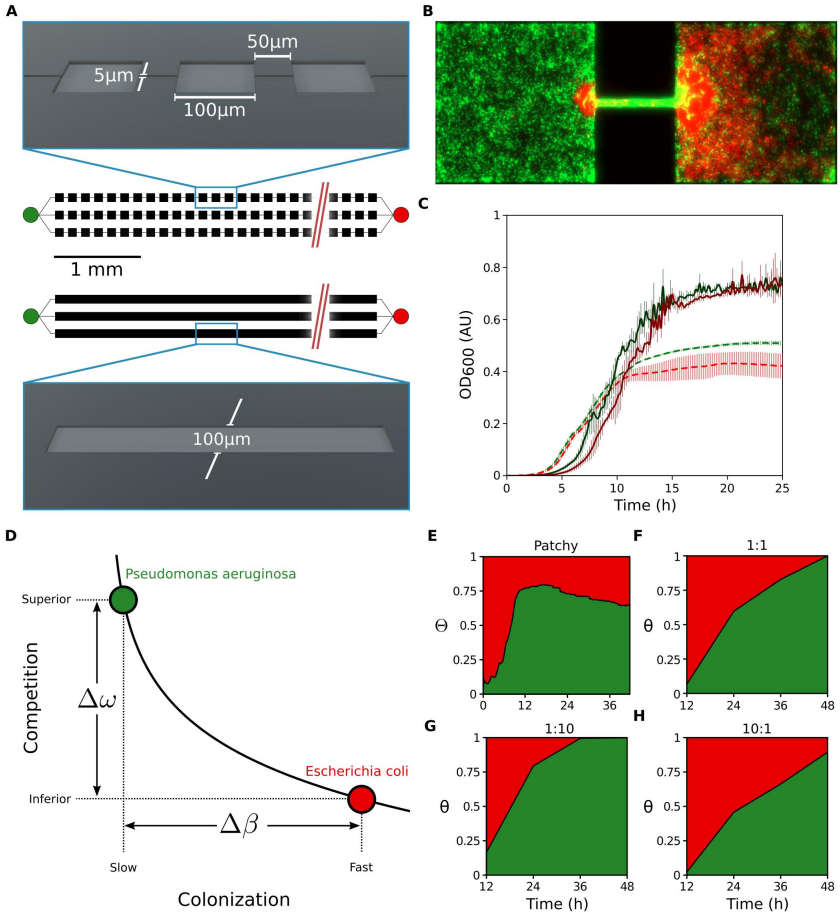

Figure 3.1: Competition colonization trade-off in micro-fabricated habitats. **A** Two different *on-chip* microfluidics-based ecosystems implementing three replica habitats each. Schematic representations and of the devices are shown. Top and bottom panels correspond to patchy and flat landscapes respectively, inoculation inlets are shown as red and green circles. For the device sketched at the bottom, length is not to scale. **B** Zoom image of a patch-corridor motif in a patchy landscape as shown in A (*top panel*), fluorescence microscopy image of RFP carrying *E. coli* competing against GFP labeled *P. aeruginosa*; scale bar is 25μm. **C** Monoculture growth assay of red (RFP) and green (GFP) labeled *P. aeruginosa* strains (solid line; PUPa3-G in green and PUPa3-R in red) and *E. coli* strains (dashed line; JEK1036 in green and JEK1037 in red) in well-mixed 96 well-plates; see Suppl. Table S1 for details on strains used. **D** Two ecological strategies: a superior competitor (high ω) but slow colonizer (low β) *P. aeruginosa* (green) and an inferior competitor (low ω) but fast colonizer (high β) *E. coli* (red); black curve represents Equation 3.1 describing the trade-off (see text). **E** *P. aeruginosa* fractional occupancy dynamics calculated as an ensemble average Θ by integrating all 72 experiments in patchy landscapes, $0 \neq \Theta \equiv \langle \bar{P}/(\bar{E}+\bar{P}) \rangle \neq 1$ (Secs. 3.2.4, 3.4.5; Table S8). This is in sharp contrast to what is observed in well-mixed experiments (**F-H**) where long-term the relative fractional abundance θ shows competitive dominance by *P. aeruginosa*, $\theta \equiv \langle N_P/(N_E+N_P) \rangle \to 1$ (Secs. 3.4.3; Table S8), regardless of the initial *P. aeruginosa* to *E. coli* abundances used at inoculation as shown here in F for 1:1, G for 1:10, and H for 10:1.

on a rather neutral ecology. We developed a spatially-explicit stochastic model of the competition colonization trade-off. In conjunction with this classical patch dynamics approach and in order to account for the effects of wave phenomena, we develop an alternative view of patchiness: introducing concepts from solid state physics, we represent the habitat structure in patchy landscapes as a periodic potential [46]. This conceptualization guides the interpretation of our microfluidics-based *on-chip* ecosystem experiments.

3.2 Results

3.2.1 Landscape ecology *on-chip*

To recreate the patchy nature of microbial habitats [135], we used microfabrication techniques [136] to generate *on-chip* landscapes where arrays of habitat patches are connected by corridors [133]. Such crystal-like habitats are models of natural patchiness. Patchiness is important because it introduces a critical length scale in the structure of the habitat [18]. This length scale determines the existence of fugitive strategies [91] which specialize in scramble competition for vacant patches (suitable locations) as opposed to excelling at interference competition for local resources within patches. To be, or not to be a fugitive strategy? This is the core of the competition-colonization (CC) trade-off. A theoretical representation of such dichotomy is sketched here in Figure 1D, a conceptual relationship linking competition (ω) and colonization (β) abilities,

$$\omega = e^{-\alpha\beta}. \tag{3.1}$$

Using microfluidics experiments, we show that if patchiness exist in the habitat, *E. coli* and *P. aeruginosa* can be positioned along this (aspect) space of differentiation. The strategy of *E. coli* corresponds to a *fast* colonizer (higher β) and *P. aeruginosa* to a *superior* competitor (higher ω). If the habitat is not patchy, the dichotomy vanishes, and so do these phenotypes (CC trade-off).

As a first approximation to patchiness in the spatial structure of natural microbial habitats, we fabricated repetitions of a patch-corridor motif (Fig. 1B) giving rise to a one dimensional array of Micro Habitat Patches (MHPs). We fabricated shallow ($h = 5$ μm), but wide ($w = 100$ μm) and rather long ($L = 12750$ μm) quasi-2D environments. Along the length axis ($x \in L$), in patchy

habitats, the patch-corridor motif $(a + b)$ repeats $n = 85$ times representing patchiness at length scale $l = a+b = L/n = 150$ μm. In this manner, we make a physical model of a "patchy landscape" (Fig. 1A, *top panel*; Fig. S2) which consists of an array of 85 MHPs which are $a = w$ wide squares, h deep and which are connected as a 1D chain by h deep, h wide, $b = w/2$ long corridors so that $L = n(a+b)$. For control experiments, we made "flat landscape" environments (see Fig. 1A, *bottom panel*) with no patchiness which are w wide, L long, h deep and consists of a single $(n = 1)$, but long $(l = L >> w)$ MHP making up a strip-like habitat.

We performed invasion-competition experiments in these *on-chip* spatially distributed environments using time-lapse microscopy of fluorescently labeled (red–green and green–red) co-cultures of strain pairs (*E. coli–P. aeruginosa*) to study cell, patch and landscape level dynamics with precision as the development of the metacommunity unfolds over 48 hours. We initiated the system with each species coming from opposite sides of the landscapes and recorded fluorescence microscopy images of the microfluidics device in 10 min intervals. Local, within MHP (spatial index k), occupancy was calculated for both *P. aeruginosa*, $P_k(t)$, and *E. coli*, $E_k(t)$, for all recorded fluorescence microscopy images (Sec 3.4.5) in a timelapse (time index, t). Figure 1E shows *P. aeruginosa* fractional occupancy dynamics, $\Theta(t)$, calculated as an ensemble average by combining the data of 72 patchy landscapes (24 experiments with 3 landscapes each). The results show a quick colonization of the landscape by *E. coli* followed by an increasing domination by *P. aeruginosa*. From about 12h till 48h the fractional occupancies change little. The landscape is dominated by *P. aeruginosa*, however in coexistence with *E. coli*; $\Theta \to 0.7$. This is in striking contrast with the results of competition experiments performed in well mixed flasks, where – regardless of the initial ratio of *P. aeruginosa* and *E. coli* cells – a steady increase in *P. aeruginosa* fractional abundance, $\theta(t)$, was seen during the full time-course of the experiments. In case of the 1:1, 1:10, and 10:1 initial *P. aeruginosa* : *E. coli* ratios this led to a total elimination of *E. coli*; $\theta \to 1$ (Fig. 1F-H).

There are several factors behind the markedly different competition outcome in patchy landscapes and mixed cultures. Dispersal/invasion strategies play a crucial role in spatially structured landscapes, but not in well mixed environments. The topology of the habitat may furthermore promote other strategies involving cell aggregation that affect the competition. We detail these in the following sections.

3.2.2 Population waves and monoculture metapopulations

Bacterial population waves have been described in the literature since the seminal work of Adler [137] and their existence is a phenomenon that appears to be robust to landscape structure [137, 138, 139, 133, 125, 134] and an integral part of bacterial dispersal strategies. They are the product of interactions between self-produced attractant fields and the chemotactic behavior of individual bacterial cells [137, 140]. These patterns of motility are known to drive quorum sensing [139], which additionally, is driven by the topology of the habitat landscape [138]. We expect that the wave dominated behavior in such landscapes sets the conditions for coexistence (Fig. 1E) due to the fugitive nature of the *E. coli* strategy. Previous work looking at bacterial mono-cultures colonizing patchy landscapes, similar to those used in this study, has shown that population waves are indeed exhibited by *E. coli* when colonizing these type of environments. After initial landscape colonization by these waves and a later expanding population front [134], bacteria develop into spatially distributed metapopulations [133]. Statistically, these population level waves are the product of directional persistence in the microscopic swimming patterns of individual cells [125]. The question that remains is how to link these waves to a mechanism preserving biodiversity in spatial environments by allowing persistence of a fugitive strategy [91].

In Figure 2 we can see the behavior of isolated metapopulations of *E. coli* (A-B) and *P. aeruginosa* (C-D) monocultures, in a patchy landscape like the one depicted in Figure 1A *top panel*. At first glance, as described by Van Vliet and collaborators [134], one notices how the landscape is colonized by a succession of waves which vary in velocity and local density. For *E. coli*, colonization of the landscape begins by a fast propagating wave ($0.78 \pm 0.2\mu$m/s). This initial wave, called α-wave [134], is of low cell density. After this fast moving wave, a larger density but slower ($0.55 \pm 0.21\mu$m/s) wave is observed; such wave is called β-wave [134]. We sketch this wave-based dispersal pattern in Figure 2E. Finally a population front (called γ-front [134]) expands into the landscape.

Notice that *P. aeruginosa* on the other hand, exhibits slower and denser waves (Fig. 2C-D) which we sketch here in Figure 2G. In Figure 1C we show that, at least in well-mixed monocultures, *E. coli* strains are faster than *P. aeruginosa* at exiting lag-phase while reaching lower densities at stationary phase. These growth differences may be interrelated to the distinct characteristics of wave formation and propagation. As the bacteria expand their range in the patchy landscape

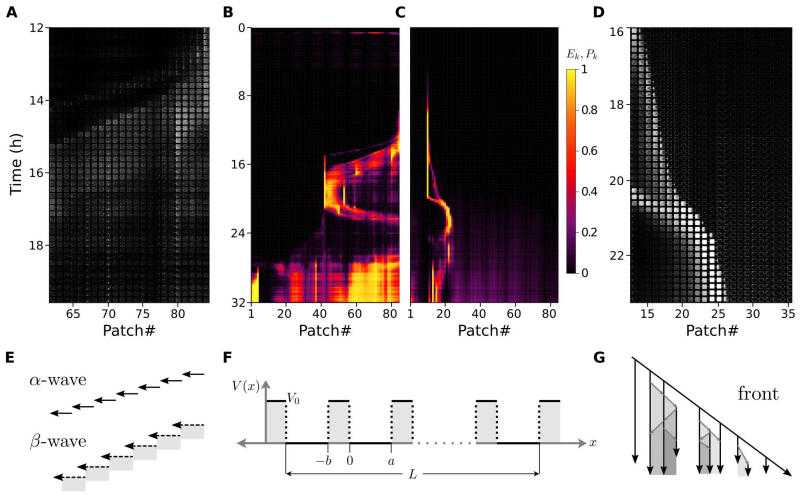

Figure 3.2: Landscape colonization by population waves of bacteria Kymographs showing the colonization of a patchy landscape by *E. coli* and *P. aeruginosa* monocultures *on-chip*. **A** Raw images of fluorescent intensity corresponding to a zoom-in view into a part of the occupancy pattern shown in B. Local (within patch) occupancy of *E. coli* E_k (**B**) and *P. aeruginosa*, P_k (**C**). Color maps in B and C corresponds to E_k and P_k respectively (see Sec. 3.4.5). **D** Raw images of fluorescent intensity corresponding to a zoom-in view into part of the occupancy pattern shown in C. **E** Sketch of the colonization wave behavior exhibited by *E. coli*. **F** Representation of an MHP array, as a periodic potential [46]. **G** Sketch of the wave behavior exhibited by *P. aeruginosa*.

the waves interact with the topology of the landscape [138] producing a bacterial metapopulation [133] which exhibits a complex phenotype of patch colonization and local extinction. Shown by Van Vliet and collaborators [134], as the wave penetrates such a landscape it experiences diffraction when interacting with corridors as they correspond to energy barriers (of height V_0; Fig. 2F). Thus, some cells keep traveling with the wave from patch to corridor (*sensu* [125]) while others leave the pack to localize and recruit to the patch adjacent to the corridor. As the traveling waves accumulate in the landscape they interact forming complex patterns of landscape occupancy. These patterns are further affected by the interactions of subsequent travelling waves with local stationary populations which are localized to patches and corridors. The nature of the spatio-temporal pattern is a phenotype which bacteria can regulate endogenously. This is a complex issue, as cells which are not travelling in waves can be both motile or aggregate into non-motile clusters. These aggregation events are highly dynamic and exist at multiple scales ranging from within patches to several adjacent patches [133, 31]. Contrary to the work of [121], which studied co-cultures of *P. aeruginosa* strains in well-mixed well-plates and where dispersal was imposed in an exogenous fashion by cross-inoculation, here two species of bacteria are free to exhibit a wave-based

range expansion and successive colonization-extinction dynamics. Can we still, in agreement with [121] and contrary to what we see in isolated well-mixed environments without cross-inoculation (Fig. 1F-H), observe coexistence between *E. coli* and *P.aeruginosa*? As we show in Figure 1E, the short answer is yes. In the following sections we describe this main result further.

3.2.3 In spatial competition, pioneering *E. coli* colonize the landscape first

Following the inoculation of the patchy device inlets with bacteria (left inlet with *P. aeruginosa*, right inlet with *E. coli*), the first MHPs are colonized by pioneer cells of *E. coli* after a delay of 3h. In the left panel of Figure 3A we show that this initial colonization by *E. coli* is often done by a low density fast traveling wave (α-wave; Sec. 3.2.2). Here we show a typical experiment where *E. coli* colonizes from the right hand side (RHS) of the device before establishing a main sub-population of high cell density which reaches 85% of local (within MHP) occupancy, E_k, after ≈ 10 hours (Fig. 3C, *top panel*). In this case, the main sub-population is localized at the left-most ($k = 1$) patch of the landscape. However, the exact location of establishment of a pioneer main sub-population varies considerably between experiments. In Figure 3B, we show a "zoomed-in view" of the first four patches ($k = 1 \cdots 4$) for four time points τ_j. We see regional metacommunity dynamics across several patches over the course of several hours; at $\tau_1 = 7.75$ hours in the left hand side (LHS) of the array, *E. coli* increases its occupancy E_1 via division and recruitment of later arrivals traveling from the RHS. Eventually this leads its main sub-population to expand in size and to become a highly condensed, localized cluster that eventually spans multiple patches and corridors by time $\tau_2 = 15.5$ hours.

Once a slower *P. aeruginosa* begins to enter the landscape ($t \approx \tau_2 = 15.5$ hours) it is first confined to patch number 1 where its local (within MHP) occupancy, $P_1(\tau_2)$, is around 30% (Fig.3C, *bottom panel*). At this stage of biofilm development, cells in these localized populations can be found in both 'planktonic' (free swimming) or 'sessile' (aggregated) states. Sessile *E. coli* cells form micro-colonies where cell aggregates attach to habitat surfaces, usually along the edges of patches and in the corridors. These aggregation events within corridors (Fig. 1B) are the basis for priority effects ultimately permitting coexistence with *P. aeruginosa* in patchy landscapes. After initial colonization, the aggregation phase is often considered the following stage in a pattern of (local sub-population) development which progresses towards its "climax stage"; a MHP which is 100%

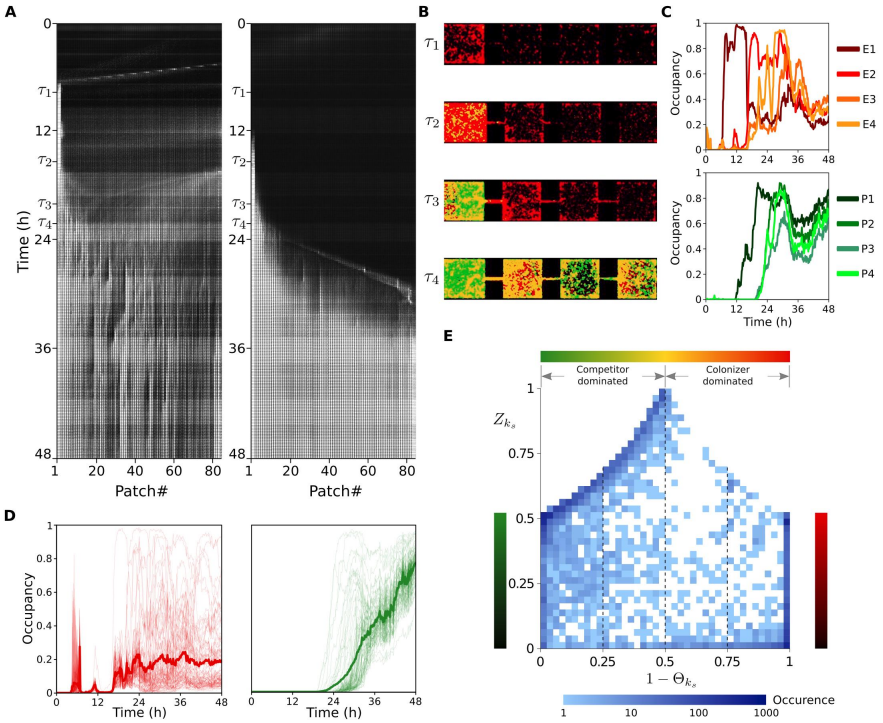

Figure 3.3: Structure and dynamics of metacommunities in patchy landscapes A Kymographs built from raw florescence images from a competition experiment between *E. coli* (*left panel*) and *P. aeruginosa* (*right panel*). **B** Zoomed-in view of four patches $k = 1 \cdots 4$ at four different time points τ_j (7.75, 15.5, 20.3, 22.5 hours)) showing succession from *E. coli* (red) colonization, *P. aeruginosa* (green) invasion as a minority and eventual coexistence. **C** Ocuppancy dynamics of *E. coli*, E_k (*top panel*) and *P. aeruginosa* P_k (*bottom panel*) for each of the MHPs shown in B. **D** Occupancy dynamics for *E. coli* E_k (*left panel*) and *P. aeruginosa* P_k (*right panel*) for all MHPs in the array shown as light red and green curves respectively. The thick curves represent spatially averaged occupancy ($\bar{E}$ in red and $\bar{P}$ in green) for all patches for *E. coli* and *P. aeruginosa* respectively. **E** Long-term local community structure after 48 hours of competition for 6120 MHPs across 72 experiments. Vertical axis represent normalized total occupancy of an MHPs, horizontal axis corresponds to relative fractional occupancy. In blue intensities we represent occurrences (see text).

occupied with biofilm [124].

In our experiments, these aggregation events are a crucial physical modification of the environment as it tends to enhance localization of the superior competitor and diminish the connectivity of the landscape and in some cases fragment it entirely. As we see here in Figure 3B, at time $\tau_3 = 20.3$ hours when *P. aeruginosa* has successfully invaded only the first patch of the landscape where it coexists with *E. coli* at high local occupancy ($\approx 80\%$). This can be appreciated by comparing values $P_1(\tau_3) \approx 0.8$ and $E_1(\tau_3) \approx 0.3$ in Figure 3C (notice, $0 \leq E_k(\tau_j) + P_k(\tau_j) \leq 2$, $\forall k, \tau_j$; see Sec. 3.4.5). It is precisely one of these aggregation events at the corridor between patches $k = 1$ and $k = 2$ that prevents *P. aeruginosa* from propagating into the right ($P_k(\tau_3) = 0$ for $k = 2 \cdots 4$).

It is only afterwards that *P. aeruginosa* manages to penetrate the corridor and invade as we see at time $\tau_4 = 22.5$ hours when all four patches shown in Figure 3B host a local population of *P. aeruginosa* with significant ($> 30\%$) occupancy ($P_k(\tau_4) > 0.3; k = 1 \cdots 4$) which after 36 hours dominates most of the landscape with local occupancy around 70% compared to 30% reached by *E. coli* as shown in Figure 3C (compare $E_k(48)$ and $P_k(48)$). This is in sharp contrast to what we see in well mixed experiments (see Fig. 1F-H) where *P. aeruginosa* always wins after 48 hours of competition ($\theta \to 1$). In these well-mixed environments, *P. aeruginosa* to *E.coli* ratios show the following patterns after 36 of hours of competition when starting from 1:1, 10:1, 1:10 ratios, respectively: 75:25, 100:0, 67:33. Comparing these results to an ensemble average obtained by pulling all our spatial experiments ($N = 72$) together, we see that in a statistical (mechanics) sense, *P. aeruginosa* coexist with *E. coli* at a 65:35 ratio in the long-term ($\Theta \to 0.65$) as shown in Figure 1E. To understand this statistical pattern further, in the following section, we focus on ecological succession.

3.2.4 *P. aeruginosa* invades later but outcompetes *E. coli* locally

In most experiments in patchy landscapes, following the initial colonization by *E. coli* we see a clear example of ecological succession, where *P. aeruginosa* enters the habitat landscape as a densely-packed front which advances and disperses into successive patches in sequence as it travels through the landscape from left to right. This initial colonization strategy of *P. aeruginosa* is qualitatively different than the one implemented by *E. coli* which comes in clear waves instead. Specifically, an example of such range expansion, can be seen in the kymograph shown in the right panel of Figure 3A and which can also be visualized in Figure 3D where the dynamics of local occupancy, P_k and E_k (thin color curves in the background), are followed for each patch in the entire landscape ($k = 1 \cdots 85$). *P. aeruginosa* occupancy ($P_k(t)$; Fig. 3A, *right panel*) demonstrates a textbook example of Skellam's "Malthusian population in a linear habitat"; a biological invasion by local populations advancing uncontested in a favorable linear landscape [141]. This is in sharp contrast to the highly fluctuating fugitive-like dynamics (*sensu* [91]) of *E. coli* occupancy ($E_k(t)$; Fig. 3A, *left panel*) which appears to be in direct response to the arrival of *P. aeruginosa*. This can be appreciated by comparing local occupancy $P_k(t)$ and $E_k(t)$ for all patches ($k = 1 \cdots 85$), as well as their landscape averages $\bar{E}(t) = (1/85) \sum_k E_k(t)$ and $\bar{P}(t) = (1/85) \sum_k P_k(t)$ (thick color

curves in the foreground), before and after $t = \tau_2$. Notice, *P. aeruginosa* enters the left most patch ($k = 1$) about 12 hours after inoculation and stays there until 24 hours when its invasion front starts moving to the right conquering patches and corridors. After 36 hours the front has expanded throughout the whole habitat landscape. As the front advances, the *E. coli* metapopulation retreats its range of high occupancy sub-populations while keeping less dense sub-populations which are less localized and fluctuate in a fugitive fashion avoiding local competition with colonization as shown in Figure 3A-D. These local community dynamics repeat themselves, one patch at a time (Figure 3B), following a classical case of ecological succession depicted in Figure 4D, where local species composition flows through the following states: (*i*) *E. coli* early colonization, (*ii*) expansion by recruitment of local sub-populations, (*iii*) competition with invading *P. aeruginosa* and eventually (*iv*) replacement of the local *E. coli* population by *P. aeruginosa*.

At the landscape scale however, looking over all patches ($\forall k_s$) in all landscapes (indexed by s), the long-term pattern of local community structure can be appreciated in more detail in Figure 3E where we plot the local community state, $[E_{k_s}(t^*), P_{k_s}(t^*)]$, after 48 hours of competition ($t^* = 48$h) for 6120 MHPs distributed across 72 landscapes with 85 patches each (*i.e.* for $k_1 = 1, \cdots, 85; k_2 = 1, \cdots, 85; \cdots; k_{N=72} = 1, \cdots, 85$). In the horizontal axis we show the fractional occupancy of *E. coli*, $(1 - \Theta_{k_s}) = E_{k_s}/(E_{k_s} + P_{k_s})$ for each patch, binned in 40 intervals of length $2.5 \cdot 10^{-2}$; thus, we represent MHPs with equal number of *E. coli* and *P. aeruginosa* at the center of the axis $(1-\Theta_{k_s}) = 0.5$. As a local community also exhibits different levels of total occupancy $Z_{k_s} = (E_{k_s} + P_{k_s})/2$, we represent the level of vacancy in the vertical axis which is also binned in 40 intervals of length $2.5 \cdot 10^{-2}$. A totally saturated patch with both species present in equal numbers corresponds to $Z_{k_s} = 1$. Such local community state $[(1 - \Theta_{k_s}), Z_{k_s}]$, plotted as point $(0.5, 1)$, is also represented as the yellow color in the gradient bar on top of the plot. As we travel from this point down the vertical axis, we represent MHPs with a 50:50 ratio of species but with increasing levels of vacancy. Traveling to the left (towards green) of the horizontal axis, we represent MHPs which are dominanted by *P. aeruginosa*. Similarly, traveling to the right (towards red), we represent MHPs with increasing numbers of *E. coli*. On the left end, at $(1 - \Theta_{k_s}) = 0$, and on the right end, at $(1 - \Theta_{k_s}) = 1$, we represent MHPs with monocultures of *P. aeruginosa* or *E. coli* respectively. Notice that due to normalization conditions, a totally saturated monoculture can only attain $Z_{k_s} = 0.5$ in the vertical axis (represented by the lateral red and green gradient bars). The color-map of blue intensities at the

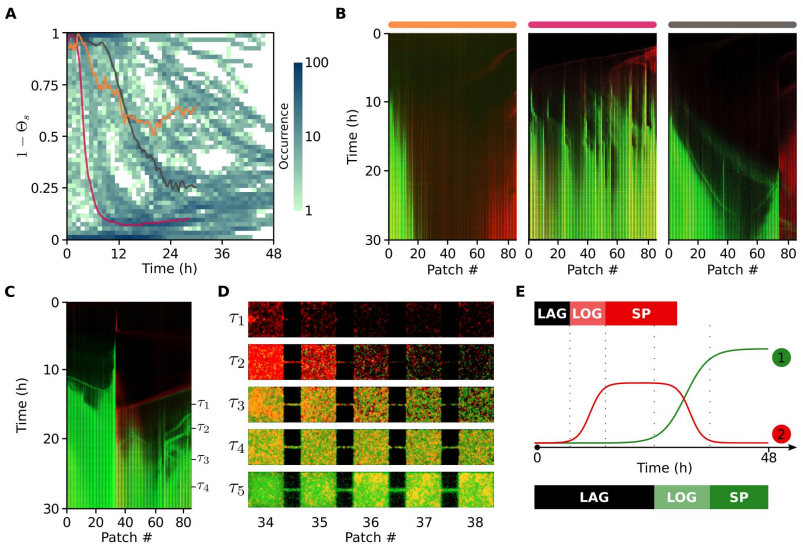

Figure 3.4: Succession, priority effects, and historical contingency A Metacommunity dynamics as binned (see text) fractional occupancy of *E. coli* averaged over all MHPs, $\bar{E}_s/(\bar{E}_s + \bar{P}_s)$, for each ($N = 72$) patchy landscape experiment, s, shown as a statistical ensemble. Color bar represent occurrences of configurations for each hour. **B** Three kymographs corresponding to three experiments s_1, s_2, s_3 represented as three color curves (orange, magenta, and grey) overlayed in A. **C** Kymograph showing colonization of a patchy landscape by *E. coli* from the right and *P. aeruginosa* from the left and right. Notice the wave of *P. aeruginosa* chasing a wave of *E. coli*. **D** Zoom-in into five MHPs belonging to the experiment shown in C, over five times steps τ_k **E** Ecological succession. A fast colonizer (red) with a shorter LAG phase is replaced by a superior competitor (green) with a longer LAG phase. After exiting LAG, both enter logarithmic (LOG) and later stationary (SP) phases of bacterial growth.

bottom, represents the frequency at which such long-term (t^*) pattern of local community structure was observed across all experiments in patchy landscapes. Here we show that, in the long-term, the most frequent (≈ 1000 occurrences) states observed fall within three classes: (i) fully occupied patches 100% dominated by *P. aeruginosa*, corresponding to the succession climax, and represented as the point $(0, 0.5)$; (ii) fully occupied patches 100% dominated by *E. coli* represented by the point $(1, 0.5)$; and (iii) extremely low density patches, 100% dominated by *E. coli* and represented by the point $(1, \epsilon \to 0)$. Intermediate levels of occurrence (≈ 100) corresponds to patches, with high levels of occupancy, $Z_{k_s} > 0.5$, which are mostly dominated by *P. aeruginosa* $(1 - \Theta_{k_s}) \leq 0.5$ or patches highly dominated by *E. coli* $(1 - \Theta_{k_s}) \to 1$ showing all levels of occupancy $0.5 > Z_{k_s} > \epsilon \to 0$. All other states are very rare showing less than ≈ 10 occurrences among 6120 sampled MHPs. These results reflect a clear long-term statistical pattern regardless of variability. To understand this pattern further, we look at the transient dynamics observed in our competition experiments.

In Figure 4A, for each landscape s we plot relative *E. coli* fractional occupancy averaged over the whole landscape, $\bar{E}_s/(\bar{E}_s+\bar{P}_s)$, in the vertical axis (binned as 48 intervals of length $2.0\bar{8}\cdot 10^{-2}$), as a function of time τ'_j binned as 48 intervals of one hour in the horizontal axis. Here, the spatial averages correspond to $\bar{E}_s = (1/85)\sum_{k_s} E_{k_S}$ and $\bar{P}_s = (1/85)\sum_{k_s} P_{k_s}$ for *E. coli* and *P. aeruginosa* respectively. Thus, for each binned time point τ'_j plotted, we have $72 \times 6 = 432$ landscape configurations, $(1-\Theta_s) = \bar{E}_s(\tau'_j)/[\bar{E}_s(\tau'_j)+\bar{P}_s(\tau'_j)]$, as we take images every 10 minutes (*i.e.* $\tau'_j = t_1^j, \cdots, t_6^j$). In total, we have $432 \cdot 48 = 20736$ configurations. The color map represents occurrences of spatially averaged *E. coli* fractional occupancy, $(1-\Theta_s)$, over all patchy landscapes over 48 hours (τ). The statistical pattern that emerges is that, early on during spatial competition ($\tau \leq 6$ hours), most occurrences (≈ 100) correspond to early colonization of the landscape by *E. coli*, $(1-\Theta_s) = 1$. The second level of occurrences (≈ 80) within this early period, correspond to the initial incursion of *P. aeruginosa* into the landscape and which is delayed respect to *E. coli* but which nevertheless later dominates $(1-\Theta_s) = 0$. Immediately after, in the follow up period ($6 < \tau \leq 12$), most occurrences still correspond to landscapes dominated by one or the other species. Mixed states occur rarely (< 10 cases) and most landscapes are either taken over by *P. aeruginosa* or recently colonized by *E. coli*. During this period, we see that the peak of occurrences (≈ 100) has shifted from most landscapes being dominated by *E. coli* to now being dominated by *P. aeruginosa*. If we consider how occurrences distribute over the plot, we can distinguish clear trajectories of competitive replacement where landscapes dominated by *E. coli* are taken over by *P. aeruginosa*. After 24 hours of competition, during the final phase of our competition experiments ($24 < \tau \leq 48$), most (65%) landscapes are dominated by *P. aeruginosa*. Notice that during this period, intermediate levels of landscape averaged fractional occupancy are also observed. The three color curves overlayed on top of Figure 4A correspond to three individual experiments shown as kymographs in Figure 4B. Such paths corresponds to three different scenarios of competition: *(i)* as in many experiments, a case (orange) where *E. coli* is capable of dominating the landscape in the long-term, $(1-\Theta_{s_1}) > 0.5$, due to fragmentation of the spatial distribution of *P. aeruginosa*; *(ii)* a *P. aeruginosa* dominated case (magenta) where *E. coli* is mostly excluded from the landscape in a quick fashion, only coexisting in low numbers, $(1-\Theta_{s_2}) \to 0$; and *(iii)* a case (grey) where, *E. coli* manages to persist at significant levels occupying $\approx 25\%$ of the landscape, $(1-\Theta_{s_3}) \to 0.25$. Although, *P. aeruginosa* always wins competition for individual patches due to its competitive

superiority when competing with localized *E. coli* sub-populations, delocalized waves of *E. coli* are always capable of outrunning their *P. aeruginosa* counterparts allowing persistence at the landscape level.

As in Figure 1E, we can integrate over all experiments (occurrences) shown in Figure 4A and define an ensemble average for fractional occupancy. Focusing on *P. aeruginosa*, this corresponds to $\Theta \equiv \langle \Theta_s \rangle = 1 - \langle \bar{E}_s/(\bar{E}_s + \bar{P}_s) \rangle$. Thus, after 48 hours of spatial competition, in almost 65% of experiments, *P. aeruginosa* dominates. In Figure 4C (and Figure S3B) we show a kymograph displaying a dramatic case of large-scale competitive dominance where it can be seen that competitive pressure by *P. aeruginosa* not only affects the dynamics of stationary (localized) populations of *E. coli*. Here, within times $12 < t < 18$ hours, a motile population wave of *P. aeruginosa* "chases" a wave of *E. coli* from the right most MHP of the landscape ($k = 85$), when at time τ_1 they are both trapped and become localized at patch $k = 34$. As the waves are trapped, we can see the materialization of the pattern of succession depicted in Figure 4D for a zoom in of this region of the MHP array at successive times τ_k. As in all experiments, what is reproduced here is the general pattern of *E. coli* colonizing first and *P. aeruginosa* colonizing second and out-competing *E. coli* locally and sometimes globally for space. Coexistence of alternative local community states can be observed even in adjacent patches as a consequence of the stochastic and history-dependent nature of patch dynamics on each individual experiment. In most of our experiments however, there is remarkable determinism, which emerges as the statistical pattern we can appreciate in Figure 4A if we only consider the temporal ordering of events of high occurrences (≈ 100). Thus, during the first 12 hours we see the development of an *E. coli* metapopulation composed of a superposition of motile wave sub-populations overlapping with localized sub-populations of variable density and spatial range. At ≈ 12 hours, *P. aeruginosa* expands through the landscape pushing localized sub-populations of *E. coli* to minority status in case of local coexistence, and away to other regions of the landscape in case of locally driving them to extinction. At multiple spatial and temporal scales we see the heuristic pattern of ecological succession depicted in Figure 4E.

3.2.5 *E. coli* aggregation in corridors enhances *P. aeruginosa* fragmentation and promotes coexistence

An important driving force for coexistence between these two species in patchy landscapes is due to habitat modification exhibited by the aggregating of *E. coli* cells primarily in corridors. Micro-colony formation in corridors can disconnect, or at least slow down, later arrivals from exploiting the resources available in patches further down the linear array. In this way these fragmentation events act as priority effects changing the course of metacommunity dynamics (Fig. 4A,B). In some instances it is a momentary delay in the expansion front of *P. aeruginosa*, while in other cases it offers *E. coli* significant extra time isolated from local competition. An example of this can be seen in the left most kymograph shown in Figure 4B where *E. coli* dominates ($(1-\Theta_{s_1}) > 0.5$). Clusters of micro-colonies aggregating in the corridors have a blockage effect shown in Figure 1B where competitive interaction is localized to the patch-corridor interface. In extreme cases this blockage turns into landscape fragmentation that is permanent and the superior competitor is unable to overcome this physical barrier in the 48hr period. When blockage is strong, the barrier is sometimes broken by *de novo* wave populations which can penetrate the competitors territory. This type of event can be seen in the right most kymograph shown in Figure 4B where a late arriving population wave of *P. aeruginosa* collides at time $t = 20.5$ hours with a localized *E. coli* sub-population aggregated at the corridor located between patches $k = 74$ and $k = 75$. This interaction can be appreciated in two zoomed views post-collision shown in Figure 5A,B. The motile population wave, consisting of swimming cells of the superior competitor coming from the left (shown in green), is first unable to penetrate the territory held by *E. coli* cells (in red) and reflects back to the LHS as well as diffracting (sensu [134]), giving rise to a *P. aeruginosa* sub-population localized at MHP number 74. Interestingly, it is from this localized sub-population that later *P. aeruginosa* periodically emits new waves as pulses of subsequently higher cell numbers which eventually manage to percolate through the colony barrier. Such wave invasions into hostile territory are reminiscent of *E. coli* invasions into landscape ecotopes with high concentration of antibiotics described elsewhere in the literature [142] and highlights the functional importance of these waves for bacterial strategies.

To test if the patchy structure of the landscape facilitated these priority effects, we ran control experiments in "flat" non-patchy landscapes (Fig. 1A, *bottom panel*) and compared to experiments

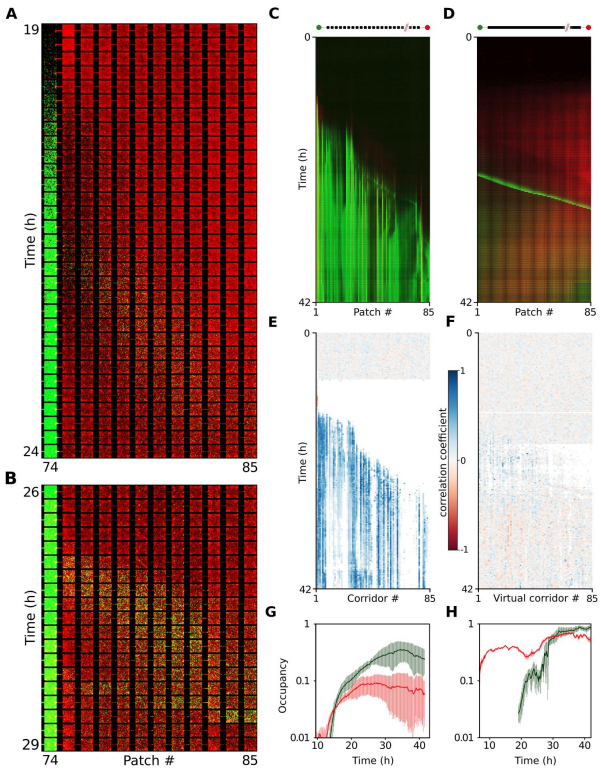

Figure 3.5: Ecological corridors: flat vs. patchy landscapes In **A** and **B**, two Zoom-ins into RHS (MHPs between 74 to 85) of the rightmost kymograph (s_3) shown in Fig. 4B for times between 19-24 (A) and between 26-29 (B) hours. **C** and **D** show Kymographs of the colonization of patchy (C) and flat (D) landscapes inoculated with *E. coli* (right) and *P. aeruginosa* (left) from the same initial cultures. **E** and **F** show the Pearson correlation coefficients between *E. coli* and *P. aeruginosa* calculated for patchy (E) landscape corridors and flat (F) landscapes virtual corridors (region of interest within the flat landscape taking the shape of corridors of patchy landscapes). **G** and **H** are semi-log plots of the average occupancy and its variance for *E. coli* (red) in patchy ($\langle \bar{E} \rangle_{\text{patchy}} \pm \sigma^2$; G) and flat ($\langle \bar{E} \rangle_{\text{flat}} \pm \sigma^2$; H) landscapes as well as for *P. aeruginosa* (green) observed in patchy ($\langle \bar{P} \rangle_{\text{patchy}} \pm \sigma^2$; G) and flat ($\langle \bar{P} \rangle_{\text{flat}} \pm \sigma^2$; H) landscapes.

ran in patchy ones (Fig. 1A, *top panel*) which were started from the same initial cultures ($n = 3$). To our surprise we also observed coexistence in the flat landscape despite the fact that *E. coli* micro-colonies are unable to fragment the superior competitor in these landscapes. Instead, coexistence is due to the emergence of a neutral ecology where species reach similarly high long-term ($t_\infty \gg 30$ hours) average occupancy, $\langle \bar{E}(t_\infty) \rangle_{\text{flat}} \approx \langle \bar{P}(t_\infty) \rangle_{\text{flat}}$, as shown here in Figure 5H. In contrast, in the patchy system, shown in Figure 5G, we see significantly different levels of long-term average occupancy $\langle \bar{E}(t_\infty) \rangle_{\text{patchy}} \ll \langle \bar{P}(t_\infty) \rangle_{\text{patchy}}$.

In Figure 5C we show 42 hours of an experiment where a *P. aeruginosa* expansion front slowly invades the patchy landscape from left to right displacing *E. coli*. In Figure 5D we show results for

inoculating a flat landscape with cells from the same ancestor cultures. In this case, contrary to what we observed in the patchy system, we consistently observed a fast traveling wave of *P. aeruginosa* (in green) which enters from the LHS and continues through the entire landscape before leaving on RHS (depicted in Fig. 5J) without diffracting nor leaving localized high density sub-populations behind as it is usually the case for *P. aeruginosa* dispersing in patchy landscape experiments (Fig. 5C; depicted in Fig. 2F). Instead, the passing wave leaves behind a homogeneous distribution of cells which after 36 hours show only minor long-term averaged occupancy differences $\Delta_{\text{flat}} \equiv \langle \bar{E}(t_\infty) \rangle_{\text{flat}} - \langle \bar{P}(t_\infty) \rangle_{\text{flat}}$ as can be appreciated by comparing Figures 5G,H. Contrary to patchy landscapes, which exhibit big difference in long-term averaged occupancy $\Delta_{\text{patchy}} \equiv \langle \bar{E}(t_\infty) \rangle_{\text{patchy}} - \langle \bar{P}(t_\infty) \rangle_{\text{patchy}}$, the flat landscapes have no intermediate patch scale and produces no separation between local population growth and landscape-scale range expansion. Computing Pearson correlations between local species occupancy in patchy and flat landscapes in competition experiments, we find that competitive hot spots (highly positive correlated regions) can be found in the corridors present in patchy landscape but not in the flat landscape as shown here in Figures 5E,F. In flat landscapes bacteria avoid each other as can be seen by the null value (in white) obtained for the coefficient of cross correlation. This spatial avoidance allows for a neutral ecology to emerge and Taylor's law [9], characteristic of patch dynamics, breaks down in flat landscapes (Fig. S4C,D). In patchy landscapes, although avoidance can be achieved within patches (Fig. S4A,B), it is not possible within corridors (Fig. 5E).

Although in patchy landscapes it usually takes *P. aeruginosa* 12 hours to enter the habitat (Fig. 5C,G), in flat landscapes this takes considerably longer; 20-24 hours (Fig. 5D,H). Notable difference is the variability in local occupancy integrated at 100×100 microns; this length scale corresponds to the scale of patchiness in the patchy landscape. Variability (standard deviation) in local long-term occupancy at this scale is considerably higher in the patchy landscape (Fig. 5G) compared to its flat counterpart (Fig. 5H). Additionally, aside from a temporary global dip in occupancy $\approx$ 24 hours, *E. coli* continues to grow in the flat landscape after the transient *P. aeruginosa* wave passes through (Fig. 5H). In fact, due to the large delay in *P. aeruginosa* entry, *E. coli* stabilizes at a higher population cell number than in patchy landscapes, however they seem more planktonic and less sessile. These "flat-habitat" populations exhibit different levels of aggregation and localization patterns than their patchy counterparts. This can be appreciated

when comparing micro-colony sizes in patchy versus flat landscapes were we observe that after 24 hour of growth, *P. aeruginosa* monocultures aggregate into mostly constant and small-sized ($< 20\mu m^2$) micro-colonies when growing in patchy landscapes while on the contrary, it aggregates into monotonically larger micro-colonies reaching sizes up to $100\mu m^2$ when growing in flat environments (Suppl. Fig. S4C,D). These observations suggest that releasing the spatial confinement of the landscape (corridors) alleviates the competition for space between sessile components of the life history and may lead to a more neutral ecology between these two species as they stay planktonic for longer. Patchy landscapes impose a characteristic length scale where co-localization of competitor populations predominantly takes place. Since we are interested in understanding coexistence in the heterogeneous soil matrix encountered by these species we further focus on the patchy habitat landscape.

The length scale $l = (a + b)$ of the patch-corridor motif (Fig. 1B), repeating every 150 μm (Fig. 2G), presents bacteria with the following dilemma: shall cells engage in exploration of the landscape, or rather focus on exploiting local opportunity. Cells naturally tend to form local populations and switch behaviour from one phase of growth to another, triggered by the topology of the local environment [138]. As the repetitive structure produces localization of populations, metapopulation development takes place [133] and the chances are increased for the bacteria to exhibit their competition-colonization strategy, which is characterized by a trade-off between abilities of populations rather than between cells. Next, to better understand the nature of succession in these metacommunity experiments we invoke a classical theory of ecology [42] in patchy landscapes.

3.2.6 Patch occupancy and the competition-colonization trade-off

The Competition-Colonization (CC) trade-off model [42, 43] has been proposed to explain the coexistence of species in a number of diverse ecosystems, from the intertidal zone to grasslands and coral reefs. This model suggests a simple but universal trade-off between competition and colonization for space to address the successional nature of such ecosystems and the limits of similarity in niche space between coexisting species. A large body of theoretical work has investigated this model often by focusing on the long-term outcome of this community with all species having the same exogenously driven local extinction rate (δ) and colonization rates (β) that are species specific [91].

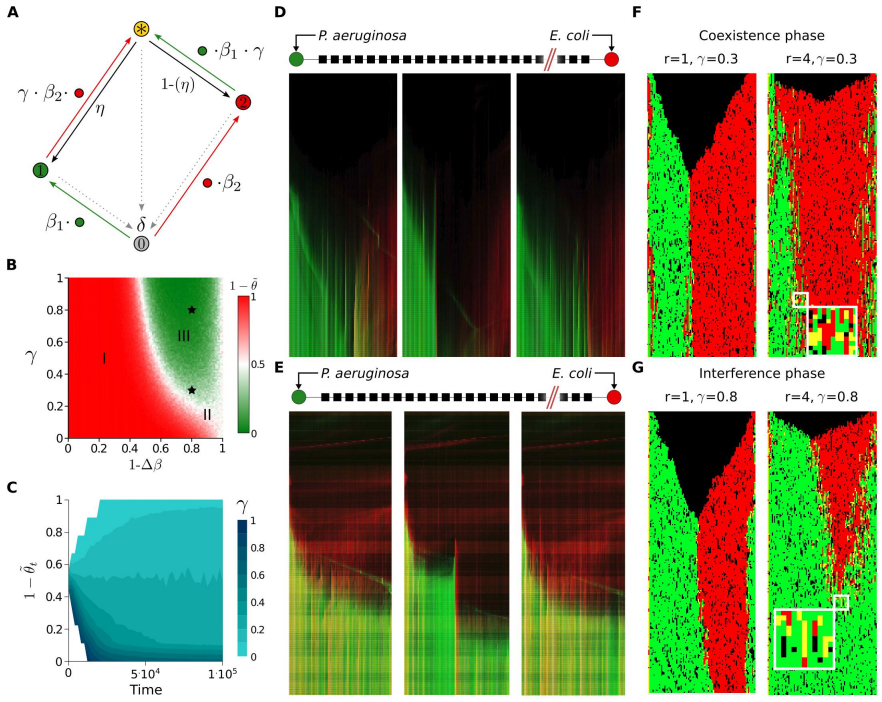

Figure 3.6: Insight from a spatial stochastic model *P. aeruginosa* dominance or coexistence with *E. coli*? **A** Schematic representation of the Markov chain describing the transitions of our spatial stochastic model; colonization rates are dependent on the state of neighboring sites. **B** Long-term behavior of our model in 2D and with nearest neighbor (n.n.) interaction ($r = 1$); We see three phases as a function of $(1 - \Delta\beta) \times \gamma$ space depicting differences in colonization $\Delta\beta$ and priority effects γ. Average colonizer fractional abundance $(1 - \tilde{\theta}) = \langle p_E \rangle / (\langle p_E \rangle + \langle p_P \rangle)$ is shown as red-to-green color map. Here $\Delta\beta = \beta_1 - \beta_2$, $\alpha = 4$, $\beta_1 \equiv 1$ and $\delta = 0.1$. **C** For a fixed value of colonization difference, $(1 - \Delta\beta) = 0.8$, metacommunity dynamics, $(1 - \tilde{\theta}_t) = \rho_E(t)/(\rho_E(t) + \rho_P(t))$, is shown for different values of priority effect parameter γ (cyan gradient bar) for the same other parameter values as in B. In **D E** we shown three kymographs from experiments where we observe regime of coexistancve (D) or dominance (E) behavior. In **F** and **G** We show 1D spatial transects of 2D simulations corresponding the exact same parameter values shown as stars in the phase space shown in B (n.n.; left panel) and for higher interaction range ($r = 4$; right). We see simulations in the (II) *coexistence* phase (F) for $\gamma = 0.3$ (F) and in the (III) *interference* phase for $\gamma = 0.8$ in G. These scenatior are both $(1 - \Delta\beta) = 0.8$.

In the strict hierarchical form of the CC model, two species are ranked $i = 1, 2$ according to their competitive abilities, which are opposite to their colonization rates, $\beta_1 < \beta_2$, such that locally the superior competitor (type 1) always out-competes the inferior (type 2) in every site. If we track site occupancy p_i we have

$$\frac{\dot{p_1}}{p_1} = \beta_1(1 - p_1) - \delta \tag{3.2}$$

$$\frac{\dot{p_2}}{p_2} = \beta_2(1 - p_1 - p_2) - \delta - \beta_1 p_1, \tag{3.3}$$

to represent such a system in a Mean Field (MF) approximation (See Table S8). In this stricked MF scenario, interference competition within sites happens infinitely fast, such that the superior competitor 'senses' a completely vacant habitat as shown by Equation 3.2. The inferior competitor on the other hand, feels as living in a dynamic landscape imposed by the superior competitor. The necessary and sufficient conditions for existence/coexistence between these two follows;

$$\Delta = \beta_1 - \delta > 0 \tag{3.4}$$

$$\Delta\beta = \beta_2 - \beta_1 > (\delta + \Delta)\frac{\Delta}{\delta}. \tag{3.5}$$

The superior competitor must colonize at a faster rate than exogenously driven to extinction ($\beta_1 > \delta$) so here Equation 3.4 is simply the condition for metapopulation persistence [20]. The inequality in Equation 3.5 tells us the value $\Delta\beta = \beta_2 - \beta_1$, exactly how much faster the colonizer must be to invade a landscape where the superior competitor is at equilibrium occupancy; this introduces a limit to similarity in aspect (niche) space [44]. This states that there exists a region in colonization space (β) where a faster colonizer but inferior competitor cannot exist. This "competitive shadow" [44], puts a limit on similarity between species and gives us the criteria for species to invade. For inferior competitors to persist they must out-colonize their superior at a rate greater than or equal to the length of the shadow (Fig. S5A).

Extensions to this theory have aimed to address some of the more unrealistic aspects of the CC model while still maintaining its generality, notably *i*) the deterministic nature of the strict competitive hierarchy and *ii*) the equivalency of colonizing vacant versus occupied patches. Calcagno and collaborators [143] addressed both of these issues and considered first, relaxing the strictly

deterministic competitive hierarchy, which by itself has been shown to make coexistence unlikely [144]. They introduced a form of priority effect ($\gamma \in [0, 1]$), such that the prior arrival of a species to a patch would affect future colonization events by competitors. As we saw before in Section 3.2.1, a competitive index ω can be defined to depend on colonization differences $\Delta\beta$ between the life history strategies of our two bacterial species (Eq. 3.1). Such competition-colonization trade-off is plotted in Figure 1D and can be linked to community dynamics as follows: After patches enter a short lived state of co-occupancy, they can be won back by a competitive lottery parameter

$$\eta_{i,j} = \frac{\omega_i}{\omega_i + \omega_j} = \frac{e^{-\alpha \cdot \beta_i}}{e^{-\alpha \cdot \beta_i} + e^{-\alpha \cdot \beta_j}} \tag{3.6}$$

which determines mean field meta-community dynamics as a balance between scramble and interference competition,

$$\frac{\dot{p_i}}{p_i} = \underbrace{\beta_i \left(1 - \sum_{i \neq 0} p_i\right) - \delta}_{\text{scramble}} + \underbrace{\gamma \sum_{j \neq i \neq 0} \left(\beta_i \eta_{i,j} - \beta_j \eta_{j,i}\right) p_j}_{\text{interference}} . \tag{3.7}$$

Unlike in the CC model with strict competitive hierarchy (Eqs. 3.2-3.3) where competition is instantaneous (Fig. S5B); in the model of Calcagno and collaborators [143], defined by Equation 3.7, resident species are not immediately overwhelmed by a superior competitor (Fig. S5C). Instead, they can invade an occupied site with some probability γ while the resident is still present, after which a biased competitive lottery representing interference competition ruled by competitive parameter $\eta_{i,j}$ (Eq. 3.6) determines whether the resident or invader succeeds in claiming the site. For two species, we simply have $\eta_{1,2} = 1 - \eta_{2,1} \equiv \eta$. From Equation 3.6 we can relate such competition bias, η, to differences in colonization ability, $\Delta\beta$ between our bacterial species using the CC trade-off relationship (Eqn 3.1) for a given strength α (Fig. S5D); if there are no differences ($\Delta\beta = 0$) then competitive ability $\eta = 0.5$ regardless of α value. A strength value of $\alpha = 0$ implies that η is the same regardless of differences in colonization, while a value $\alpha = \infty$ on the other hand implies an absolute competitive hierarchy (*sensu* [43]). An intermediate value of $\alpha = 4$ means that a superior (type 1) competitor which has 80% of colonization ability of its fugitive (type 2) counterpart ($\Delta\beta = 0.2$), has around 70% more chances of winning the competitive lotery; $\eta(0.2) \approx 0.7$. These qualities of a

system like Equation 3.7 reflect our experimental observations, where often a MHP, first colonized by *E. coli*, is eventually invaded by *P. aeruginosa* and often, but not always taken over by the later. However, spatially explicit interactions are missing from this picture based on differential equations. Inspired by these theoretical developments [143] as well as our empirical observations described in previous sections, we developed a spatially-explicit stochastic (toy) model [16] based on Interacting Particle Systems (IPS). We incorporate a localized mixed state where both species can occupy a common site at the same time with the condition they are locked into an interference competition program. While locked on this localized state, no dispersal takes place, only the competitive lottery. Such a mixed state, not present in spatially-implicit model of Equation 3.7, is something we often see in our experimental observations.

We consider a spatially explicit stochastic process $\xi_t : \mathcal{L} \to \mathcal{S}$, mapping sites on a discrete lattice $\mathcal{L}$ to the set of states $\mathcal{S} = \{0, 1, 2, *\}$ representing the local community states: vacant site (state 0), site occupied by superior competitor (state 1), fast colonizer (state 2) or both (mixed state $*$). Lattice reactions are sketched as a Markov chain in Figure 6A and correspond to: (i) a disturbance regime/clearance rate where all occupied sites, $\{1, 2, *\}$, turn vacant at rate $\delta \equiv 0.1$; (ii) a difference $\Delta\beta$ in the colonization ability between fast $\beta_2 \equiv 1$ and slow $\beta_1 = 1 - \Delta\beta$ (dispersal) strategies; (iii) a competition bias $\eta = (1 + e^{\alpha \cdot \Delta\beta})^{-1}$ in favor of the superior competitor controlled by parameter α modulating the trade-off; and (iv) a priority effect parameter γ controlling the existence of the mix state. Interactions occur in a neighborhood $\Omega(x, r)$ of radius r around a focal site $x \in \mathcal{L}$ in a lattice of sites which can be arranged in one or two dimensions. We varied the strength of the CC trade-off (α; Fig. S5E-G), as well as the range of interactions r and lattice dimensions (Fig. S6A-H) to test the robustness of our simulations (for model details see Sec. 3.4.6). We performed numerical studies of our model and explored the parameter space $[(1 - \Delta\beta) \times \gamma]$ representing competitor's (type 1) colonization ability $(1 - \Delta\beta)$ and different levels of priority effects γ. Guided by the experimental focus of this work, we kept initial conditions always the same to mimic our experiments' initial configuration at inoculation; each type starting from clusters separated at different inoculation points. (see Sec.4.4.2).

In Figure 6B we show our model's long-term behavior (phase space), for a 2D lattice, with nearest neighbor (n.n.; $r = 1$) interactions. We recognize three metacommunity phases when looking at the distribution of *P. aeruginosa* fractional occupancy ()$overparameterspace$[(1-$\Delta\beta$) $\times$ γ]: (I) a

scramble phase (red), where only the fast colonizer survives; (II) a *coexistence* phase (white), where both strategies persist; and (III) an *interference* phase (green), where the superior competitor wins. The stars we overlay on top correspond to two simulation scenarios shown on the left panels of Figure 6F,G. Here we show the same parameter values as in B,C with n.n. interactions ($r = 1$) as well as a slightly larger interaction range ($r = 4$; Fig. 6F,G *right panels*). Notice that the larger the interaction range, the more prevalence of mixed state $*$ is observed. In Figure 6D,E three microfluidics experiments in patchy landscapes are shown to exemplify patterns similar to the phases ($\tilde{\theta}$) of our 2D model; *coexistence* phase (Fig. 6D) as well as *interference* phase (Fig. 6E). Fixing the value representing colonization differences, $(1 - \Delta\beta) = 0.8$, we can think of individual experiments with bacteria as different values of γ representing priority effects which vary stochastically. Although this is not accounted for explicitly in our model, it nevertheless provides a useful framework. Using a value $\alpha = 4$ with a 20% difference ($\Delta\beta_0 = 0.2$) in dispersal ability (70% chances of loosing interference competition; $\eta(0.2) = 0.698$); in Figure 6C we show the average dynamics of the colonizer fractional occupancy $(1 - \tilde{\theta})$, for different scenarios of priority effects (γ). Notice the importance of parameter γ in determining trajectories of competitive replacement as well as long-term patterns of species dominance (phases). For a 20% decrease in cross-colonization rate due to priority effects ($\gamma = 0.8$), we obtain a scenario within the *interference phase* and the competitor pushes the colonizer off the landscape as shown in Figure 6E,G. Decreasing the value of parameter γ, reducing the cross-colonization rate of occupied sites, we obtain another ecological scenario we observed in experiments. Namely, when *E. coli* persists due to the blockage of patch-corridor interfaces which delays and fragments the colonization by *P. aeruginosa*. Such scenario occurs for parameter $\gamma = 0.3$ for which simulations lay within the *coexistence phase* as is shown in Figure 6D,F. Here we show such a simulation next to three kymographs of experiments where the landscape is shared between both species.

In one dimensional lattices, there is no coexistence regardless of the range of interactions or their localization (Fig. S5E-G). In two dimensions, global interactions cause the *coexistence phase* to shrink significantly when compared to short range counterparts (Fig. S6). Another important difference is when comparing a spatial construction based on Equation 3.7 with no mix state with our full model with mix state. The mix state allows for the separation of scramble and interference interactions. A consequence of this separation is that the mix state sequesters occupied sites from

participating in the purely spatial process (scramble competition). This has a habitat destruction/fragmentation effect which causes the superior competitor to reach its extinction threshold as $\gamma \to 0$. For a fixed value of $\gamma = 1$, no priority effects, we distinguish two critical values $\Delta\beta_c^*$ and $\Delta\beta_c^{**}$ delimiting the three phases at the top of the figure. If the difference in colonization ability is large, $1 > \Delta\beta > \Delta\beta_c^*$, we are in the *scramble* phase (red) and only the colonizer dominates; If the difference is of intermediate magnitude, $\Delta\beta_c^* > \Delta\beta > \Delta\beta_c^{**}$, we are in the *coexistence* phase; and if small differences are considered, $\Delta\beta_c^{**} > \Delta\beta \geq 0$, we are in the the interference phase (green). When no differences exist, $\Delta\beta = 0$, the system is in a *neutral* phase (white) as the lottery has no bias ($\eta = 0.5$), regardless of the strength of the trade-off (α). This neutral case $\Delta\beta = 0$ allows us to appreciate the role of γ which induces fragmentation in the spatial colonization process and leads to an extinction threshold at γ_c. We scan along a fixed transect $(1 - \Delta\beta_0) = 0.8$ across phase space by varying parameter γ from no priority effects ($\gamma = 1$) to full cross colonization inhibition ($\gamma = 0$). Along this transect we cross two transitions between phases: (i) a boundary between *interference* and *coexistence* and (ii) a boundary between *coexistence* and *scramble*. Thus, at intermediate values of priority effects we can expect coexistence for a pair of strategies with a small difference in colonization, $0 < \Delta\beta_0 < 0.3$. The sequestration from the colonization process, produced by localization of the interference interaction, has a critical role in modulating coexistence in our model. This result is congruent with our experimental finding that *E. coli* coexist with *P. aeruginosa* by a localization and fragmentation mechanism (priority effects).

3.3 Discussion

Performing biophysical experiments with spatially explicit meta-communities of bacteria *on-chip*, we have shown that *E. coli* is a fast colonizer but poor competitor while *P. aeruginosa* is a slow colonizer but superior competitor enacting a competition-colonization trade-off scenario when competing in patchy environments. This result constitutes empirical evidence highlighting the relevance of an otherwise abstract ecological theory to microbiologists at large. Moreover, we further developed ecological theory and used it to understand the empirical patterns observed.

In well-mixed monocultures (Fig. 1C), strains of *E. coli* show an approximate 3 hour lag phase while strains of *P. aeruginosa* start growing after approximately 6 hours but reach a considerably

higher (optical) density. The spatial behavior of these strains in monoculture experiments in patchy landscapes (Fig. 2) show that *P. aeruginosa* exhibits slower population waves as well as a larger spatial lag phase. Behavior of these monoculture metapopulations is consistent with the claim, supported by our competition experiments (Fig. 1E-H), that these two species of bacteria are related to one another by a competition-colonization trade-off (Fig. 1D) modulated by the structure of the habitat (Fig. 5 and Fig. S4).

In patchy environments (Fig. 1A, *top panel*), dispersal strategies play a crucial role structuring ecological communities. A bacterial life-history resonates with such periodic structure [138, 139] and selects patterns of localization which reflect a balance between exploiting local patches by entering stationary phase programs or exploring the landscape searching for new colonization opportunities. In flat habitats (Fig. 1A, *bottom panel*) of approximately equivalent volume but which do not have such repetition pattern separating the habitat into patches and corridors, a neutral ecology emerges (Fig.5H). Our *on-chip* microbial metacommunities are not only composed by sub-populations which are localized but also made of non-localized sub-populations corresponding to traveling waves. Such population waves generate dispersal structures which only makes ecological sense when colonizing patches. It is for this reason we see ecological succession clearly take place at the scale of patches (Figs. 3B,4D), while at the landscape level colonization-extinction and fugitive dynamics dominates (Fig.3D). Our flat habitats which offers no corridor-to-patch transitions not only induce a different ecology (competition-colonization versus neutral) but also give rise to a different pattern of micro-colony structure in monocultures (Fig. S4E,F). Together, these two habitat types (Fig. 1A) allowed us to study the roles patchiness plays in structuring an ecological community made of two species of bacteria. It is the enhanced importance of colonization-extinction dynamics in the patchy landscape (Fig. 5G; Suppl. Fig. S4C) which allows for a textbook example of ecological succession to be exhibited by these species of bacteria. Although each individual experiment in patchy landscapes deviated from the heuristic pattern depicted in Figure 4E in a multi-scale stochastic fashion, an ensemble average can be constructed for community dynamics (Figs. 1E,4A) as well as long-term community structure (Fig. 3E).

An observed mechanism for coexistence in patchy landscapes is habitat fragmentation by strong blockage of patch-corridor interfaces (Figs. 1B; 3B; and 5A,B). In general, this is responsible for holding back *P. aeruginosa* invasions which in some cases can become ultimately fragmented from

entire regions of the landscape. From the perspective of ecological succession however, coexistence is a transient state as waiting for long-enough time, waves of the superior competitor will break through (Fig.5A,B). Corridors are landscape ecotopes where strong interactions between *P. aeruginosa* and *E. coli* take place (Fig. 5E). By delaying *P. aeruginosa*'s arrival, *E. coli* increases its window of opportunity for local development. In the end, as any fugitive species, *E. coli* wave populations disperse away from competitors and recruit cells from its localized subpopulations in the process. The longer time *E. coli* has free of competition, the more it increases its chances against *P. aeruginosa* and sometimes, due to priority effects, can even come to dominate (Fig. 4A,B).

In flat landscapes we consistently observe that *P. aeruginosa* enters the habitat as a fast population wave shown in Figure 5D and sketched in Figure 5J. Notice, this is in contrast to what we observe in the patchy habitat (Fig. 5C); where *P. aeruginosa* enters as a slower metapopulation front depicted in in Figure 2G. Patchiness modulates the metapopulation phenotype by causing population waves to diffract as they travel the landscape encountering different barriers to their propagation (Figs. 2F, 5K). *E. coli* disperses via α and β waves [134] in patchy landscapes (Fig. 2A,B), penetrates the flat landscapes in even faster waves that we can barely capture in timelapses (Fig. 5C,D). From a biophysical point of view, the repetitive motif of patches and corridors (Fig. 1B) makes our model habitats resemble to a periodic potential like the one shown in Figure 2G. Such potentials, introduced by Kronig and Penney [46] to calculate wave functions of electrons in crystals, may be useful to understand the behavior of invasion waves corresponding to non-localized populations of bacteria traveling throughout our patchy habitats. This interpretation can help us understand the role played by characteristic length scales present in the habitat in structuring ecological communities [18] dominated by invading wave populations. An interesting consequence of such interpretation is the possibility of Anderson localization mechanism [145]. Anderson localization is a wave phenomenon, where randomness/disorder over a periodic potential leads to localized wave functions (of electrons). The lack of disorder otherwise leads to a diffusion of the wave function. A similar mechanism could structure the spatial distribution of wave populations. As species modulate each other's landscape, *E. coli* cells can modulate the potential seen by *P. aeruginosa*'s waves introducing randomness to the value of the potential barrier height via niche construction occurring in corridors. In this way *E. coli* can induce strong localization in the spatial distribution of *P. aeruginosa*'s metapopulation. In patchy landscapes, occupancy clusters in a band-gap fashion

characterized by zones of high cell density (bands) separated by zones (gaps) of low density (Fig. S3). Stronger localization benefits fugitive *E. coli* as larger clusters of vacancy are available for colonization within gaps in the distribution of *P. aeruginosa*. This further highlights the importance corridor interactions have in determining landscape-wide patterns of community structure as "band-like" occupancy distributions are ubiquitous in our experiments.

Guided by our results from competition experiments (Sections 3.2.3–3.2.5), we extended the CC model of Calcagno and collaborators [143], Equation 3.7, to consider the spatial structure of scramble and interference competition dynamics explicitly. Moreover, we considered interference competition acting separately from scramble competition. While alternative theoretical frameworks could be justified [115], one thing is certain; precise details of the spatial structure in our *on-chip* habitat landscapes determines the scale at which ecological dynamics are most prominently on display. This is clear as we observed strikingly different outcomes when comparing between flat and patchy landscapes (see Sec. 3.2.5).

By varying the spatial structure of our habitat landscape and starting with identical inoculated populations we were able to replay the community assembly process in experimental conditions which corresponded to different coordinates along the niche-neutral continuum of the competition colonization framework. For our patchy landscape, this allowed us to focus on the competition and colonization dynamics of individual patches rather than just single cells or the entire meta-community. The stochastic spatial model presented here (Secs. 3.2.6 and 3.4.6) provided us with the right level of biological abstraction and attention to spatial structure to lend insight to our experimental observations. Specifically, the spatially explicit nature of priority effects in our model make it possible to qualitatively understand the large-scale space-time dynamics of our experiments (Fig. 6).

Results from numerical simulations of our model (in 2D, with n.n. interactions) show that the *scramble* phase (red in Fig. 6B) stretches further (see also Fig. S5C) than we anticipated. Furthermore, we see a qualitative change in the trade-off mediated *coexistence* phase such that a nearly neutral (avoidance) ecology ($\Delta\beta \to 0$) also permits coexistence regardless of priority effects ($\forall\gamma$). Particularly relevant for the interpretation of our experiments, is that we also find coexistence for strong priority effects ($\gamma \to 0$) and small differences in colonization ($0.4 > \Delta\beta > \epsilon \to 0$). This cannot be obtained simply by lifting Equation 3.7 to become a spatial stochastic

process (Sec. 3.4.6), therefore, localization of co-occupancy (mix state $*$) is a necessary condition (Fig. S6). The localization of competitive interference interactions, where priority effects (γ) slow down patch expansion of the superior competitor and in the extreme case freeze it entirely. For slow colonizer/strong competitor strategies, far to the left of fecundity space ($1 - \Delta\beta$), the risk of becoming fragmented from vacant patches is important. Limited to a small region of the landscape, due to rapid expansion by the faster colonizer, strong competitors are then destined to go extinct. In our model, competitive advantage comes at a topological price as the mix state cannot propagate to adjacent vacancy. By varying spatial structure experimentally we could manipulate the location along the trade-off manifold in which community assembly occurred. Despite features of the model framework which are confirmed by our experiments, our spatial competition results suggest fundamental aspects such as wave mechanics are missing and need to be developed in our theory to better link up to our experiments. One clear insight of both our model and interpretation based on potentials is the importance of priority effects which determine patterns of competitor co-localization.

Conclusion

The competition-colonization trade-off is not dead! Using micofabricated habitats *on-chip*, we have shown that indeed when habitats are patchy there is a competition colonization trade-off structuring a bacterial metacommunity. In this context *E. coli*, a fugitive species, is a fast colonizer which locally loses competition to superior competitor *P.aeruginosa*. Priority effects enhanced by *E. coli* niche construction in corridors can modulate the pattern of localization of *P.aeruginosa* limiting its dispersal. We understand such modulation as occurring by the Anderson localization [145] mechanism. As *P.aeruginosa* strongly localizes, it releases space (larger gaps and longer delays) for *E.coli*'s utilization.

3.4 Methods

3.4.1 Strains and growth conditions

Experiments were performed using strains of *E. coli* (JEK1036 and JEK1037) and *P. aeruginosa* (PUPa3-G and PUPa3-R) labeled with Green and Red Fluorescent Proteins (GFP and RFP). Strain details are listed in Table S1. For both species, strains are isogenic except for fluorescence labeling. It is clear from Figure 1C that red and green strains for both *E. coli* and *P. aeruginosa* show similar growth pattern, while the different bacterial species evidently display distinctive behavior.

Single colonies for both *E.coli* and *P.aeruginosa* were grown from $-80°$C glycerol stocks on solid LB agar plates (LB Broth EZMix, Sigma-Aldrich + 1.5% Bacto Agar, MOLAR Chemicals) and subsequently inoculated in 3 ml Lysogeny Broth medium (LB Broth EZMix, Sigma-Aldrich) for 16h$\pm$30min (O/N) at 30°C, 200rpm. For *P. aeruginosa*, 50μM of Ampicilin (Amp) and Gentamicin (Gm) was added. Overnight cultures of *E. coli* (*P. aeruginosa*) were back-diluted 1:1000 (1:500) in 3ml LB medium with 1mM IPTG (50μg/mL Amp and Gm) and grown to an optical density at 600nm (OD_{600}) of 0.3. Cultures were then centrifuged at 350G for 10 minutes, after which the supernatant was removed and cells were resuspended in LB medium containing 1mM IPTG. PUPa3-R and PUPa3-G maintain their plasmids over the course of the experiment (48h) in absence of antibiotics Amp and Gm in the growth media. Stability of the plasmid was confirmed by comparing cell number in bright field and fluorescence images over a period of 3 days (results not shown).

3.4.2 Well-plate Assays

Cultures of JEK1037/36 and PUPa3-G/R were grown overnight until stationary phase and back-diluted 1:1000. Once back-diluted and cultures had reached an $OD_{600} = 0.3$ they were again back-diluted 1:100 into a 96 well-plate well reaching a final volume of 100μL. Monoculture growth patterns were evaluated in 96 well-plates using fresh LB. Plates were incubated in a Synergy two microplate reader at 30°C and, in-between periods of shaking, OD_{600} measurements were acquired every 10 minutes for a total of 48 hours. A total of 6 replicates were used for each of the 4 strains shown in figure 1C.

3.4.3 Well-mixed competition experiments

Cultures of JEK1037 and PUPa3-G were grown overnight until stationary phase and back-diluted 1:10000 in 25mL of fresh LB and 1mM IPTG grown in 150mL Erlenmeyer flasks resulting in a 1:1 initial cell density *E. coli*:*P. aeruginosa*. Asymmetric initial conditions (10:1 and 1:10) were also tested on the same day. Each experimental set-up was performed with 3 replicates. Flasks were placed in a shaking incubator set at 30°C and 100rpm for a total of 48 hours. Optical density measurements (OD_{600}) were taken every 12 hours in parallel with cell counting measurements. For cell counting measurements, 1mL sample cultures were diluted to $OD_{600} = 0.4$. From this, 1μl droplets were placed on 1.1mm thick agar pads (freshly made before every measurement). Droplets were allowed 5 minutes to absorb to agar pads before placing a cover-slip on top, this ensured an even distribution of cells in a symmetric, circular Region Of Interest (ROI). Images were acquired in the center of this ROI using a 40X Nikon Plan Fluor objective giving a field of view of $(413 \times 348.4)\mu m^2$ (See Sec. 4.4.3 for the full microscopy configuration). Using ImageJ [146] we counted the average number of *E. coli* ($\bar{N}_E$) and *P. aeruginosa* ($\bar{N}_P$) cells in the ROI. The relative fractional abundance of *E. coli* in well-mixed communities (θ), plotted in Figure 1F-H, was calculated as $\bar{N}_E/(\bar{N}_E + \bar{N}_P) \equiv \theta$.

3.4.4 Microfluidic device fabrication and preparation

Microfabricated devices used in this study consist of two inlet holes (1.2mm) on opposite sites with 3 parallel landscapes, each with arrays of 85 habitat patches ($100 \times 100 \times 5\mu m^3$) connected by corridors ($50 \times 5 \times 5\mu m^3$) or one long quasi-2D environment ($12750 \times 100 \times 5\mu m^3$). These devices are depicted in Figure 1A and shown using Scanning Electron Microscopy (SEM) in Figure S2. Devices were fabricated using soft lithography techniques [136]: A silicon wafer was coated with a thin film (5μm, height of the device) of the negative photoresist SU-8 (SU-8 2005, MicroChem) and the design of the device was written into the resist with a laser pattern generator (μPG 101, Heidelberg Instruments) to fabricate a master mold on which Polydimethylsiloxane (10:1 PDMS:curing agent, Sylgard 184, Dow Corning) was deposited to yield an elastomeric stamp that was covalently bonded to a glass cover slip by oxygen plasma activation (29.6 W, 400mTorr, 45 sec; PDC-002, Harrick Plasma) of both the PDMS and glass parts.

Microfluidic experiments

For each run of a device (with 3 habitat landscapes each), either the red PUPa3-R or green PUPa3-G strain of *P. aeruginosa* is used with the green JEK1036 or red JEK1037 *E. coli* strain, respectively. This way experiments are done with a green-red or red-green pair of *P. aeruginosa* and *E. coli*.

Prior to inoculation, the devices were wettened with LB + 1mM IPTG. Then, 1μl culture of *P. aeruginosa* (red/green) and *E. coli* (green/red, respectively) was pipetted into the inlet holes on opposite ends of the device. Once both sides were inoculated, the device was sealed with fast curing PDMS (Kwik-Sil Silicone Elastomer, World Precision Instruments). A water tight wall is made around the perimeter of the sealed device on the glass slide using four 24 $\times$ 60mm coverslips which were previously 'painted' up-right onto the glass-slide using fast curing PDMS. The sealed device was then submerged in Milli-Q water for the remainder of the experiment to prevent the device from drying out. During the 48hr time-lapse microscopy experiment, the microscope set-up was equipped with an incubator enclosure (Okolab) by which temperature is controlled at 30°C during the image acquisition of the device.

3.4.5 Image acquisition and data analysis

Devices were imaged at 10 minute intervals using a Nikon Eclipse Ti-E microscope equipped with 10X Nikon Plan Fluor objective, GFP and mcherry fluorescence filter sets (49002 49008, Chroma Inc.), Andor Neo sCMOS camera (Andor Technology plc.), LUMEN 200 Pro metal arc lamp (Prior Scientific Ltd.) and a Prior Proscan II motorized stage (Prior Scientific Ltd.) was used for scanning. The NIS Elements Ar software (Nikon Inc.) was used for image acquisition and data processing and image analysis was carried out using ImageJ and Python. Fluorescence intensity is a poor estimation for biomass due to differences in expression among cells. To avoid this problem we use a custom script in ImageJ to convert all images to occupancy data for each of the two strains used in an experiment.

Local occupancy within patches (MHPs)

After background correction is performed on each image a threshold pixel value is calculated based off the corresponding auto-fluorescence for each of the color channels used (red and green). This is performed at every time point for each channel (strain). When the value is above this threshold, the pixel ($0.803\mu m^2$) is considered occupied by that strain (value of 1), otherwise it is vacant (value of 0). Using the ROImanager in ImageJ [146], a custom mask was fitted at each patch for each experiment allowing us to consider occupancy values at the patch level for each strain. *E. coli* occupancy for a MHP indexed by k is denoted as E_k and *P. aeruginosa* is written as P_k. Notice that occupancy is normalized per channel, thus $0 \leq E_k \leq 1$ and $0 \leq P_k \leq 1$. With these measurements per MHP $\{P_k, E_k\}$; we calculated total MHP occupancy $Z_k = P_k + E_k$ and fractional occupancy of *P. aeruginosa* $\Theta_k = P_k/(E_k + P_k)$ and *E. coli* $(1 - \Theta_k) = E_k/(E_k + P_k)$. We characterized a local MHP community at location k at time t as $\{\Theta_k, Z_k\}$ or $\{(1 - \Theta_k), Z_k\}$ depending if focus is on *P. aeruginosa* or *E. coli* respectively.

Notice, while experiments are carried out with both green-red and red-green pairs of *P. aeruginosa* and *E. coli*, all figures, with exception of supplementary material Figures S9 and S10, (which correspond to a catalog for our experiments), if colored, images are colored green for *P. aeruginosa* and red for *E. coli*. This is done to facilitate easy interpretation of the results and comparison to the model presented.

3.4.6 Stochastic Spatial Model

We consider a spatial stochastic process $\xi_t : \mathcal{L} \to \mathcal{S} = \{0, 1, 2, *\}$ [16]. Thus, a lattice site $x \in \mathcal{L}$ at time t is in state $\xi_t(x) = s_x \in \mathcal{S}$. These states are vacancy $\{0\}$, occupancy $\{1,\ 2\}$, and localized co-occupancy $\{*\}$. Our model is ruled by reactions which take place only if lattice sites are adjacent. Such adjacency dependence in our model is controlled by a radius r for which the interaction neighborhood $\Omega(x, r)$ is defined. Thus, interactions take place only if the site y representing the source of propagules is in the vecinity $\Omega(x, r)$ of the focal site x being colonized, $\mid x - y \mid \leq r; \forall x, y \in \mathcal{L}$. Reactions are shown in Figure 6B and are the following. Particle extinction $s_x \to 0_x$, affecting occupied sites ($s_x \neq 0$), occurs at a rate δ which does not depend on the state of near-by sites. When we say that an event (local extinction) occurs at rate δ, we mean that

the times τ_i between successive occurrences (lifespan of the occupied states) have an exponential distribution with parameter δ; that is, $\mathcal{P}(\tau_i \leq t) = 1 - \exp(-\delta t)$. Colonization reactions, all depend on the state of near-by sites as they are the sources of colonization propagules. We assume that only states 1 and 2 can spread the process in space by wave emission. The mixed state $*$, is assumed to be localized and with no emissions so it cannot infect near-by sites. This co-occupancy state represents co-localized populations of competitors engaged only in interference competition. To access this state depends on near-by occupancy however, as cross colonization is needed. This cross colonization depends on priority effect γ and adjacency of propagule sources. Vacant sites (0_x) can be colonized, $0_x + s_y \rightarrow s_x + s_y$, at rate β_{s_y}/z by propagules coming from near-by sites in state $s_y \in \{1, 2\}$ where z is the number of neighboring sites. Here z is the number of neighbors to x within $\Omega(x, r)$. Sites occupied by type i can be cross-colonized by type $j \neq i$ by reaction, $i_x + j_y \rightarrow *_x + j_y$ or $j_x + i_y \rightarrow *_x + i_y$ occurring at rate $\gamma \cdot \beta_{s_y}/z$ for $s_y \in \{1, 2\}$ (priority effects). When a site is co-occupied, the local community is localized and its members cannot spread to near-by sites. State * decays to each of the (not localized) types (state 1 or 2) by a reaction representing the competitive lottery $*_x \rightarrow s_x \in \{1, 2\}$ occuring at rate η for type 1 and at rate $(1 - \eta)$ for type 2 and which is determined by Equation 3.6. We also considered a spatial version of Equation 3.7 by ignoring the mix state $*$, and consider a restricted set of states $\mathcal{S} = \{0, 1, 2\}$. We define a spatially explicit version of Equation 3.7 by implementing the transitions shown in Figure S5C as lattice reactions of an IPS. We also studied such construct (Fig. S6E-H) along our full, $\mathcal{S} = \{0, 1, 2, *\}$, model including the mix state (Fig. 6A) for different strength α, interaction range r and lattice dimensions (Figs. S5,S6).

Numerical Simulations

The C programming language was used to implement simulations of the stochastic spatial model using the Mersenne Twister algorithm [147] for pseudo random number generation. For plotting the spatio-temporal patterns of individual simulations in Figure 6F,G we used the GTK+ library. In order to obtain results shown in Figures 6B,C,F,G; S5E-E; S6C,D,G,H a two dimensional (2D) lattice $\mathcal{L}$ composed of 100×100 sites and periodic boundary conditions. As initial condition, in all simulations, the lattice was seeded with 5 sites occupied by the superior competitor (state 1) and fast colonizer (state 2) strategies each. Simulations were also conducted in 1D lattices (Fig.

S6A,B,E,F) A 100×100 sweep of the $[(1 - \Delta\beta) \times \gamma]$ parameter space was performed. Individual colored pixels constitute long-term results of individual simulations. For each run, after converging to a statistical steady state (after $1 \cdot 10^5$ time steps) an ensemble average was then computed over the next 10^3 time steps. In figure 6B we show results for local ($r = 1$) interactions and intermediate strength ($\alpha = 4$) of the trade-off.

science$_a dvances_r eferences$

3.5 Supplementary Material

3.5.1 Mean Field Approximation

The MF for the system $\xi_t : \mathcal{L} \to \mathcal{S} = \{0, 1, 2, *\}$ which corresponds to two types: a superior competitor (type 1) and a fast colonizer (type 2),

$$\dot{p}_1 = \beta_1 p_1 p_0 - \delta p_1 + \eta p_* - \gamma p_1 p_2 \beta_2 \tag{3.8}$$

$$\dot{p}_2 = \beta_2 p_2 p_0 - \delta p_2 + (1 - \eta) p_* - \gamma p_2 p_1 \beta_1 \tag{3.9}$$

$$\dot{p}_* = \gamma(\beta_1 + \beta_2) p_1 p_2 - (1 + \delta) p_*. \tag{3.10}$$

The proportion of empty site being $p_0 = 1 - p_1 - p_2 - p_*$.

3.5.2 Equilibrium analysis

First we consider re-writing the proportion of empty sites as $p_0 = 1 - (p_1 + p_2) - p_*$ and set up the sytem,

$$0 = \beta_1 \hat{p}_1 \hat{p}_0 - \delta \hat{p}_1 + \eta \hat{p}_* - \gamma \hat{p}_1 \hat{p}_2 \beta_2 \tag{3.11}$$

$$0 = \beta_2 \hat{p}_2 \hat{p}_0 - \delta \hat{p}_2 + (1 - \eta) \hat{p}_* - \gamma \hat{p}_2 \hat{p}_1 \beta_1 \tag{3.12}$$

$$0 = \gamma(\beta_1 + \beta_2) \hat{p}_1 \hat{p}_2 - (1 + \delta) \hat{p}_*. \tag{3.13}$$

Rearranging we get

$$\hat{p}_1[\beta_1\hat{p}_0 - \delta] = \gamma\hat{p}_1\hat{p}_2\beta_2 - \eta\hat{p}_* \tag{3.14}$$

$$\hat{p}_2[\beta_2\hat{p}_0 - \delta] = \gamma\hat{p}_2\hat{p}_1\beta_1 - (1-\eta)\hat{p}_* \tag{3.15}$$

$$\hat{p}_*(1+\delta) = \gamma(\beta_1+\beta_2)\hat{p}_1\hat{p}_2. \tag{3.16}$$

and immediately know from Equation 3.16 that,

$$\hat{p}_* = \gamma\frac{(\beta_1+\beta_2)}{(1+\delta)}\hat{p}_1\hat{p}_2 = \gamma\lambda\hat{p}_1\hat{p}_2 \tag{3.17}$$

where $\lambda = \frac{(\beta_1+\beta_2)}{(1+\delta)}$. Replacing this in Equations 3.14 and 3.15 we get,

$$\hat{p}_1[\beta_1\hat{p}_0 - \delta] = \hat{p}_1[\gamma\hat{p}_2(\beta_2 - \eta\lambda)] \tag{3.18}$$

$$\hat{p}_2[\beta_2\hat{p}_0 - \delta] = \hat{p}_2[\gamma\hat{p}_1(\beta_1 - (1-\eta)\lambda)] \tag{3.19}$$

Taking $\hat{p}_*$ out of the picture for now and assuming $p_{1,2} \neq 0$,t

$$\beta_1\hat{p}_0 = \gamma\hat{p}_2(\beta_2 - \eta\lambda) + \delta \tag{3.20}$$

$$\beta_2\hat{p}_0 = \gamma\hat{p}_1(\beta_1 - (1-\eta)\lambda) + \delta \tag{3.21}$$

We also notice,

$$\hat{p}_0 = 1 - (p_1+p_2) - p_* = 1 - (p_1+p_2) - \gamma\lambda\hat{p}_1\hat{p}_2 \tag{3.22}$$

and finally get

$$\beta_1[1 - (p_1+p_2) - \gamma\lambda\hat{p}_1\hat{p}_2] = \gamma\hat{p}_2(\beta_2 - \eta\lambda) + \delta \tag{3.23}$$

$$\beta_2[1 - (p_1+p_2) - \gamma\lambda\hat{p}_1\hat{p}_2] = \gamma\hat{p}_1(\beta_1 - (1-\eta)\lambda) + \delta \tag{3.24}$$

and now p_0 is also out of the picture. A simple change and,

$$\beta_1[1-(p_1+p_2)] - \beta_1\gamma\lambda\hat{p}_1\hat{p}_2 = \gamma\hat{p}_2(\beta_2-\eta\lambda)+\delta \quad (3.25)$$

$$\beta_2[1-(p_1+p_2)] - \beta_2\gamma\lambda\hat{p}_1\hat{p}_2 = \gamma\hat{p}_1(\beta_1-(1-\eta)\lambda)+\delta \quad (3.26)$$

to get

$$\beta_1(1-p_1-p_2)-\delta = \gamma\hat{p}_2\{[\beta_2-\eta\lambda]-\beta_1\lambda\hat{p}_1\} \quad (3.27)$$

$$\beta_2(1-p_1-p_2)-\delta = \gamma\hat{p}_1\{[\beta_1-(1-\eta)\lambda]-\beta_2\lambda\hat{p}_2\} \quad (3.28)$$

then

$$\beta_1(1-p_1-p_2)-\delta = \gamma\hat{p}_2\{\beta_2-\lambda[\eta+\beta_1\hat{p}_1]\} \quad (3.29)$$

$$\beta_2(1-p_1-p_2)-\delta = \gamma\hat{p}_1\{\beta_1-\lambda[(1-\eta)+\beta_2\hat{p}_2]\} \quad (3.30)$$

where the LHS represents scramble competition for space and the RHS interference competition.

We can see that

$$\beta_1-\delta = [\gamma\beta_2-\lambda\gamma\eta+\beta_1]\cdot\hat{p}_2-(\lambda\gamma\beta_1)\cdot\hat{p}_1\hat{p}_2+\beta_1\hat{p}_1 \quad (3.31)$$

$$\beta_2-\delta = [\gamma\beta_1-\lambda\gamma(1-\eta)+\beta_2]\cdot\hat{p}_1-(\lambda\gamma\beta_2)\cdot\hat{p}_1\hat{p}_2+\beta_2\hat{p}_2 \quad (3.32)$$

which means that

$$1-\frac{\delta}{\beta_1} = \hat{p}_1+\left(\frac{\gamma}{\beta_1}[\beta_2-\lambda\eta]+1\right)\cdot\hat{p}_2-(\lambda\gamma)\cdot\hat{p}_1\hat{p}_2 \quad (3.33)$$

$$1-\frac{\delta}{\beta_2} = \hat{p}_2+\left(\frac{\gamma}{\beta_2}[\beta_1-\lambda(1-\eta)]+1\right)\cdot\hat{p}_1-(\lambda\gamma)\cdot\hat{p}_1\hat{p}_2 \quad (3.34)$$

which we write as

$$P_{01} = \hat{p}_1+\epsilon_2\cdot\hat{p}_2+\epsilon\cdot\hat{p}_1\hat{p}_2 \quad (3.35)$$

$$P_{02} = \hat{p}_2+\epsilon_1\cdot\hat{p}_1+\epsilon\cdot\hat{p}_1\hat{p}_2 \quad (3.36)$$

where we then scale and sum to get

$$P = \frac{1}{2}[P_{01} + P_{02}] = \frac{1}{2}[\epsilon_1 + 1] \cdot \hat{p}_1 + \frac{1}{2}[\epsilon_2 + 1] \cdot \hat{p}_2 + \epsilon \cdot \hat{p}_1 \hat{p}_2. \tag{3.37}$$

Parameters correspond to

$$\epsilon = \gamma\lambda \tag{3.38}$$

$$\epsilon_1 = \gamma\left[\beta_1 - \lambda(1-\eta)\right]\beta_2^{-1} + 1 \tag{3.39}$$

$$\epsilon_2 = \gamma\left[\beta_2 - \lambda\eta\right]\beta_1^{-1} + 1 \tag{3.40}$$

and all only depend on γ and $\Delta\beta = \beta_2 - \beta_1$. If we fix $\beta_2 = 1$ and take $\beta_1 = 1 - \Delta\beta$ and remember that $\eta = [1 + e^{\alpha\Delta\beta}]^{-1}$ and that we had defined $\lambda = (2 - \Delta\beta)/(1 - \delta)$ to simplify calculations. Thus,

$$\epsilon = \gamma\frac{2 - \Delta\beta}{1 - \delta} \tag{3.41}$$

$$\epsilon_1 = \gamma\left[1 - \Delta\beta - \frac{2 - \Delta\beta}{1 - \delta} \cdot \frac{1}{1 + e^{-\alpha\Delta\beta}}\right] + 1 \tag{3.42}$$

$$\epsilon_2 = \gamma\left[1 - \frac{2 - \Delta\beta}{1 - \delta} \cdot \frac{1}{1 + e^{\alpha\Delta\beta}}\right]\frac{1}{1 - \Delta\beta} + 1 \tag{3.43}$$

So if $\gamma = 0 \Rightarrow \epsilon = 0$ and $\epsilon_k = 1$. If $\gamma = 1$, and $\Delta\beta = 0$ we get

$$\epsilon = \frac{2}{1 - \delta} \tag{3.44}$$

$$\epsilon_1 = 2 - \frac{1}{1 - \delta} \tag{3.45}$$

$$\epsilon_2 = 2 - \frac{1}{1 - \delta} \tag{3.46}$$

which when $\delta = 0$ we have $\epsilon_1 = \epsilon_2 = 1$ and $\epsilon = 2$ so $P = \hat{p}_1 + \hat{p}_2 + 2\hat{p}_1\hat{p}_2 = 1$.

Table 3.1: S1: Bacterial strains

Strain ID	Plasmid	Characteristics	Reference
E. coli			
JEK1036		W3110; lacZY::GFPmut2	[31]
JEK1037		W3110; lacZY::mRFP1	[31]
P. aeruginosa			
PUPa3-G	pKR-C12	PUPa3; Gm^R Amp^R; pBBR1MCS-5 carrying PlasB–gfp(ASV) Plac–lasR	[148],[149]
PUPa3-R	pKR-C12	PUPa3; Gm^R Amp^R; pBBR1MCS-5 carrying PlasB–dsRed(ASV)Plac–lasR	[148]

3.5.3 Tables & Additional Figures

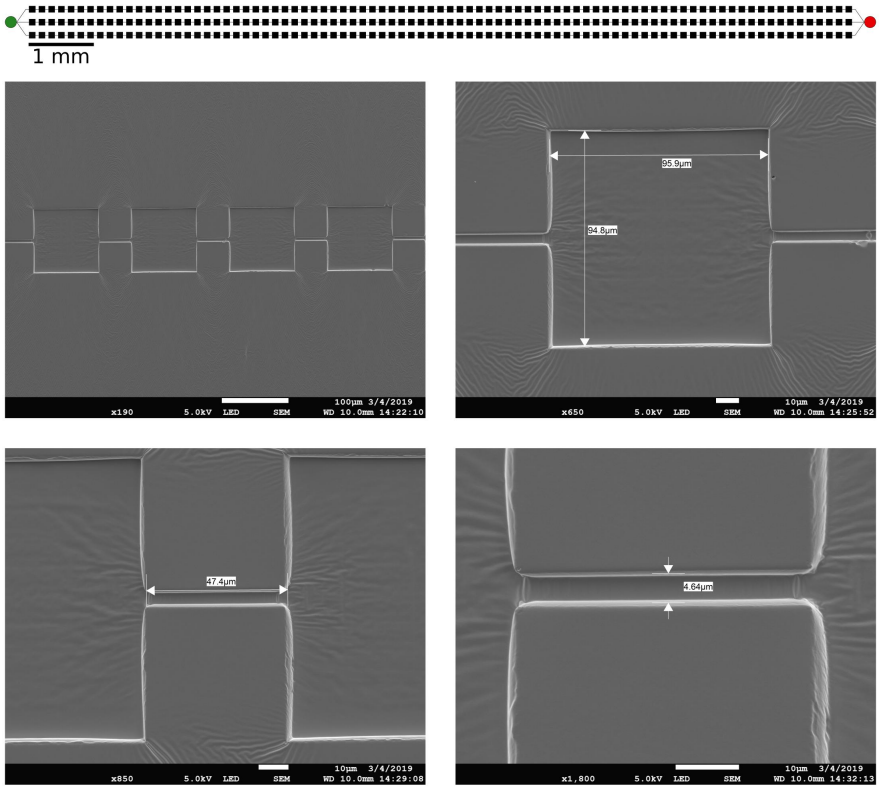

Figure 3.7: S2: Microfluidic devices Scanning Electron Microscopy (SEM) images of an MHP array (patchy landscape) in the microfluidic devices depicted in Figure 1A (*top panel*). To make this SEM, freshly made PDMS devices were sputter coated using a Q150T ES turbomolecular pumped coater leaving a 15nm gold film deposition. Devices were then placed in a JSM-7100F Thermal field emission electron microscope for imaging.

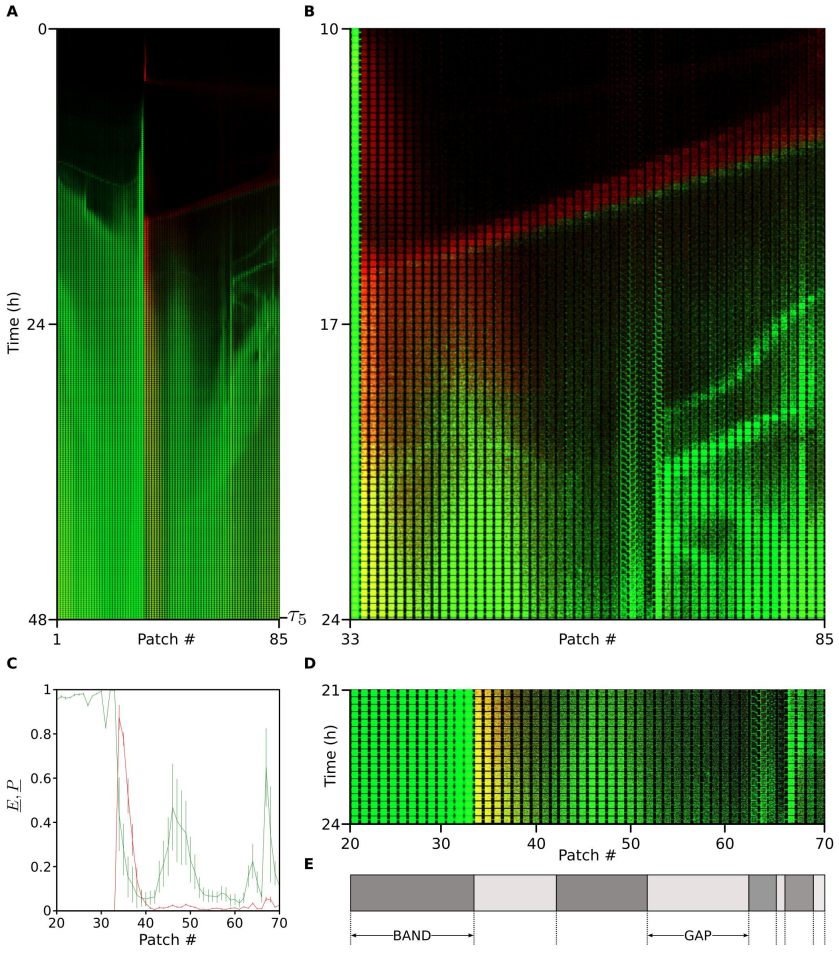

Figure 3.8: S3: Structure and dynamics of a bacterial metacommunity In **A** we shown the complete (85 MHPs; 48 hrs) kymograph partially shown in Figure 4C,D. A Zoom-in to a region of space ($33 \leq k \leq 85$) and time ($10 \leq t \leq 24$) within this kymograph is shown in **B**. Notice the fine structure of the spatio-temporal dynamics of the bacterial metacommunity. Between times ($10 \leq t \leq 17$) a *P. aeruginosa* wave (green) chases an *E. coli* wave (red) from left to right. Later, ($17 \leq t \leq 24$) we see two meso-scale *P. aeruginosa* structures. One is located on the left ($k \approx 46$) and the other on the right ($k \approx 83$). These structures form and interact by emitting and absorbing waves. On the left most side we see the MHP ($k = 34$) part of the ecological succession described in Figure 4D. In **C**, we zoom in further and take an average of 3 hours of occupancy data for *E. coli* ($\underline{\mathrm{E}}_k = (18)^{-1} \sum_{21<t\leq 24} E_k(t)$; red) and *P. aeruginosa* ($\underline{\mathrm{P}}_k = (18)^{-1} \sum_{21<t\leq 24} P_k(t)$; green) for each MHP ($20 \leq k \leq 70$) shown in **D**; a ROI of kymograph shown in A. **E** Bands/gap structure of *P. aeruginosa*'s $\underline{\mathrm{P}}_k$.

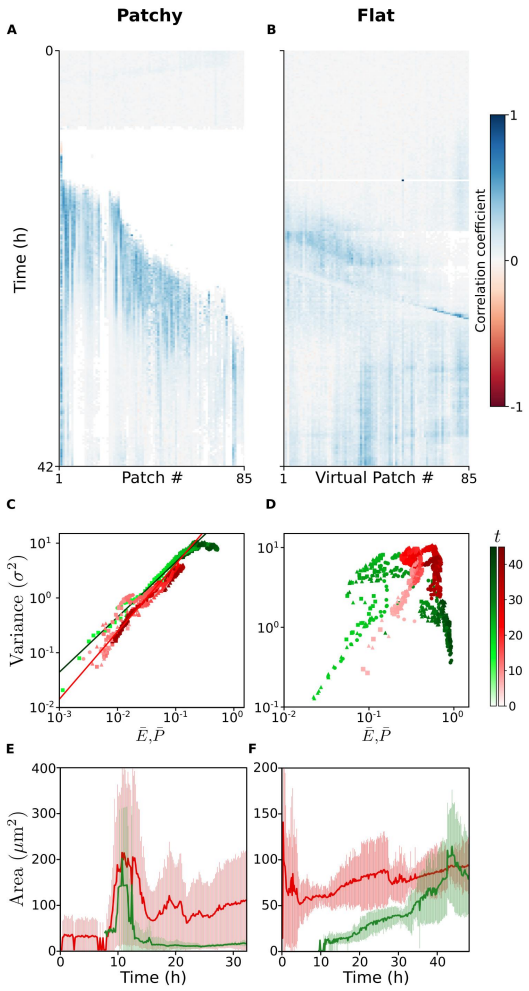

Figure 3.9: S4: Patchy versus Flat landscapes revisited As in Figure 5E,F in the main text, in (**A**- **B**) we plot Pearson coefficients between red and green channels for competition experiments as well as showing an analysis of Taylor's law in (**C** -**D**) in patchy (A,C) and flat (D, B) landscapes. Similarly, but for mono-culture experiments, in (**E** -**F**) we show the dynamics of the size of micro-colonies, in patchy (C,E) and flat (D,F) landscapes. Plotting regional variability σ^2 v.s. average % occupancy $\bar{E}, \bar{P}$ we test for Taylor's law [9]; which holds (power law pattern) in C but not in D. The size (μm^2) of micro-colonies (cell clusters) follows very different dynamics in patchy (E) and flat (F) landscapes. In C-F, Colors represent *P. aeruginosa* (green) and *E. coli* (red). Symbols in (C,D) represent replicas and the color gradients are time dimensions. The light thin regions in (E,F) correspond to deviations from the mean, σ and the dark thick curve is the mean for $n = 3$ landscapes each.

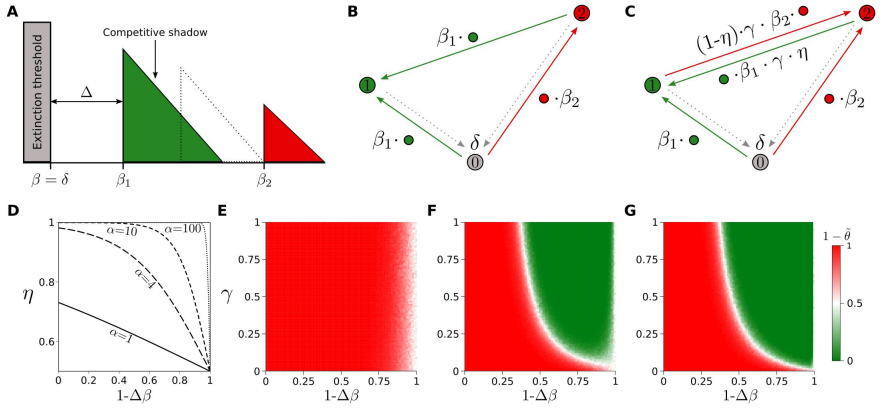

Figure 3.10: S5: Models of the competition-colonization (CC) trade-off A Niche competitive shadows in the CC model [44]; **B** Markov chain of the CC model [44]; **C** Markov chain of the Calcagno model [143]; **D** Strength of interference competition advantage, η, expressed as a trade-off with competitive ability, $(1-\Delta\beta)$, for four different strengths, α, of the trade-off. **E-G** show our spatial (2D; $r=1$) model's parameter space $[\gamma,(1-\Delta\beta)]$ for three of the trade-off strength values shown in D which are $\alpha=1$ (E), $\alpha=10$ (F), and $\alpha=100$ (G); value of $\alpha=4$ is shown in main text's Figure 6B.

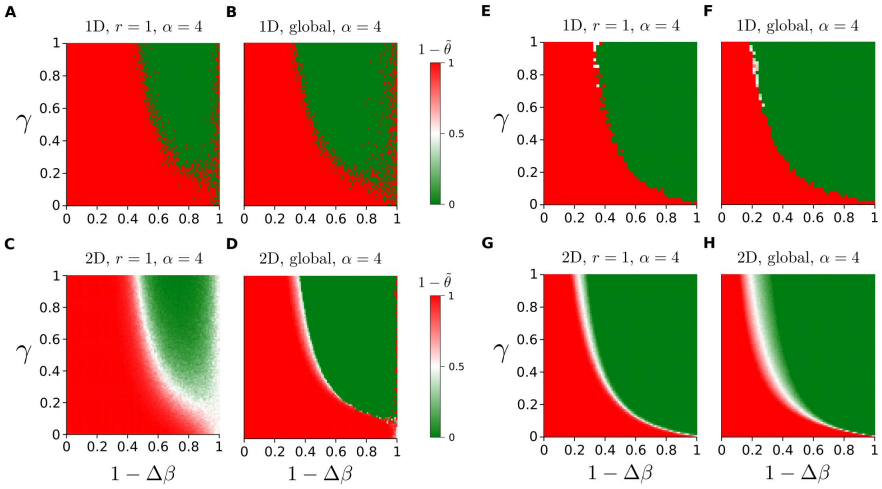

Figure 3.11: S6: Topological considerations Independent of the model and strength of the CC trade-off, we can think on different dimensionality (1D, 2D, or 3D) or the extent of spatial interactions (r) when considering reactions between sites. Fixing strength for the trade-off, $\alpha=4$, we can consider a spatial version of Calcagno's model and/our our formulation in 1D or 2D for local (nn) or global dispersal. The phase space over $[\gamma,(1-\Delta\beta)]$ is shown for our IPS model implemented on a 1D lattice **A-B**, considering local (nearest neighbor) dispersal, $r=1$ (A) and global (full lattice) dispersal $r=r_{\max}$ (B) interactions, and also on a 2D lattice **C-D** for local (C) and global (D) interactions as well. A spatially explicit stochastic implementation of the Calcagno picture is shown in **E-F** for the 1D implementations for local (E) and global (F) interactions as well as in 2D **G-H** for local (G) and global (H) respectively.

Table 3.2: S7: Glossary

Term	Meaning	Refs.
Biophysics		
bacterial waves	Motile bacteria swim together as cell packs	[137, 125]
α-wave	First, fast, low density wave of bacteria	[137, 134]
β-wave	Second, slower, higher density wave of bacteria	[137, 134]
γ-front	After initial waves, a refracting front follows	[134]
microfluidics	Manipulation of small volumes of fluids	
microfabrication	Using (soft/hard) lithography techniques to build microfluidics devices	[136]
ecology *on-chip*	Applying landscape ecology to guide microfabrication of microbial ecosystems	[133]
arrays of MHPs	Using microfabrication and microfluidics to capture patchiness in microbial habitats	[133]
periodic energy potential	Used to represent a solid crystal (of atoms)	[46]
band (gap) structure	In periodic potentials waves structure in bands	[46]
delocalized cells	Cells traveling in waves (sessile or pelagic)	
localized cells	Non traveling "resident" cells (sessile or pelagic)	
Anderson localization	wave phenomenon, where randomness/disorder over a periodic potential leads to localized wave functions (of electrons)	[145]
Microbiology		
bacterial community *on-chip*	Synthetic microbial ecosystem (*e.g.* soil) *on-chip*	[135]
bacterial chemotaxis	Motile bacteria responds to chemical fields	[137]
biofilm	Development program; bacteria attached to surfaces	[124]
lag phase	First phase of colony development with no growth	
log phase	Logarithmic growth phase of a culture/colony	
stationary phase	Phase where growth comes to a halt	
sessile	Cells aggregated to surfaces/each other	
pelagic	Cells swimming in the liquid interface	
Ecology		
landscape ecology	Scaling ecology from locality to landscapes	[18]
habitat patch	Spatially discrete, ephemeral, favorable conditions	
patchy landscapes	Habitats which are collections of patches.	
occupancy (vacancy)	Local patches, are occupied or vacant	
Taylor's law	Local abundance/occupancy relates to its regional variance as a power law	[150, 9]
lattice model (IPS)	Spatially explicit models of site occupancy	[16]
metapopulation	A population of populations	[20]
metacommunity	A collection of metapopulations of $\neq$ species	[21]
CC trade-off	Trade-off between competition and colonization	[42]
fugitive strategies	A life history focused on scramble competition	[91]

Table 3.3: S8: Symbols

heightSymbol	Meaning
Experiments	
$k \in \{1 \cdots 85\}$	Index of a Micro fabricated Habitat Patch (MHP);
E_k, P_k	Local occupancy within MHP number k
	The symbols E_k and P_k correspond to
	E. coli and *P. aeruginosa* respectively.
$k_s \in \{1 \cdots 85\}; s \in \{1 \cdots 72\}$	index for MHP number k in MHP array s
E_{k_s}, P_{k_s}	Local occupancy within MHP k_s in array s
$\bar{E}_s, \bar{P}_s$	Spatial average across MHPs (k) in MHP array s;
	$\bar{E}_s = (1/85) \cdot \sum_{k_s} E_{k_s}$ and $\bar{P}_s = (1/85) \cdot \sum_{k_s} P_{k_s}$.
$Z_{k_s} = (E_{k_s} + P_{k_s})/2$	Normalized total occupancy in MHP k_s in array s
$\Theta_{k_s} = P_{k_s}/(E_{k_s} + P_{k_s})$	Fractional occupancy of *P. aeruginosa* in MHP k_s in array s
$(1 - \Theta_{k_s}) = E_{k_s}/(E_{k_s} + P_{k_s})$	Fractional occupancy of *E. coli* in MHP k_s in array s
$\Theta_s = \bar{\Theta}_{k_s}$	*P. aeruginosa* fractional occupancy averaged across MHPs in s
$(1 - \Theta_s) = 1 - \bar{\Theta}_{k_s}$	*E. coli* fractional occupancy averaged across MHPs in s
$\Theta = \langle \Theta_s \rangle$	Ensemble average of Θ_s across all arrays (n=72)
N_E, N_P	Number of cells of *E. coli* (N_E) and *P. aeruginosa* (N_P)
θ	Fractional density of *P. aeruginosa* in well-mixed environments
	averaged across experiments $\theta \equiv \langle N_P/(N_E + N_P) \rangle$ (n=3)
t	Time t in experiments is a full-landscape image scan
	then a picture scan is taken every 10 minutes at $t + \jmath \cdot \delta t$
τ_j, τ'_j	A time point $t = \tau_j$ or a collection of successive times τ'_j
Theory	
$\Delta\omega$	Difference in interference competition ability
$\Delta\beta$	Difference in scramble competition ability; $\Delta\beta = \beta_2 - \beta_1$
α	Strength of the trade-off model between competitive abilities
$\xi_t : \mathcal{L} \to \mathcal{S}$	Spatial stochastic process describing the state of sites at time t
$\mathcal{L}$	Lattice sites $x, y \in \mathcal{L}$ can be arranged in 1D ($\mathcal{L}_{1D}$) or 2D ($\mathcal{L}_{2D}$)
	with boundary conditions, $\mathcal{L}_{1D} \cong \mathbb{Z}_{100}$ and $\mathcal{L}_{2D} \cong \mathbb{Z}^2_{100\times100}$
$\mathcal{S} = \{0, 1, 2, *\}$	Set of states. Each lattice site can be in a state of this set
$\Omega(x; r)$	Interaction neighborhood $\Omega \in \mathcal{L}$ with radious r around x
	so we have that $\Omega(x; r) = \{y \in \mathcal{L} :\mid x - y \mid \leq r\} \subset \mathcal{L}$
β_1, β_2	Colonization rates indexed such $\beta_1 < \beta_2 \equiv 1$
	Competitor type (state 1) represents *P. aeruginosa*
	and colonizer type (state 2) corresponds to *E. coli*.
$(1 - \Delta\beta) = \beta_1$	Superior (interference) competitor's colonization ability
γ	Degree of priority effects (rate of co-colonization modulation)
η	Interference competition bias on a localized competitive lottery
δ	Clearance rate (local extinction) of a sub-population
ρ_P, ρ_E	Proportions of sites held by type 1 (ρ_P) or type 2 (ρ_E)
$\tilde{\theta} = \rho_P/(\rho_E + \rho_P)$	Fractional occupancy of competitor type (state 1)
$(1 - \tilde{\theta}) = \rho_E/(\rho_E + \rho_P)$	Fractional occupancy of the colonizer type (state 2)
$(1 - \tilde{\theta}_t) = \rho_E(t)/[\rho_E(t) + \rho_P(t)]$	Dynamics of colonizer's fractional occupancy

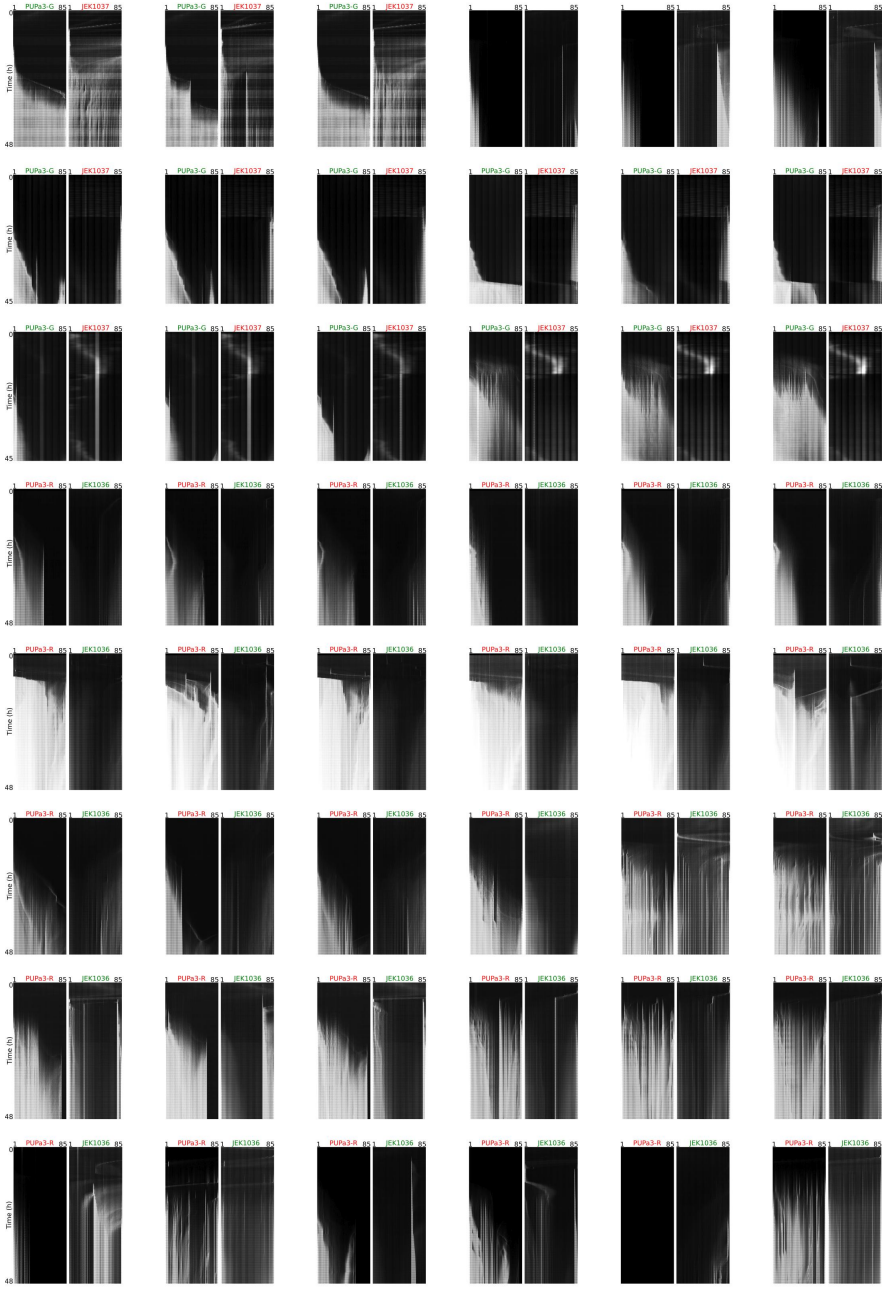

Figure 3.12: S9: Raw image kymographs pairs (GFP and RFP) of 48 experiments For information on strains see Table S1. Each kymograph pair S9KG$[r, c]_{L,R}$ where r, c are *row* and *column* in the Figure and L and R correspond to *left* and *right*.

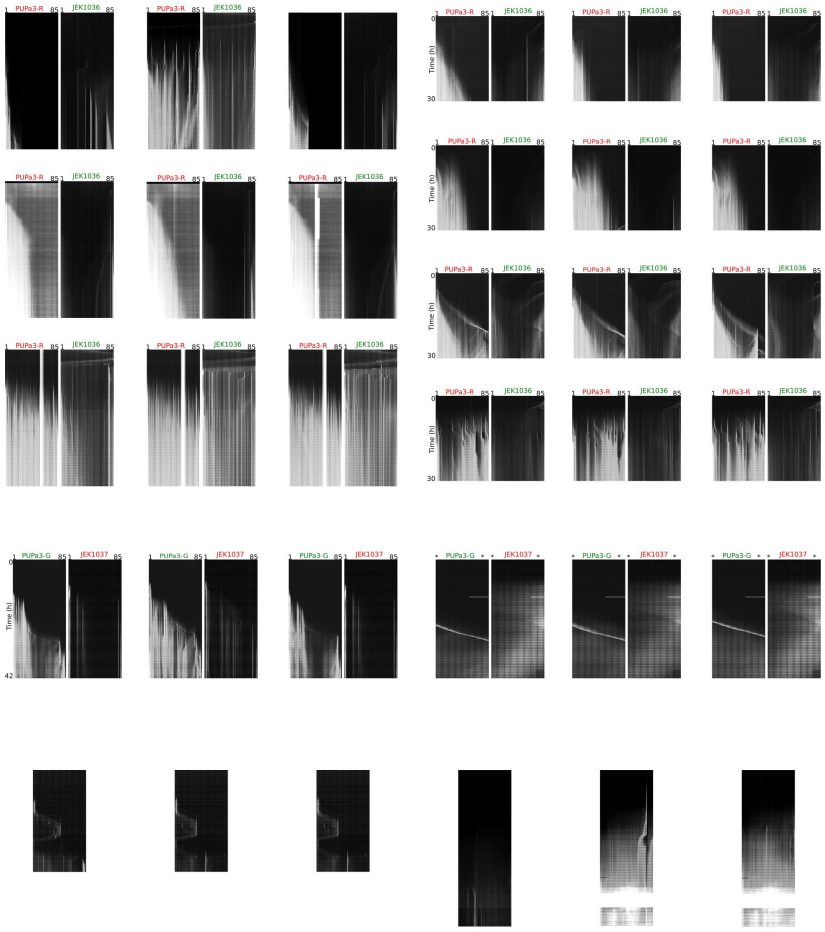

Figure 3.13: S10: Raw image kymographs pairs (GFP and RFP) experiments. For information on strains see Table S1. As in Fig S9 here in **A** we have kymograph pairs S10A$_K G$[r,c]$_{L,R}$ to refer to data on patchy landscapes; In panel **B** we show experiments S10B$_K G$[r,c]$_{L,R}$ corresponding to 3 flat landscape kymographs corresponding to parchy landscapes.... **C** Kymograph data corresponding to monoculature experiments in patchy and flat landscapes.

Chapter 4

One Slope Doesn't Fit All: Landscape Structure Changes Taylor's Law in Microbial Metapopulations

The only things that can be universal, in a sense, are scaling things.

-Mitchell Feigenbaum

Taylor's law is an empirical law in ecology which asserts that the fluctuations in populations is a power law function of the mean. Here we provide experimental evidence that bacterial metapopulations in patchy habitat landscapes on microchips follow this law. Furthermore, we find that an increased randomness of patch-connecting ecological corridor size leads to a qualitative transition in the fluctuation scaling. Future work is discussed as is a possible connection to other scaling laws of ecology.

4.1 Introduction

Developing a statistical mechanics characterizing patterns of microbial species abundance and distribution is a fundamental goal of ecology [151, 7]. One such pattern is Taylor's Law (TL) which states that the variance in the number of individuals of a (meta-) population is related to the mean by a power law [152]:

$$\sigma_\phi^2 = c\langle\phi\rangle^\alpha \tag{4.1}$$

This statistical emergent property of populations was first shown empirically by L.R. Taylor when he compiled census data of several organisms, including macro-zooplankton, worms, insects, mites and fish [152]. Since this landmark paper, TL as a statistical phenomena has been observed far beyond the scope of ecology, present in cell biology [153], linguistics [154], social science [155] and even number theory [156] in mathematics (See [150] for a review).

The case for TL Universality in ecological populations has been strengthened, more recently having been confirmed in microbes in the human gut [157], hot spring [158] and several other microbiomes [159]. While the phenomena of power law scaling appears to be a universal property of populations, the slope (α) varies: In his own words, Taylor considered α to be the 'index of aggregation' ranging from near regular dispersion $\alpha \to 0$, to random (i.e. Poisson) $\alpha = 1$ to highly aggregated $\alpha \to \infty$. Given the cornucopia of slopes these results produced, he considered α to be a characteristic feature of the organism in question.

Beyond simply the verification of its existence, TL has provided insight into aspects of spatial ecology, including a connection with the Moran effect [160], which describes the synchronization of dispersed populations within a landscape that are environmentally correlated [161]. While underlying mechanisms for the origins of differing α's are still up for debate [162, 163, 164], one thing is certain; α varies considerably from organism to organism and from landscape to landscape.

Despite the recognition that landscape structure impacts metapopulation dynamics [165], as of yet, no connection has been made explicitly between the physical properties of ecological landscapes and its impact on the slope (α) of the metapopulation. In order to perform such an investigation requires precise control of physical properties defining the landscape in question.

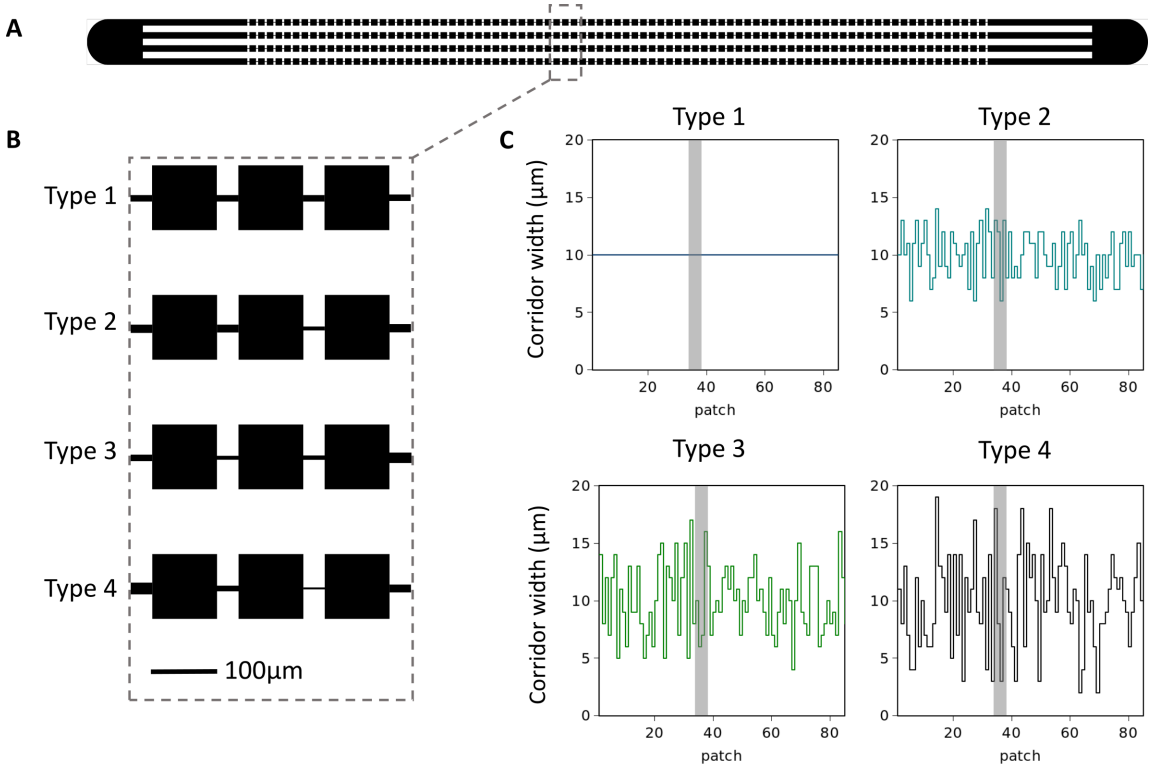

Figure 4.1: Microfluidics device: A) A sketch of the microfluidics device with single inlets on each side leading into 4 parallel habitat landscapes B) Zoom-in view of patch-corridor structure in each of the 4 parallel landscapes. For type 1 corridor width is kept constant at 10μm. Types 2-4 the average width is also 10μm but variance around the mean increases from type 2 to 4. This can be appreciated in C) where we show the pattern of corridor widths used for each landscape type. Grey shading indicates location of zoom-in.

In this short report, we show results from microfluidic experiments (see Materials and Methods) using a single species of bacteria, *Escherichia coli* (*E.coli*), which is known to form a metapopulation in such micro-habitat patch landscapes (Fig 1A) and, therefore suitable for studying in the context of TL [133]. As a first step in connecting landscape microbial ecology to Taylor's Law, we wanted to know the following; *(i)* does the long-term metapopulation occupancy structure display a discernible α? And, if so, *(ii)* is α landscape structure dependent?

4.2 Results

To answer these questions we compared TL outcomes for *E.coli* metapopulations living in different landscape types (Fig. 1). In order to achieve this, we studied the distribution of *E.coli* occupancy in microfluidic devices which consist of microscopic chambers (patches) connected by

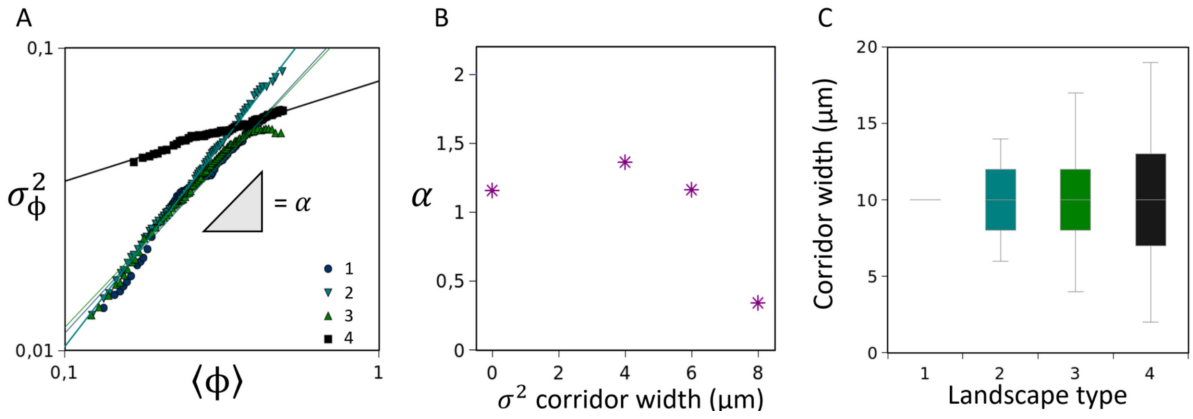

Figure 4.2: Landscape dependency of Taylor's Law in a bacterial metapopulation: A) The relationship between the average occupancy of a patch, $\langle\phi\rangle$, and its variance, σ^2_ϕ, over (n = 31) replicates and across all patches (85) generates the unique Taylor's Law (TL) for each landscape type. The slope of TL, α, is plotted against the variance of corridor width (randomness) defining landscape types in B). In C), a box plot of corridor widths around the mean (10μm). Four variances were used in this study, ($\sigma^2 = 0, 4, 6, 8\mu$m).

narrow channels (ecological corridors). Here, the only difference between landscape types was the within-landscape corridor width variance (see Figure 1C) which we refer to as *randomness*.

For landscape types 1-3 we see α values between 1-1.5 which falls within the range commonly found in the literature [150]. Strikingly, beyond some critical level of randomness ($6\mu\text{m} < \sigma^2_{crit} < 8\mu\text{m}$) the slope of our TL ($\alpha$) changes abruptly in landscape type 4 (Figure 2A-B).

When interpreting these results, one must consider two regimes of the metapopulation occupancy: For relatively 'dilute' sub-populations occupying patches in the metapopulation, where landscape occupancy $\langle\phi\rangle << 1$, type 4 patches have a significantly higher fluctuation around the mean than equivalent mean occupancy patches in landscape types 1-3, L.H.S. figure 2A. In short, the normalization constant (c) is characterized as follows: $c_4 > c_{1-3}$. However, given the scaling behavior observed, $\alpha_4 < \alpha_{1-3}$, this disparity diminishes as we consider more concentrated patches in the metapopulation $\langle\phi\rangle \to 1$, and even flips in the case of landscape type 2.

A key takeaway from our results is that we see the fluctuation scaling of bacterial metapopulations change with landscape modifications. Particularly, beyond some level of randomness within the ecological corridors of the landscape a transition occurs in the statistical properties of the metapopulation distribution. From these experiments, the transition appears to be abrupt, as we see a relatively consistent value for α below σ^2_{crit}, i.e. landscape types 1-3. This 'basal' α value while differing quantitatively between the three landscape types remains qualitatively the same,

lying between a random/Poisson distribution ($\alpha = 1$) and aggregated/gamma distribution ($\alpha = 2$). Counter-intuitively, landscape randomness (above σ^2_{crit}) induces a qualitative change driving the metapopulation to be more uniformly distributed ($\alpha < 1$).

4.3 Discussion

It remains to be seen exactly how these metapopulations arrive at this alternative statistical equilibrium. It is well-known that *E.coli* collectively migrate into such landscapes as traveling chemotactic waves [125, 134]. Therefore, following the range-expansion dynamics of pioneering population waves is a logical next step in answering this question. Furthermore, previous investigations by van Vliet et al. using the same strain and similar microfluidics devices, also designed with shared inlets leading to multiple landscapes, yet without variance in ecological corridor width, showed strikingly similar patterns of colonization and occupancy [134]. In fact, van Vliet et al. found more similar occupancy patterns for experiments performed with shared inlets and identical colonies than those performed on independent inlet devices and different colonies. Taking this into account and the extensive number of replicate colonies performed for this investigation suggests that our results are a property of the spatial biology at play and not a methodological artifact, nor a stochastic feature of under-sampling.

Our results reflect the conclusions of Reuman et al. suggesting α is not only a trait of a species, originally asserted by Taylor, but likely a tunable characteristic which responds to external factors as in the case of the Moran effect, *sensu* [160], or in this case – landscape properties. One question which remains is if there exists a 'basal' α for populations which is only perturbed by exceptional exogenous forces within the landscape or strong trophic or competitive interactions. That we should see such shifts in the scaling exponent α driven by external factors does not diminish the utility of TL, rather it refines our understanding and in fact marks the development and progress of other ecological scaling laws [166]. In this light, pursuit of these questions will aid in finding connections between TL and other ecological scaling laws which is an exciting and ongoing effort [167]. It is clear, extensions to the microbial world are in order and likely to provide unexpected results. This is especially the case given the known disparity of metabolic scaling observed between prokaryotes and the more commonly studied metazoa [168]. Notwithstanding, we believe controlled spatial

experiments like those made accessible through the lab-on-a-chip framework will play an important role.

4.4 Supporting information

4.4.1 Strains and growth conditions

Experiments were performed using *E. coli* (JEK1036) labeled with Green Fluorescent Protein (GFP) [133]. Single colonies were grown from $-80°$C glycerol stocks on solid LB agar plates (LB Broth EZMix, Sigma-Aldrich + 1.5% Bacto Agar, MOLAR Chemicals) and subsequently inoculated in 3 ml Lysogeny Broth medium (LB Broth EZMix, Sigma-Aldrich) for 16h±30min (O/N) at 30°C, 200rpm. Overnight cultures were back-diluted 1:1000 in 3ml LB medium with 1mM IPTG and grown to an optical density at 600nm (OD_{600}) of 0.3. Cultures were then centrifuged at 350G for 10 minutes, after which the supernatant was removed and cells were resuspended in LB medium containing 1mM IPTG.

4.4.2 Microfluidic device fabrication and preparation

Microfabricated devices used in this study consist of two inlet holes (1.2mm) on opposite sides with 4 parallel landscapes, each with 1-dimensional arrays of 85 habitat patches ($100 \times 100 \times 5\mu m^3$) connected by corridors with constant lengths (50μm) and depths (5μm) but with different widths. The statistics of width distributions for landscape types 1-4 is shown in the main text, figure 2C, and patterns were maintained for all experiments, figure 1C.

Devices were fabricated using soft lithography techniques [136]: A silicon wafer was coated with a thin film (5μm, height of the device) of the negative photoresist SU-8 (SU-8 2005, MicroChem) and the design of the device was written into the resist with a laser pattern generator (μPG 101, Heidelberg Instruments) to fabricate a master mold on which Polydimethylsiloxane (10:1 PDMS:curing agent, Sylgard 184, Dow Corning) was deposited to yield an elastomeric stamp that was covalently bonded to a glass cover slip by oxygen plasma activation (29.6 W, 400mTorr, 45 sec; PDC-002, Harrick Plasma) of both the PDMS and glass parts.

Microfluidic experiments

Prior to inoculation, the devices were wettened with LB + 1mM IPTG. Then, 1μl culture was pipetted into one inlet hole. Once inoculated on one side, the device was sealed with fast curing PDMS (Kwik-Sil Silicone Elastomer, World Precision Instruments). A water tight wall is made around the perimeter of the sealed device on the glass slide using four 24×60mm coverslips which were previously 'painted' up-right onto the glass-slide using fast curing PDMS. The sealed device was then submerged in Milli-Q water and placed into an incubator at 30°C for 48hrs.

4.4.3 Image acquisition and data analysis

After 48h of incubation, devices were imaged using a Nikon Eclipse Ti-E microscope equipped with 10X Nikon Plan Fluor objective, GFP fluorescence filter set (49002 Chroma Inc.), Andor Neo sCMOS camera (Andor Technology plc.), LUMEN 200 Pro metal arc lamp (Prior Scientific Ltd.) and a Prior Proscan II motorized stage (Prior Scientific Ltd.) was used for scanning. The NIS Elements Ar software (Nikon Inc.) was used for image acquisition and data processing and image analysis was carried out using ImageJ and Python. Fluorescence intensity is a poor estimation for biomass due to differences in expression among cells. To avoid this problem we use a custom script in ImageJ to convert all images to occupancy data.

Local occupancy within patches (MHPs)

After background correction is performed on each image a threshold pixel value is calculated based off the auto-fluorescence for the green color channel used. When the value is above this threshold, the pixel (0.803μm^2) is considered occupied (value of 1), otherwise it is vacant (value of 0). Using the ROImanager in ImageJ [146], a custom mask was fitted at each patch for each experiment allowing us to consider occupancy values at the patch level. Occupancy for a MHP indexed by k is denoted as ϕ_k, thus $0 \leq \phi_k \leq 1$. Running $n = 31$ replicates, an average, $\langle\phi\rangle$, and variance, σ^2_ϕ, is calculated for each patch, k, within each of the 4 landscape types, rendering $85\text{x}[\langle\phi\rangle, \sigma^2_\phi]$ data points. These values are shown as a log-log plot in Figure 2A of the main text with a best fit power law. The value of the slope for each landscape type TL is plotted in Figure 2B of the main text.

Chapter 5

Ecology for physicists: the dynamics of cells in spatially structured habitats

This web of life, the most complex system we know of in the universe, breaks no law of physics, yet is partially lawless, ceaselessly creative.

- Stewart A. Kauffman

Cells are individuals and thus an ecological view of cellular behavior is critical for generating understanding of biological dynamics of cell assemblages. The goal of this manuscript is to introduce cell biophysicists with the relevant ecological theory as well as to review recent studies of cell biophysics in micro and nano structured environments where an ecological interpretation of results can be useful. In particular, I revise theories which are relevant to understand the biology and ecology of the cell's microenvironment and how to scale from individual cells to the global structure of the cellular assemblage. Finally, I discuss possible directions for future experiments and theoretical work aiming at understanding cellular tissues as communities of cells in an adaptive landscape physically implemented as a collection of weakly-connected micro-environments (local niches).

5.1 Introduction

Recent efforts to understand the physics of active matter [169] have emerged as a candidate framework to construct a physical theory of life [170], in parallel developments some new ideas from non-equilibrium statistical mechanics begin to offer a view of biological adaptation as resonance between molecular networks and environmental oscillations [171]. To place these theoretical approaches, together with data coming from cell biophysics experiments, in a biological context we will review the literature where cell systems have been studied by setting up artificial ecologies *on-chip* and use them to layout our view of what is useful to know from ecology. The idea is to introduce physicists to the relevant biological aspects we consider important to connect what otherwise is a diverse set of experimental observations in biological physics. The aim, is to link up these experimental data sets with ideas from theoretical biology, and it is to this goal that we start with a discussion of the biological cell instead of focusing on questions about the origin of life on Earth [172], or what life is from an information point of view [173], we will rather focus here on the ecology of biological cells.

5.1.1 The physical biology of the cell

Cells are individuals! Before any macroscopic multicellular entity populated this planet, individual cells were the only biological individuals. Let's not focus on the question of their origin but first on, 'What are they?' Biology, exhibits an infinite diversity of phenomena which is instantiated by a diversity of cells, their communities and the environments they construct in the process of going along with their life history strategies. The first thing cells construct is themselves, a process known as *Autopoiesis* [174] (see Section 5.2.1). To construct themselves, cells, rather than needing to self re-produce, need to self produce. If the later is achieved, the former inevitably is too. Thus, reproduction is nothing more than a fracture, which preserves autopoiesis. To achieve this, cells only need to grow in a supporting environment until they reach a critical body size at which point cell division takes place automatically. However, the finite nature of cells means that in order to grow, a minimal set must act as a simpler version of von Neuman's universal constructor [175], in the sense of Langton [176]. We think it is this theoretical framework, that is best suited to understand the biological cell as a soft-matter molecular machine. The developments at the interface of chemistry

and biology led to the revolution of molecular biology [177], today developments at the interface between physics and biology are making a new revolution. Bio-nanotechnologies are producing experimental observations highlighting the role of physics, while developing a physical biology of the cell [178]. Classical cell theory consists of three tenants: (i) all living organisms are composed of one or more cells; (ii) the cell is the basic unit of structure and organization in organisms; (iii) cells arise from pre-existing cells. It is at this level of organization, and its associated temporal and spatial scales that all the action takes place, in our view, everything else emerges from here. From what cells are, and from what they are doing.

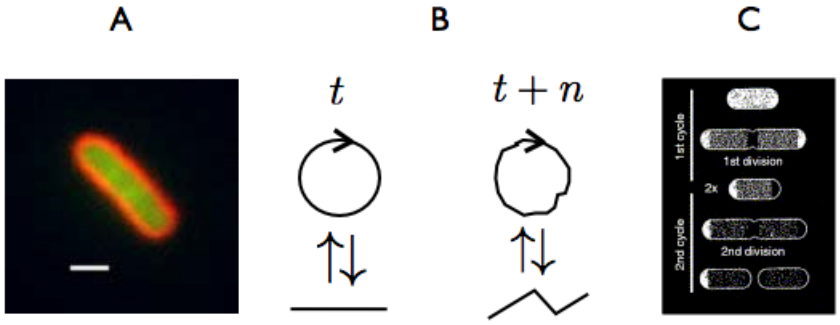

Figure 5.1: The bacterial cell (A) Single cell of *E. coli* is shown here, where the scale bar correspond to 1μm. In green the cell's interior shown by expressing GFP fluorescence and the cell boundary shown in red by the action of a dye acting on the bacterial cell wall; (B) A representation of an autopoietic machine and the process of autopoiesis; At time/configuration t, a self-determined and self referential machine is coupled to its environment by its own structure, a phenomena known as structural coupling. (C) Image is reproduced from [179] showing the distribution of cell wall protein after removal of radio label, we can see how bacteria's growth process concentrates at the middle, leaving the poles frozen.

Biophysics of bacteria

As explained in subsection 5.1.1, biology's natural scale of organization is the biological cell, inspired by the approach of one of our favorite textbooks [178], we adopt the *E.coli* cell as our standard cell. In Figure 5.1A, we can see a cell of a typical strain expressing GFP on its body where its boundary is shown in red, using a dye for the cell wall. Such a cell of this bacteria, is considered here as our model individual and from this point of view, we summarize the ecology that we consider important to understand recent biophysical experiments with cells in general.

Table 5.1: Glossary of biological terms

Term	Definition
Cell	basic unit of structure and organization in living organisms
E. coli	bacteria
Autopoiesis	
Autopoietic machine	
Structural coupling	
Allometric scaling	

5.2 Ecology of individuals

Individuals are finite entities in space, they have boundaries, and in time, they are born and they die. The relationship between an organism and its environment is the focus of autoecology and one of its most important results is the principle of energetic equivalence of metabolism which is the basis of metabolic ecology.

5.2.1 Molecular autopoiesis and individuality

To generalize our description from the *E.coli* standard to other cell types, we appeal to the theory of autopoiesis where cells are all equivalent to autopoietic machines operational in the molecular domain defined by chemistry. A system is autopoietic [180] if: (i) it has a semi-permeable boundary, (ii) the boundary is produced from within the system, and (iii) it encompasses reactions that regenerate the components of the system. Structural coupling refers to the mutual co-dependence of non-destructive perturbations between the individual (autopoietic machine) and its environment and it is the loci of behavior and cognition. The machine and its environment co-determine one another, so from moment t both in a given configuration, can be transformed by n iterations into a new co-state as depicted here in Figure 5.1B. Such a machine $\mathcal{M}$ exists in the context of an ecological niche $\mathcal{N}$ reflecting the physical conditions needed for instantiation.

On natural drift and resonant adaptation

An alternative view to Darwinian selection, is a more neutral approach where individuals, drift [181] while co-determining environmental changes, this also in likes where simple arguments about coupling could offer alternative explanations to adaptation [182]. We believe there is a lot to do here and this is a very exiting area of biophysical research.

5.2.2 Body size, shape and the age of individual cells

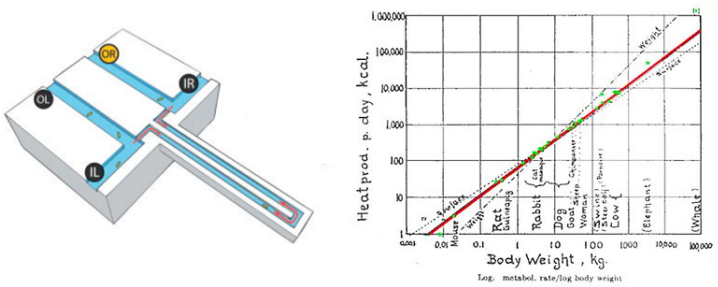

Figure 5.2: Keibler's law Body size predicts metabolic rate for multiple scales of biological organization. This energetic equivalence scales our view from *E.coli* to individuals operating at higher mass scales. (A) Cantilever shaped micro fabricated channel which can be used to calculate the weight of individual bacterial cells by measuring the resonance frequency shift [183] (B) Relationship between body size (in grams) and metabolic rate (in Watts/hour) from [184]

As individuals are finite in space, they have size, form and lifespan. One of the most studied attributes of individuals is body size.

Body size

It is important to remember the universal character of metabolic equivalence and the fact that we can scale many functions y of individuals to their body mass z by using $y = \alpha z^{\beta}$ using a scaling constant α and exponent β. The set of relationships of several biological attributes y_k have with body mass are known as allometric relationships. Unlike in multicellular organisms, where an economy of scale is achieved as body mass increases ($\beta \sim 0.75$) Figure 5.2, allometric scaling of single celled organisms is super-linear ($\beta \sim 1.72$) [168]. This reflects the adaptive process expressed by [182] where single cells, structurally coupled to their environment, are driven by their surroundings to dissipate increasingly more energy. Larger cells equates to superior dissipation.

Ecophysiology of single cells: bacteria's body size

Metabolic activity powers everything a cell can do, since for everything they need a supply of free energy and a sink of entropy. Measuring size [183] by measuring the resonant shifting of

micro-fluidic cantilevers.

Shape-shifting bacteria

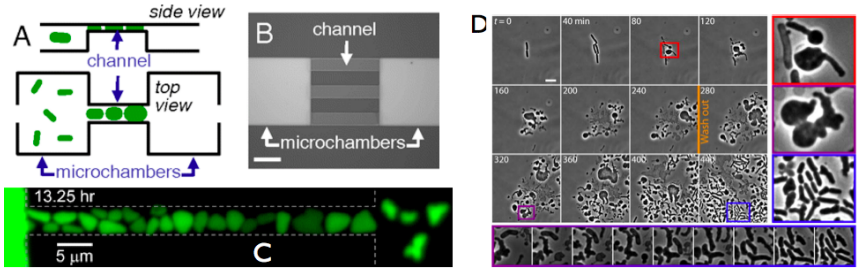

Figure 5.3: Cell shape Rod shaped bacteria can shape shift into a several alternative shapes know as L-forms which are alternatives to the (normal) N-form.

The cell of bacteria shown in Figure 5.1A is the most common shape *E. coli*'s cell adopt when growing exponentially. Let's denote this rod shape, as normal. Therefore the cell shape is referred as the N-form. This nomenclature is needed due to phenotypic plasticity in cell shape. It is know, that in the presence of wall-acting antibiotics, L-forms can be observed. Just as with antibiotics, when subjected to extreme confinement, bacteria also exhibit a remarkable plasticity in cell shape, a fact I learned, when my colleague Peter Galajda discovered it by serendipity while making nano-slits when we were postdocs at Princeton learning from Bob Austin.

The age of bacteria

Bacteria which divided asymmetrically have been long model system for cell aging [185], more recently even *E. coli*, which was thought as dividing symmetrically indeed doesn't. The model cell takes cell-damage and thus, cells with older poles have lower survival. Taking protein aggregates with them [186] ensures the dissipation of damage from the population and this is its evolutionary origin [47].

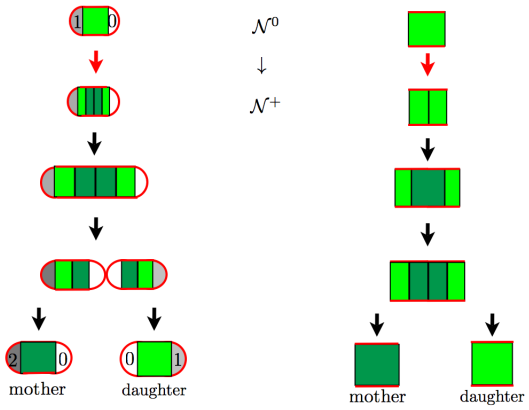

Figure 5.4: Cell growth and division When the fundamental niche is activated $\mathcal{N}^0 \rightarrow \mathcal{N}^+$, we observe that cells resting in a quiescent state of their cell cycle known as G_0 switch into an active state were cell division take place (Interface I and Mitosis M). Left, a cell with a recently made pole (state 0) on the right, and a one generation old pole on the left (state 1) activates after a succession of transformations, reproduces itself leaving a mother cell with a two generations old pole and a daughter cell with the same age structure as the original cell.

5.3 Ecology of populations

5.3.1 The role of the micro-environment: from the "Mother Machine" to the "Death Galaxy"

Exponential growth and environmental resistance

Notice the that the goal of the mother machine (see Fig.5.6A; [187]), is to study a single cell (the mother), which is assumed to be in a physiological state, where the cell is growing at a constant rate g (which at 37°C is $\approx 5\%\text{min}^{-1}$; Fig. 5.6B), as it would be in a population experiencing logarithmic growth. This means, the mother cell is growing and dividing at a constant rate every 20 minutes. The mother cell is constantly generating a cohort of daughter cells that disperse outwards from the dead-end end of the μ-channel towards the exit, where cells are taken away by a larger (high-flow) channel collecting them from the μ-channels and finally flushing them off the chip downstream through an outlet. This daughter-cell removal service, an "ecosystem service" provided by the flow channel and implemented by the device architecture, prevents density-dependent processes from affecting the physiology of the mother cell and therefore ensuring a constant division rate (fecundity) for the cell located at the dead-end end of the μ-channel.

If we focus on the mother cell, at a length scale of 3 μm, we have an ecological individual (see

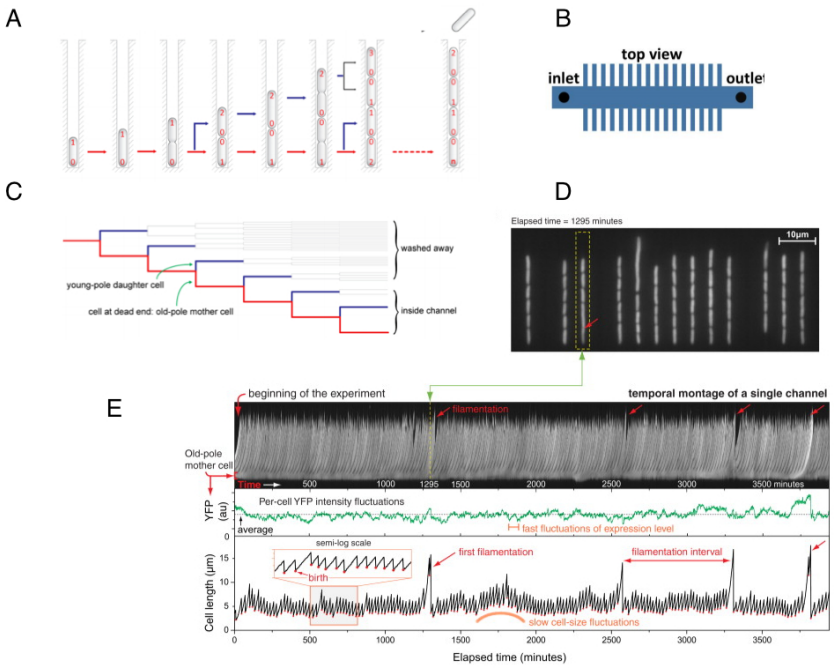

Figure 5.5: Cell growth and division in the mother machine (A) Sketch of a μ-channel population in the mother machine; (B) Sketch of the mother machine device, where many μ-channels converge to a main flow channel which take cells away from a mother living in a cript a the end of the channel (trenches); (C) Cell progeny; (D) A typical fluorescent image of cells living in the device during 1295 minutes; (E) Mother cell growth dynamics (see text);

other section) dividing constantly over its lifespan. On the other hand by focusing on the whole length of the μ-channel, at the scale of tens of μm, we have a linear chain of cells propagating outwards. This group of cells, "a μ-channel population", persists by constant renewal of daughter cells which are produced by the mother cell to replace the removed ones. Daughter cells are removed from the system at a timescale determined by cellular growth rate and the length of the μ-channel. We can ensure homogeneous habitat conditions along these μ-channels by building them no longer than a few cell-lengths. Daughter cells need to be removed quickly, otherwise environmental resistance emerges in the system. Exponential Growth [189] occurs when a population experiences no environmental resistance to its growth potential and therefore its number of individuals $N(t)$ increases exponentially at a constant "per-capita" growth rate r also known as the Malthusian parameter M,

$$M \equiv r = \frac{1}{N}\frac{d}{dt}N = \frac{d}{dt}\ln N.$$

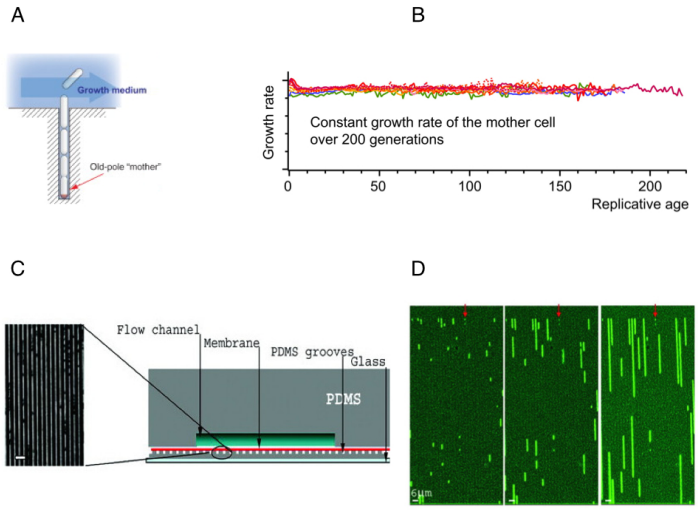

Figure 5.6: Microfluidic ecosystems and the cell μ-environment. (A) Sketch of a mother machine device individual μ-channel hosting a local population of cells; (B) Growth rate of mother cells vs their replicative age at 37°C in rich media (tick marks are % of full cell elongation per min); (C) Scheme of a μ-channel population array ecosystem (scale bar is 5 μm), multiple parallel μ-channels equipped with a membrane for the supply of fresh media and waste removal; (D) Snapshots of the spatial dynamics of linear populations, scalebar = 6 μm, times (in h:min) are 0 : 00 (left), 0 : 59 (center), (right) 1 : 45. Notice some cells do not grow (red arrow). Images are reprinted from [187] (A,B) and from [188] (C,D).

Density dependence

An alternative construction could be used to grow longer population chains. One solution could be to make longer μ-channels while providing habitat renewal in their interior. If we consider longer μ-channels where the removal of cells is done at their ends [188] we still need to make sure the chemistry at the middle is similar to the entrances. If the channels are too long, diffusion from the ends will not be enough to transport nutrients inside and waste outside them. For this reason, these longer μ-channels are also equipped with a membrane at the top for nutrient delivery and waste removal from a reservoir compartment not available to cells (see Fig.5.6C). This compartment and membrane are meant to homogenize the chemistry of the μ-channels, but it does not remove the mechanical interactions between near-by cells accumulating within the μ-channel. With this device, several linear populations can be monitored. In Figure 5.6D we can see three time snapshots of such linear populations, expanding in both directions along μ-channels. At the interior of these channels, away from the ends where removal of cells happens, cells accumulate and start crowding one another.

Under these conditions, although the accumulation of waste and nutrient depletion can be prevented by exchange with the reservoir, an ecosystem service provided by the membrane, cell-cell interactions cannot be avoided completely which will cause processes in the physiology of individual cells to manifest affecting their reproductive potential. This however is the hallmark of environmental resistance, differentiation, and the departure from the "null ecology" scenario. The effects local cell densities have upon a population's physiologically determine birth and death process. This physiological response of individual cells is known as density-dependence. Traditionally, the most simple theoretical description of "a population", incorporating density-dependent regulation, is given by Verhulst's logistic equation [190] which tracks the number $N(t)$, of "individuals" in a certain place. Here we can write as

$$\frac{1}{N}\frac{d}{dt}N = r \cdot \left(1 - \frac{N}{K}\right), \tag{5.1}$$

stressing the role density-dependence has in modifying the Malthusian parameter characterizing individual growth rate. Here two basic parameters come to mind: the growth rate r, and the "carrying capacity" K which corresponds to the long-term number of individuals, of a given life history strategy, a local environment can support within a given ecosystem context. In a test tube environment, shaking is usually applied to provide a well-mixed population where all cells interact with all of the others. This produces a mean-field effect where the population density $\phi = N/K$ affects the growth of individuals. In this normalised coordinate, the dynamics correspond to,

$$\frac{1}{N}\frac{d}{dt}\phi = r \cdot (1 - \phi). \tag{5.2}$$

To prevent the undesired effects which local cell densities have upon one another, the chemostat was developed [191] to study microbial populations in a particular ecological scenario. This corresponds to a steady state population, a constant density scenario, where cells are assumed to be independent from (and equal to) one another. This "null-ecology" ensures that all cells have the same physiological state since the environment is assumed now not only to be well mixed as in the batch culture but fresh growth media is constantly provided as well as waste removal. This ensures an ecosystem with a high productivity regime (nutrients are constantly flowing in) but also a disturbance regime (biomass is constantly flowing out). Notice, in this scenario, biomass can be

removed as a tunable parameter known as the dilution rate D. As with the mother cells in the mother machine, the state of a cells in the chemostat are believed to be in a "mid-log" like state. Such "population" must constantly replace the removed biomass. Cells are executing a growth and division program and that the steady state is achieved by balancing growth rate with the dilution rates. A μ-chemostat can be constructed using microfluidic-based pipes and valves [192] (see Fig.5.7A) in order to make a two-state device which can be run in "continuous circulation" or "cleaning and dilution" modes. This way, what the macroscopic chemostat does in parallel, here is divided into two modes of operation. To make up for this, we can run many of them in parallel. In the continuous circulation mode, a loop chamber which can be addressed by individual segments, holds a circulating population. At some moments depending on the desired dilution rate D, segments are selected, cells are then destroyed and flushed out, and then refilled with fresh media once again made available for immediate colonization from the adjacent segments in the loop. Circulating this procedure through the 16 segments making up the loop we can introduce a disturbance regime to prevent the population in the loop from reaching stationary phase. Depending on ecosystem parameters (productivity and disturbance) we observe different patterns of population dynamics.

In Figure 5.7B we see seven curves representing population dynamics data from such μ-chemostats growing *E.coli* strain MG1655 all exhibiting a logistic growth pattern as envisioned by Verlhust [190]. The variability in growth rates and equilibrium densities are notable. The first two curves correspond to data from runs at 32°C, but with different growth media (productivity) and dilution rates (disturbance), (1) MOPS EZ Rich + 1.1 M glucose, $D = 0.34$ h^{-1}; (2) MOPS EZ Rich + 0.11 M glucose, $D = 0.30$ h^{-1}. Less disturbance in (1) compared to (2) generates higher population grow rate. Better productivity of (2) compared to (1) leads to higher yields of biomass. At lower temperature, at 21 °C, we have the following curves for three productivity scenarios (low, intermediate, and high) and several dilution rates, (3) LB + 0.5 g/L bacto-tryptone, $D = 0.24$ h^{-1}; (4)LB + 0.5 g/L bacto-tryptone, $D = 0.30$ h^{-1}; (5)LB + 3 g/L bacto-tryptone, $D = 0.37$ h^{-1}; (6)LB + 0.5 g/L bacto-tryptone, $D = 0.37$ h^{-1}; (7) LB + 0.1 g/L bacto-tryptone, $D = 0.37$ h^{-1}. For the same intermediate productivity level (0.5 g/L bacto-tryptone), the condition with less disturbance (3) when compared with (4) reaches higher yields as expected. When disturbance is similar and high (dilution rate $D = 0.37$ h^{-1}), the condition with high productivity (5) reaches the highest yield when comparing with intermediate (6) and low (7) productivity. The lowest productivity regime

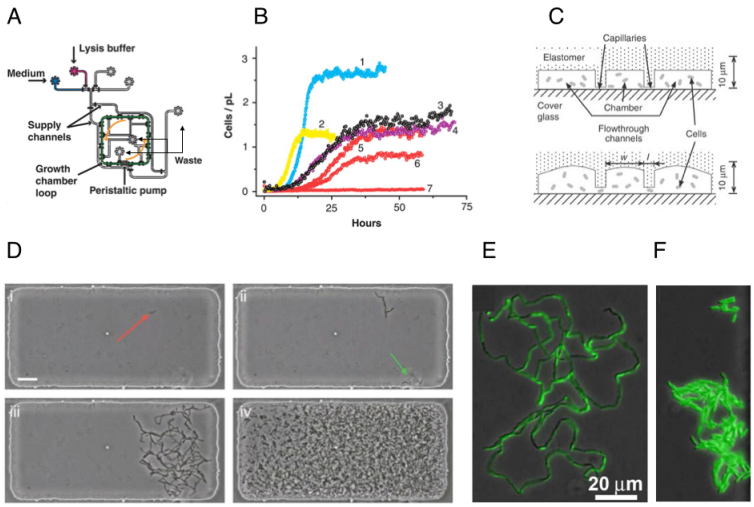

Figure 5.7: The μ-chemostat and other habitats (A) Chemostat design based on micron scale pipes and valves where cells inhabit a loop-chamber, (B) Local population dynamics in the μ-chemostat depicted in (A). Colors and numbers represent different parameters (see text); (C) Microfluidic device consisting of 10 μm-tall chambers connected with actuated capillary channels. These capillaries can be closed (top), rendering a collection of isolated growth μ-chambers and open (bottom) to connect them and isolate cells via flow; (D) Spatial population dynamics of a non-motile *E.coli* (JM109) at T=35°C, where a μ-chamber population develops from one single cell (red arrow) (i) into couple of clusters (green arrow), and finally into a cell-network like structure of individual cells expanding throughout the chamber (time in hours: i = 0, ii= 3, iii=5, iv=8), scalebar = 20μm; (E,F) quorum sensing and cell-cell attachments on early colony formation for autoinducer (AI) concentrations 5nN (E) and 10nM (F). Images, modified from [192] (A,B) and [193] (C-F).

(7) corresponds to a chemostat configurations known as the wash-out scenario where persistence is not possible due to the low levels of productivity and high rates of dilution (disturbance). In this device, when there is no disturbance (active removal of biomass) biofilms take over the fluidic channels within $\sim$ 48 hours.

Alternatively, if we are interested in tracking populations develop without disturbance (no biomass removal), we can use similar channels and valves manipulated by pressure, to create an array of μ-chambers and capillaries [193]. In Figure 5.7C, we depict such a construction. This device also works as a two-state (eco) system where by applying pressure a configuration consisting of connected μ-chambers develops through opening capillaries (bottom panel). When pressure is removed, capillaries close (top panel), the systems consist of a collection of μ-chambers where cells

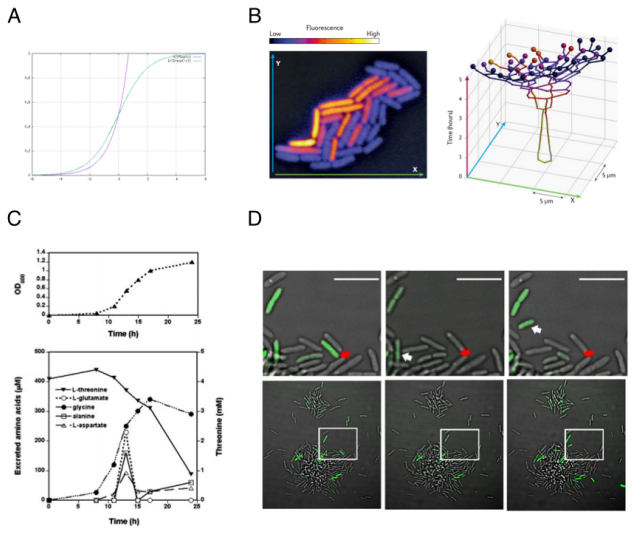

Figure 5.8: Environmental resistance and micro-scale local differentiation (A) Exponential (red) and logistic (geen) functions; (B) Individuality and differentiation, a 35 cell 2D cell population pic of snapshot on the Left panel and on the Right panel a spatial differentiation dynamics and lineage tree since the μ-colony was develop from one cell,Fluorescent level induction is controlled by flagellinC promoter; (C) Population development and habitat conditioning; (D) Quorum sensing activation and differentiation, scale bar= 5μm ; Images, modified from [194] (B), [195] (C), [196] (D).

can be observed (see Figs. 5.7D-F). An example of such μ-chamber population is shown here in Figure 5.7D where a single cell (i) of non-motile strain JM109 of *E. coli* grows into a small cluster of cells which later divides into two (ii) and then expands and begins to conquer space from the right side to the left side of the μ-chamber (iii) to finally cover all the μ-chamber and reaching a steady state consisting of a complex cellular network dominated by cell-cell attachments (iv). The detailed spatial structure of such a cellular network is sensitive to the chemical environment as shown in Figure 5.7E,F. Overlays of epifluorescence and phase contrast images to show the response of such cell network to exogenous auto inducer (AI) added to the media. Cells contain a reporter construct which induces GFP upon activation. At, 5nM (Fig. 5.7E) we observe the cells exhibit much more variability in their induction levels while at 10nM AI (Fig. 5.7F) concentrations not only produce higher average levels but less variability. The spatial structure of the network is also affected since at higher levels of AI, the network is denser since cell-cell connections are less abundant as strain JM109 separate more often after divisions and therefore grow less las linear filaments of cells attached at their ends.

In Figure 5.8A, we see a growth pattern with no environmental resistance resulting in an exponential curve (red), the simplest representation of the biology of constant growth at a single cell level. Therefore if we start with some scale of biomass $q_0 \equiv \ln N_0$ already accumulated at some time, the scale after some elapsed time t, is $q(t) \equiv \ln N(t)$ which corresponds to

$$q(t) = q_0 + r \cdot t,$$

where $r = \dot{q}$ is the growth rate. Due to a fact pointed out by Malthus, this geometric grow, and its associated ecosystem demand, cannot be matched by resources which is assumed to grow linearly. Therefore, we often observe that environmental resistance kicks in and does so in a heterogeneous fashion, such that not cells are affected and/respond differently. The simplest representation of these scenario is depicted by the logistic curve (green).

$$\phi(\tau) = \left(1 + e^{-\tau}\right)^{-1}.$$

The onset of environmental resistance is shown here in Figure 5.8B a strain of Salmonella enterica subspecies enterica serovar Typhimurium developing from a single cell to a 35-cells μ-colony (left panel). We can see the lineage tree (right panel). The level of fluorescent induction is controlled by a promoter and shows spatial heterogeneity in induction levels. A non-induced perimeter surrounds an induce core cluster. Here cell crowding is the obvious stressor. Crowding is a prevailing conundrum who's effects we have discussed in the context of single lineages, in the mother machine, as well as in macroscopic well mixed test tube cultures. In Figure 5.8C we can see how a batch culture of *E.coli* (top) can change the composition of numerous metabolites (bottom) as it develops from low cell density, into a stationary phase culture at carrying capacity [195], [197]. Although this is a mean field setting, it reflects the results of the behavior of single cells which regulate their cell cycle by switching from actively dividing $\uparrow$ to an inactive $\downarrow$ non dividing phenotype. In spatial cases, for example when a cell is attached to a biofilm cluster, we can see that QS induces individual cells to stochastically leave the cluster and disperse as shown in Figure 5.8D and reported in [196].

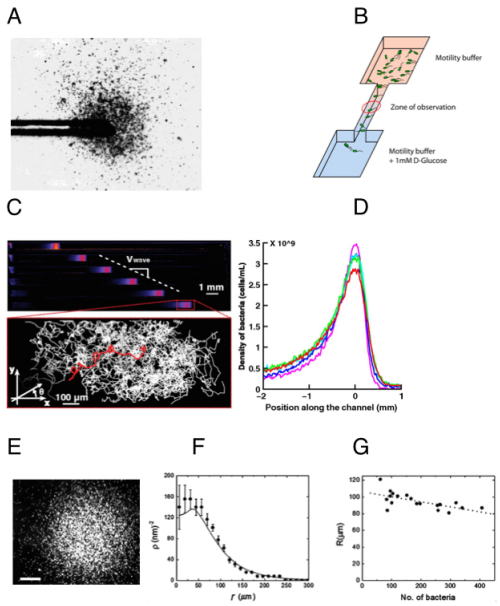

Figure 5.9: Population waves and propagule fronts. (A) Capilary assay showing, bacterial cells 'flocking' towards the source of a chemotactic gradient; (B) A two habitat-one channel device to study chemotaxis migration along a gradient; (C) Kymograph showing a bacterial population wave propagating along the channel (top) while each individual cell trajectory executes a run and tumble based random walk; (D) Wave profile of bacterial density along the channel; (E) Cell cluster formed by chemotactic aggregation; (F) Cell density vs cluster radius; (G) Distribution of radii vs cell density. Images, modified from [137] (A), [198] (B-D), [199] (E-G).

Dispersal, propagules, and travelling populations

When local conditions become unfavorable, individuals can disperse to a new suitable location. QS is necessary to sense space and reach active growth in confined droplet populations [200] as well as in triggering departure from a cell cluster [196]. When departure from the local environment takes place, motility is driven by chemotaxis [137], [198], [199]

In Figure 5.9A we can see a classical experiment [137] where *E. coli* cells swim towards a pipette tip following a gradient of attractant. Such behavior is advantageous when searching for suitable locations to attach and differentiate. In Figure 5.9B we depict a two patch system connected by a corridor where a gradient in glucose has been established. As bacteria swim up the gradient along the corridor a population front travels along the channel at a constant speed (see Figures 5.9C (top panel) and 5.9D) as individual bacteria perform bias random walks (see Figure 5.9C, bottom panel). Another example of how bacterial cells can regulate their run and tumble behavior and in

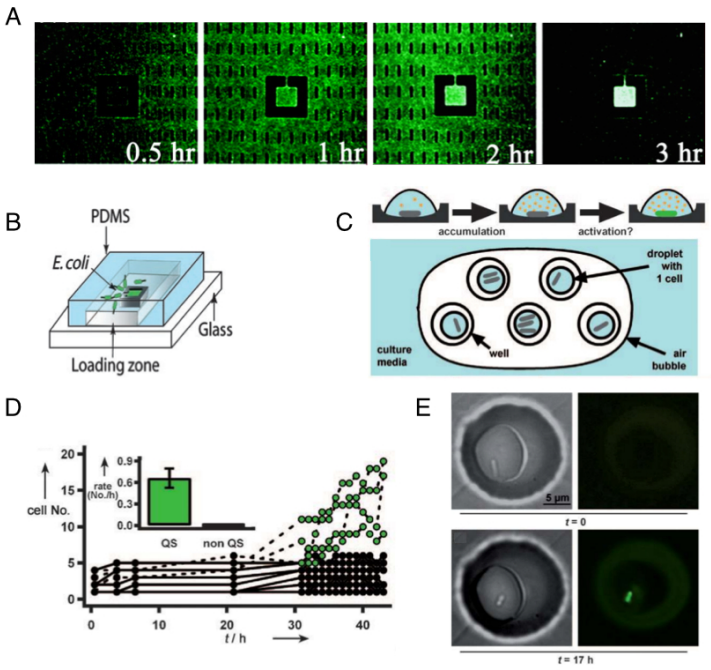

Figure 5.10: Sensing quorum and/or densities (A) Spatial population dynamics of a motile *E. coli* strain travelling as a population wave which passes by and self-congregates into a square chamber; (B) Sketch of the PDMS device used in A, (C) Sketch of droplet-based population device, where cell can be isolated and population can be grown from them; (D) After, 30 hours quorum sensing is activated in single cell droplets which start dividing (in green activated cells). (E) A tipical picture of the experiments that generate the data in D. Images, modified from [195] (A,B) and [200] (C-E).

this manner a spatially structured motile populations formed, Figure 5.9E. Here a ball of cells of a 100μm in radius (see Figure 5.9F) is achieved by inducing chemotaxic collapse [199] regardless of cell density as shown in Figure 5.9G. The lesson being, regardless of the stochasticity of single cell motility patterns, cell populations can self organise to either localised [199] or travelling populations [198].

5.3.2 Micro Habitat Patches

Populations can travel as a dispersal strategy. As soon as local opportunities are detected at some location, **recruitment** begins and a localized population is founded. This new sessile population undergoes different degrees of aggregation, integration, and differentiation. As shown in Figures 5.10A and 5.10B, spatial confinement can nucleate the recruitment of a sessile population in a given location and therefore induce cell localisation. Such colonisation phenomena and the

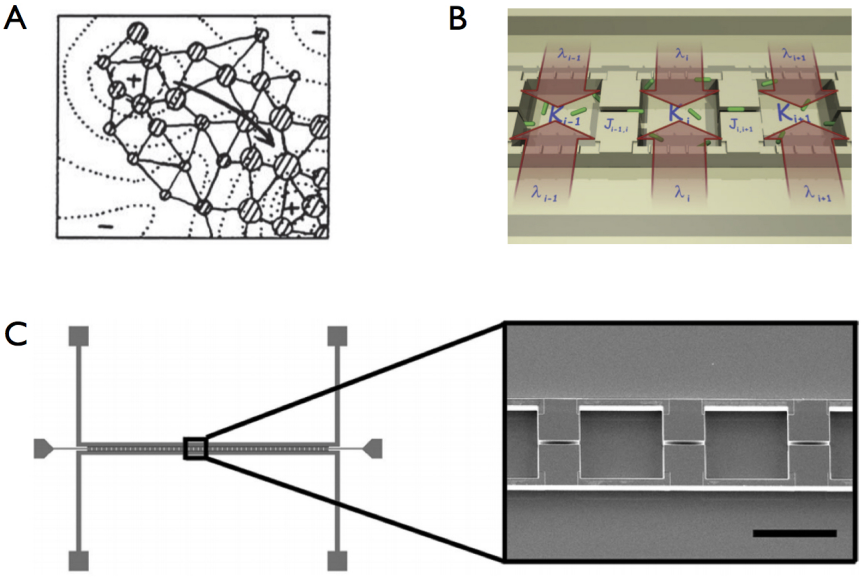

Figure 5.11: Microfabricated Habitat Patches (A) Sewall Wright adaptive landscape with a metapopulation of local races; (B) Concept of a linear chain of habitats with some capacity and renewal services; (C) TEM of microfabricated device, scale bar is 100 μm. Images modified from [201].

posterior extinction of the formed population due to depletion of growth conditions is the base for the theory of **meta-populations**.

Metapopulation theory

Colonization-extinction dynamics taking place at much larger scales of space and time give rise to a metapopulation. Richard Levins' [202] famous "population of populations" can be depicted, in the simplest mean field scenario, by tracking the proportion p of occupied habitat patches

$$\frac{d}{dt}p = \beta p(1-p) - \delta p$$

within the landscape given rates of colonization β and extinction δ. As long as $R_0 = \beta/\delta > 1$ the metapopulation will persist with long-term equilibrium occupancy of $1 - R_0^{-1}$. For a deeper insight on metapopulation theory see [203].

Local races and adaptive landscapes

Notice the scenario above assumes mean field like dispersal where all patches are accessible, in a more realistic lattice scenario, local correlations due to limited dispersal as well as adaptation to local conditions give rise to the emergence of local races. These provide stepping stone mechanisms [204] where a network of local races make-up a metapopulation spanning an **adaptive landscape** [205] characterized by fitness peaks and valleys. In Figure 5.11A we see an heuristic sketch of such network over an adaptive surface.

5.3.3 Bacterial metapopulation dynamics

With the discussion surrounding Fig5.9 one can emphasize a spatial scale over others, and permit cells to colonize an array of patches forming a network of locally adapted demes. In this light, habitat landscape constitute a crystal-like structure of repeated elements, where spatial confinement create a network of discrete **habitat patches** connected by **ecological corridors** which facilitates dispersal between patches. Using microfabrication techniques [201] we can implement a simple **array of microfabricated habitat patches** (MHPs) to model a spatially distributed habitat landscape composed of multiple μ-habitats locations.

MHPs are therefore individual islands of habitat able to support a local population with the most immediately needed services –space and nutrients. Notice, the act of living degrades local conditions, therefore these need to be restored for sustained persistence. This makes the implementation of **habitat renewal services** an important consideration! In Figure 5.11B we see a sketch of the MHP concept where at some rate λ_i, determined by the strength of coupling to a reservoir, growth media conditions in a given location i are restored. As life-cycles propagate from location to location, we need more than one of these locations and a way for organisms to disperse among them. The ecological corridors are confided spaces allowing propagule dispersal but not population development which we expect to localise on the MHP sectors of this crystal lattice. In Figure 5.11C we see a linear landscape consisting of 85 MHPs coupled to a reservoir of growth media by nano-slits on top and bottom sides of each MHP. The landscape is homogeneous in the sense $\lambda_i = \lambda_j$ for all MHPs in the array. Each of the MHPs in the array are 25 μm deep and have a basal area of 100×100 μm^2.

In Figure 5.12A we see a kymograph with the meta-population dynamics of E. coli WT strain

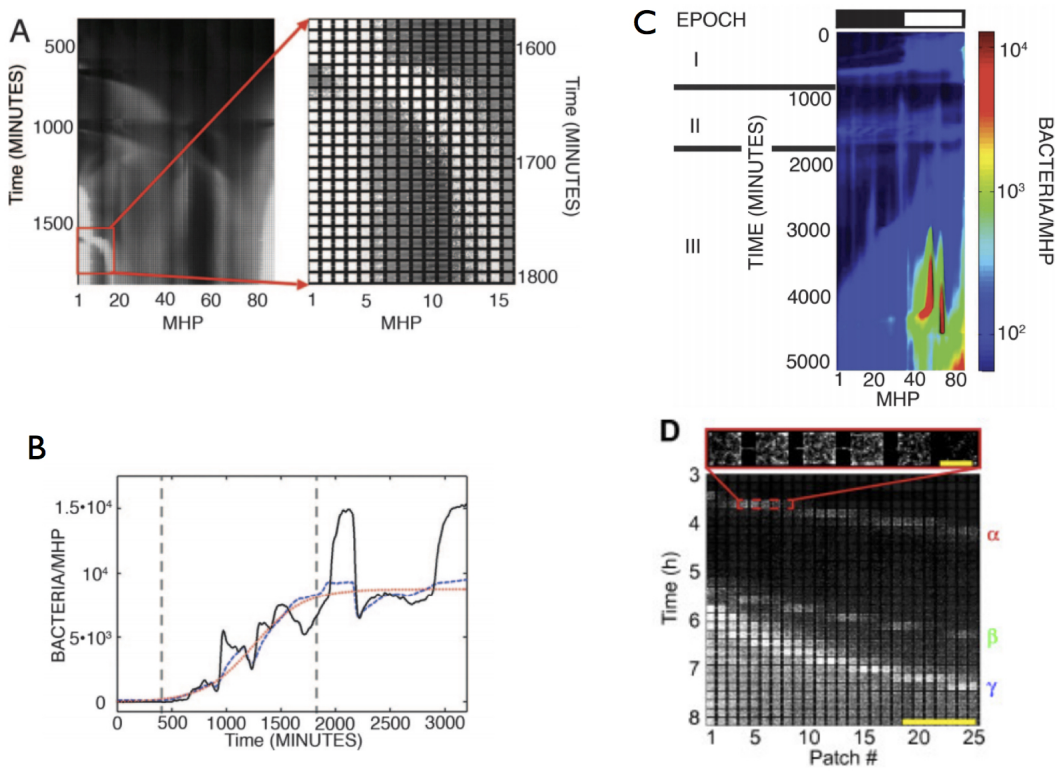

Figure 5.12: Bacterial adaptation to micro fabricated landscapes of habitat patches (A) Metapopulation dynamics in a all-open MHPs array starting from all MHPs inoculated at $t = t_0$. (B) Global $\Phi(t)$ vs local $\phi_k(t)$ densities (C) Two-region landscape made of NP and NR MHPS (D) All-closed MHPs, thus $\lambda_i = 0$ for all i.

(JEK1036) labeled with GFP growing in a device like in the one shown in Figure 5.11C. The data shown corresponds to images I_t taken 10 minutes apart and stacked on top of one another making a kymograph. On the right of the Figure 5.12A we see a zoom into an amazing **condensed structure** that is born between MHPs 1 and 5 after 20 hours of growth in the device. Further on it begins to branch into two similar structures where an aggregated mother sessile population gives birth to a daughter sessile population placed 5 MHPs to the right between MHPs 15 and 20. This **forking** raises many interesting questions. In the hours before, the bacteria has already broken up in into a network of local sub-populations connected by dispersal. Aggregation phenotypes emerge at multiple scales spanning multiple MHPs. Using the MHP as a unit of integration, we integrate fluorescent intensity in I_t for all pixels within an MHP located at k in the array and produce $\phi_k(t)$,

which if we can integrate across all MHPs gives a global landscape-wide density $\Phi(t)$. Figure 5.12B shows the global intensity $\Phi(t)$ in blue and $\phi_{k_0}(t)$ in black as well as a logistic fit to the dynamics of $\Phi(t)$ in red. By comparing Figures 5.12A and 5.12B the forking condensed structure only emerges after the global landscape has reached steady state at 1800 minutes (32 hours) post inoculation.

In Figure 5.12C depicts a plot of $\phi_k(t)$ for the same strain (JEK1036) cultured now in a **two-region landscape** where the left side of the array is made of MHPs with no service $\lambda_i = 0$ while the MHPs on the right side has habitat renewal $\lambda_i \neq 0$. These two regions are represented on the top panel in black and white respectively. Initially (Epoch I) after inoculating all MHPs at $t = t_0$, bacteria mostly prefer the white side of the landscape. After 24 hours (720 min) a wave to the left spread from the population has established on the right side. After numerous fast wave incursions into the black side during Epoch II, localized populations are established at several MHPs. Finally, in Epoch III a low density ($\phi \approx 10^2$ cells per MHP) front expands slowly across the landscape from right to left. Additionally, much higher density class aggregates ($\langle\phi\rangle_k \approx 10^4$ cells per MHP) develop at the landscape scale in the white region on the right side. This shows the role of $\lambda_i \neq 0$ in supporting higher density. Habitat renewal services also plays a role in supporting developmental complexity as condensed dynamic structures seem to only emerge in these MHPs. Are these complex structures only possible at high cell numbers? What are the levels of integration in these cell assemblages? In Figure 5.12D a series of **invasion waves** are visible, with pelagic motile populations, coming from the left, entering the array of MHPS. Initial conditions are now different as cells are inoculated only at the left inlet of the device and must swim into the array of MHPs. The array shown here has no renewal services ($\lambda_i = 0$) and slightly shallower depth (5 μm) of MHPs but otherwise of the same dimensions. Sequential traveling population waves α, β, γ of decreasing velocity and increasing density $\tilde{\phi}_k$ with $k \in \{\alpha, \beta, \gamma\}$, emitted into the landscape. We use tilde and greek index to distinguish delocalized travelling populations (propagules) from sessile or pelagic populations that are localized to a particular MHP; for this we use ϕ_i with $i = 1 \cdots 85$ for the case of Figure 5.12D. This emission phenomena was described by Adler [137] and depicted here in Figure 5.13A whereupon starting from a inoculation spot at the center of a soft agar plate containing growth media, radially expanding rings emerge. More specifically, a **mother colony** establishes at the inoculation site. After some development time it **emits a series of populations waves** which travel outwards over the habitat surface as rings. Inoculation in the case of Figure

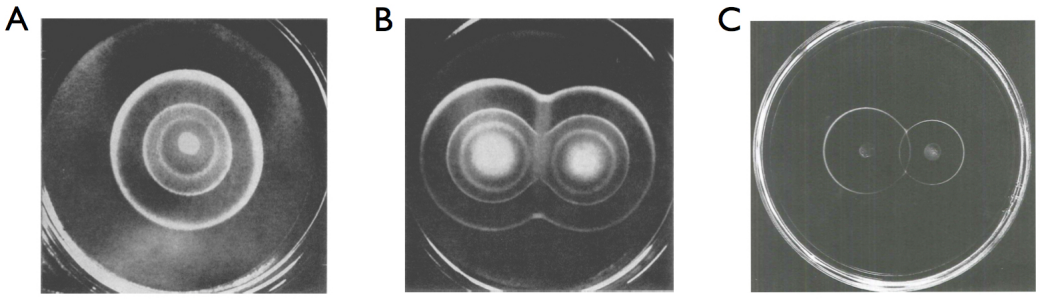

Figure 5.13: Adler rings occur when inoculating a soft agar plate with bacteria. (A) Adler rings correspond to population waves travelling away from the mother population; (B) destructive collisions between waves of the same metabolic type; (C) constructive collisions between waves of different metabolic type. Images modified from [140].

5.12D, leaves a single mother population in the inlet of the device. It is this mother population that is the source of the travelling population waves observed in the kymograph. For the case of Adler's rings they have been described to perform metabolic transformations as they travel through the surface of the agar plate. Each of these rings is made of cells metabolising specific nutrients from the growth media. Let's denote this set of components as $\mathcal{N}_k$. If two colonies of the same type, separated at a distance, emit waves, they will collide, coalesce and travel perpendicular to their direction before collision as shown here in Figure 5.13B. If we make sure the colonies are using different metabolic components $\mathcal{N}_k$ and $\mathcal{N}'_k$ with $\mathcal{N}_k \cap \mathcal{N}'_k = \emptyset$ then the mother colonies will emit travelling populations which DO NOT collide and exhibit constructive interference (Fig. 5.13C) at the collision point, instead passing one another. The question is can we guide these population waves in order to structure dispersal patterns? The answer is to guide microfabrication with principles from landscape ecology.

Landscape ecology and patch dynamics

As a sub-discipline of ecology, landscape scology is particularly interested in the role habitat distribution and abundance, located within a larger spatial context (the landscape), as well as the topological properties of such, play in effecting the works of ecosystems. Analogies between the connectivity of habitats within landscapes [84] and percolation theory [206] as well as other topics in condense matter physics have always been a bridge between ecology and physics. Most of the

concepts in landscape ecology evolved from the theory of island biogeography [207]. Opportunity comes in patches at multiple scales of space and time [208]. From the point of view of life cycles, every location is transitory and to propagate from location to location is life's final dilemma.

Island biogeography The Theory of Island Biogeography (TIB) attempts to explain the diversity of species present in islands in terms of their two attributes: (i) island size, and (ii) distance to a main land. In these efforts it connects the biology of populations with spatial features (area) of discrete units of habitat (patches) and their distance to a mainland harboring viable populations.

The connection is provided by a balance between colonization-extinction processes as well as characteristics of metapopulations to predict the equilibrium biodiversity of the island. By considering features of the island, such as the the size and distance from the mainland, important ecological features like island carrying capacity, local extinction rate and colonization rate change.

An observer following the dynamics of small islands, far from a mainland, are likely to see low colonization rates and high extinction; given a smaller size, stochastic events are more likely to drive newcomers to an untimely local extinction. On the other hand, large islands in close proximity to mainlands are likely to see high rates of colonization from the mainland and low rates of local extinction given its abundant space/resources. Following some period of time, once the island converges to its carrying capacity, a balance must be made between rates of colonization and extinction. In this way, newcomers are less likely to find success upon arriving to this saturated island and, given the packing, currently established species may be driven to extinction. Thus the island itself will go through different phases, such that the species present will also change over time, shifting from fast colonizers to superior competitors. The details of which we will discuss further in 5.4.1.

The role dispersal in supporting co-existence Thinking on a system of n species ($\mu = 1 \dots n$) distributed over m connected patches ($i = 1 \dots m$), Levin [209] studied,

$$\frac{d}{dt}\phi_i^\mu = F(\vec{\phi}_i) + J_{i,j}^\mu. \tag{5.3}$$

Where the reaction term, $F(\vec{\phi}_i)$ represents community dynamics (see Section 5.4) and $J_{i,j}^\mu$ the migration of species μ from patch j into patch i. Focusing on a two patch system [210] shows how

dispersal can stabilise coexistence between competing types at both within patch (local) as well as at the landscape level (global). Thus when considering competition between types, breaking up habitat into smaller connected units can favor coexistence. Thus by using confinement, ecological corridors act as wave guides for dispersing populations. When connecting MHPs with such corridors we allow for **dispersal strategies** to be exhibited by the bacterial population. Dispersal, in turn, opens up a space of coexistence for different types of bacteria to coexist in the system. These different types can be species, strains, or alternative functional phenotypes from genetically similar cells. By imposing a regular structure of confinement defining patches (MHPs) and corridors we force the cells to partition between traveling $\tilde{\phi}_k$ and localised sub populations ϕ_k.

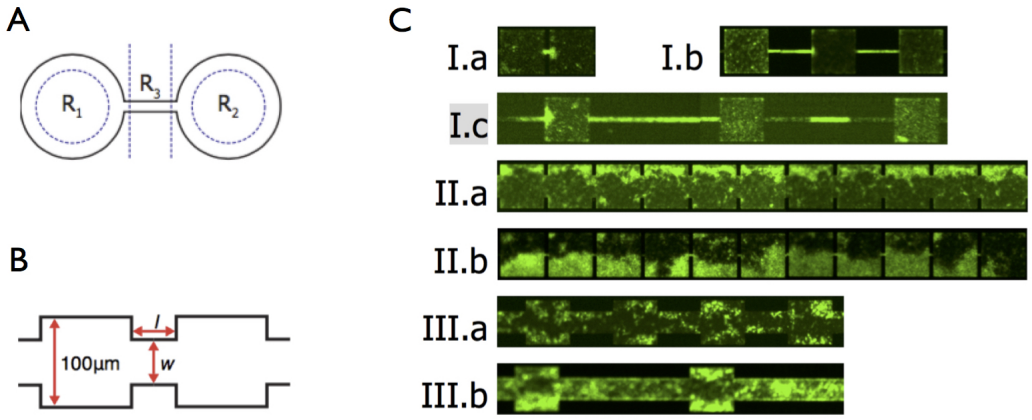

Figure 5.14: Lanscape ecology and microfabricated confinment (A) Compact domain of habitat $\mathcal{H} = R_1 \cup R_2 \cup R_3$. (B) Idealize MHP dimensions where an habitat patch is distinguished from an ecological corridor. (C) Different microfabricated landscapes with different geometric parameter l and w of the ecological corridors connecting MHPs. Images modified from [211]

The role of confinement in supporting inhomogeneous distributions The continuous analogy of the system represented by Equation 5.3,

$$\frac{\partial}{\partial t}\phi_i^\mu = F(\vec{\phi}) + J^\mu \tag{5.4}$$

was studied by [212] over a compact domain like the one shown here in Figure 5.14A. If the system considering only the reaction term ($J^\mu = 0$ in eq. 5.4) has multible stable states, then the full

system ($J^{\mu} \neq 0$) allows for non-uniform solutions provided that the connector region R_3 is narrow enough compared with regions R_1 and R_2. The lesson to be learned is that the shape of the domain matters! It matters not only to make quorum and other social concerns of individual cells but it allows for coexistence of local demes (slightly different and localised populations) and travelling populations acting as propagules of a dispersal strategy. The frequencies of trans-locations between patches is then a new axis of differentiation [213]. In Figure 5.14B we see a sketch of two-patch system where two MHPs are connected with an ecological corridor of length l and width w. In Figure 5.14C we can see that by growing our familiar friend JEK1036 in three different corridor geometries (I, II, III) we can see how the results of [212] inspired the work of [201] when choosing parameters of ecological corridors. Long and narrow corridors (type I) are well suited to localise the demographic process to the MHPs and regard them only as connectors with a small effect upon the local population dynamics. In type I geometries where patches and corridors are well defined, populations partition into localized and travelling populations.

From biofilms to dynamic clusters

The scale at which cells modify their surrounding environment is enormous. This presents the greatest challenge when applying ecology to understanding cell assemblages. Very quickly, cell-to-cell signalling mechanisms give rise to coordinate collective behavior. The level of coordination and the extent such behavior modifies the environment is tremendous. Early examples of bacterial collectives like biofilms 2D, in MHP ecosystem we see large condensed structures capable of amazing coordination.

Synchronisation We know that cultures of *E. coli* can be synchronised by shifting cells from a key point in development, entry into stationary phase, back to fresh media [214]. In Figure 5.15A we can see how cells from entry into stationary phase (red) and not in other phases of growth (blue) are synchronised when shifted to the fresh media. Revisiting these results under the light of Figure 5.12A, we wonder how the pattern of synchronicity of cell division and the assumption of overlapping generations apply to members of a condensed structure like the one observed. If generations do not overlap and reproduce in sync we must replace Equation 5.2 by the logistic map

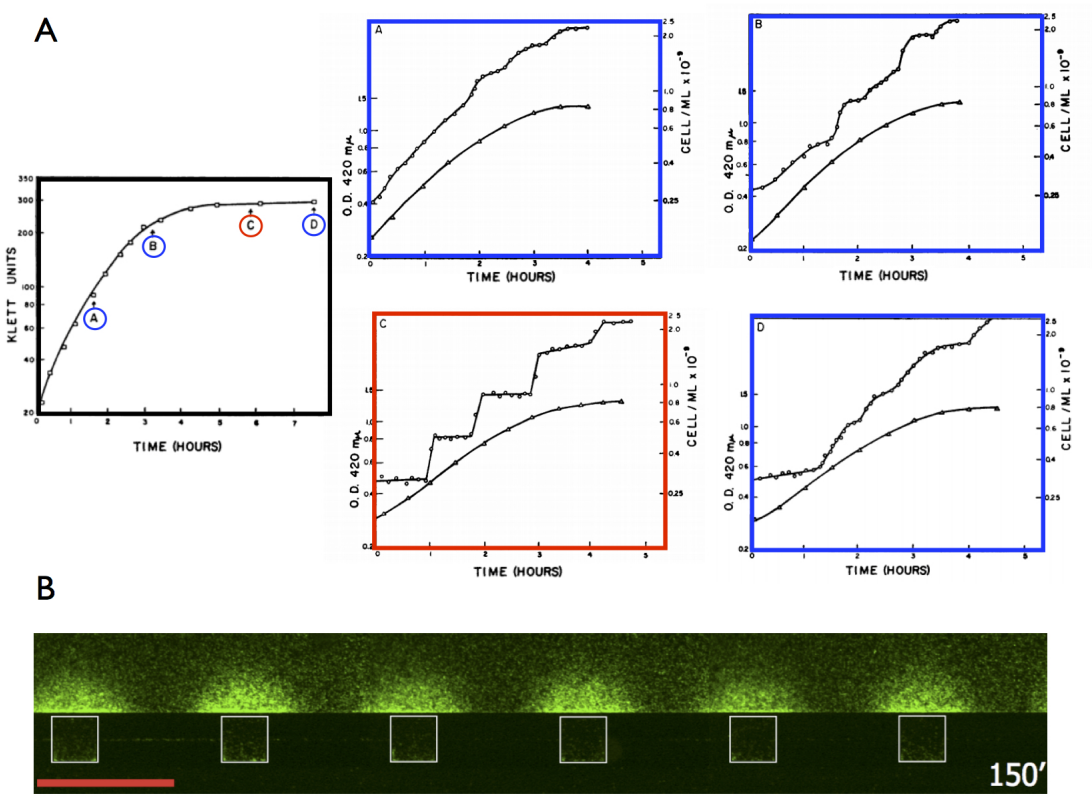

Figure 5.15: Synchronisation of division and coordination of swimming. (A) We can Sync cells by stationary phase method. Imaged modified from [214] (B) Cells coordinate their swimming in response to demographic states of near-by populations. Scalebar is 300 μm. Imaged modified from [211].

$$\phi^{t+1} = r \cdot \phi^t \cdot \left(1 - \phi^t\right) \tag{5.5}$$

which opens the door to all the complex associated dynamics [215].

Localization As bacteria are know to aggregate attracted by self-produced chemical gradients they can produce complex patterns of localisation at the level of swimming cells [199] in bulk cultures as well as in MHPs [211]. In Figure 5.15B we can see how as cells condition MHP environments, chemical gradients attract populations in the reservoir. These populations can aggregate in response to gradients generated by another population living within the MHPs in the array. These aggregates are dynamically created and destroyed and localise to the nano-slits coupling between reservoir and

the MHPs. MHPs undergo a cycle of colonization, grow and conditioning, and local extinction. After being exploited and degraded (conditioned), a location can renew its habitat thanks to the ecosystem service of habitat renewal which is provided by nanoslits. As locations can be re-set to suitable state, spatial ecosystems are excitable media and population outbreaks act as excitations that travel the landscape of patches. Here the population in the reservoir acts as an indicator of patch dynamic regimes of the MHPs.

5.3.4 Population waves and metabolic entanglement

An interesting lesson about collective identity in bacterial colonies can be obtained by colonizing a simple 1d MHP array from opposite ends by 2 strains that are only different by a neutral marker.

Initial conditions A **very important consideration** to make when thinking about competition between bacterial strains are the initial conditions used when inoculating the microfluidic devices. The experiments which start with a 1:1 spatially homogeneous mixture of two strains are different of experiments which start with bacteria colonising as they expand their range in a microfluidic device. This is due to the extreme level of habitat conditioning.

Strain identity and marker neutrality

To see this phenomena we can think of two strains that are only different on a neutral marker but which behave the same as they are genetically identical except for the genetic locus of the marker. in Figure 5.16 we show two strains of WT *E. coli* which we paint with fluorescent proteins (FP). When using neutral markers on the same genetic background such as WT strain of *E. coli*, we should expect coexistence regardless of the original abundances. Moreover, given enough time, relative abundances should converge to equal partitioning. Images in Figure 5.16 use these neutral markers to distinguish between WT strains JEK1036 marked with green FP (GPF) and WT strain JEK1037 marked with red FP (RFP). Both markers are inserted in the lac operon and induced with IPTG and are expected to have no influence in population performance and except for this

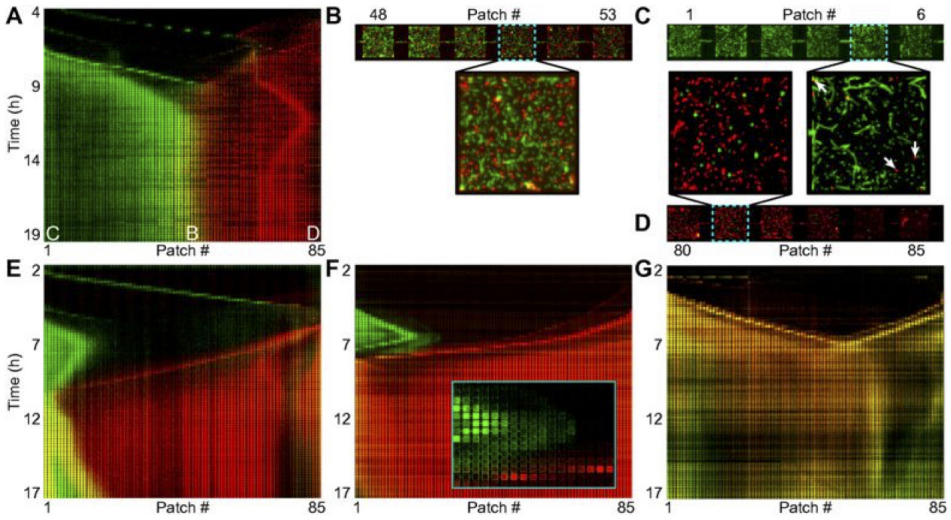

Figure 5.16: Self or non-self? Inoculating a device like in Fig. 5.11B with $\lambda_k = 0$ with strains only different by carrying GFP or RFP at the lac operon. (A) Red and green strains coming from opposite sides come to a division of the array with no mixing at the landscape level. (B) At the middle of the array, around MHPs 48 and 53 we see coexistence of both cells in similar abundance at both extremes we find cells of the other type as minorities within a majority of green as shown here for MHPs 1 and 6 (C) or red (D) for MHPs between 80 and 85. (E) In some experiments one type (red) displaces the other from the array. Here we see that after an initial incursion across the landscape made by a travelling green populations, a red front progresses from right to left until conquering almost the whole landscape. (F) Action at a distance is observed in experiments where biofilms seem to communicate from one extreme of the array to the other. In the inset we see the green population turn around before the red front moves in. (G) If a well-mixed mother population was made 1:1 before inoculation and then from this yellow mix we inoculate from left and right sides, the mixture never separates even though its spatial distributions presents zones of high and low abundance. Images modified from [216].

locus, the strains are genetically identical. Thus from Equation 5.2 we get

$$\frac{1}{N_i}\frac{d}{dt}N_i = r \cdot \left(1 - \frac{1}{K} \cdot [N_i + N_j]\right), \tag{5.6}$$

for $i \neq j \in \{R, G\}$. As populations develop however, they secrete small molecules which cell membranes are permeable to and therefore connect the metabolic status of cells near-by. Populations also actively regulate transport of amino acids that act as chemo attractants and repellents shaping motility patterns. This allows populations to develop a sense of identity that goes beyond sharing the genetic background of their ancestors.

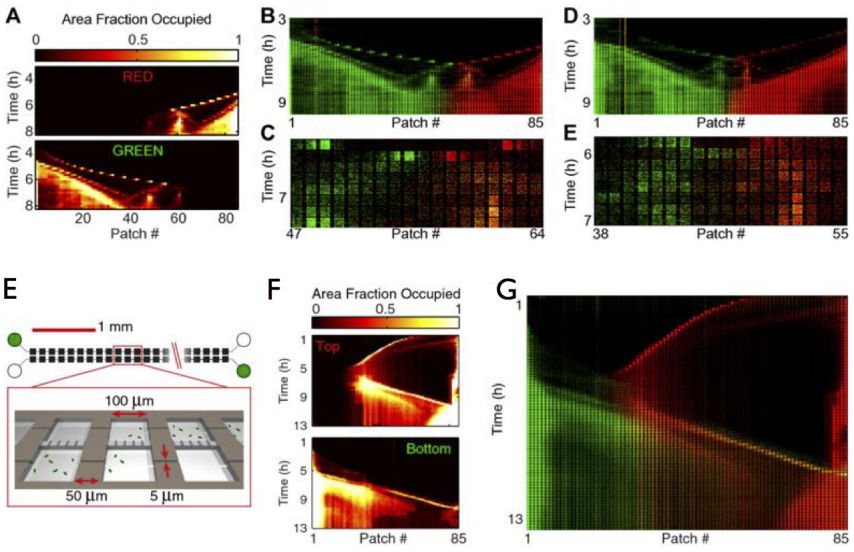

Figure 5.17: Collisions of population waves. (A) occupancy (top panel) calculated from images from the red (middle panel) and green (bottom panel) channels. (B) A typical collision observed between 3 and 9 hours of growth during initial invasion. (C) Zoom into the collision seen in B. (D) A similar collision as shown in B, but occurring on a different array of patches inoculated from the same mother population as B. (E) Zoom into the collision seen in D. Images modified from [216].

Biofilm action potential and electric communication

Besides quorum sensing [217] an incredible recent discovery is electrical communication in *bacillus subtilis* biofilms. The work of [218, 219] open up new possibilities. For example, we no longer find the long-distance interaction in Figure 5.17F so weird since this type of communication could easily explain time-scales of repulsion.

5.3.5 Landscape ecology and the evolution of antibiotic resistance

Interesting results have emerged from work in MHP landscapes in order to probe the relationship compartmentalized landscapes and adaptation to antibiotic gradients. A two-patch MHP array with a sharp gradient over the connecting ecological corridor known as *heaven and hell* (see Fig. 5.20); and a 1200 hexagonal array of MHP with a gradient over many MHPs know as the *dead galaxy* (see Fig. 5.22). These studies show similar as well as contrasting results regarding the dynamics of range expansions into antibiotic regions of a landscape.

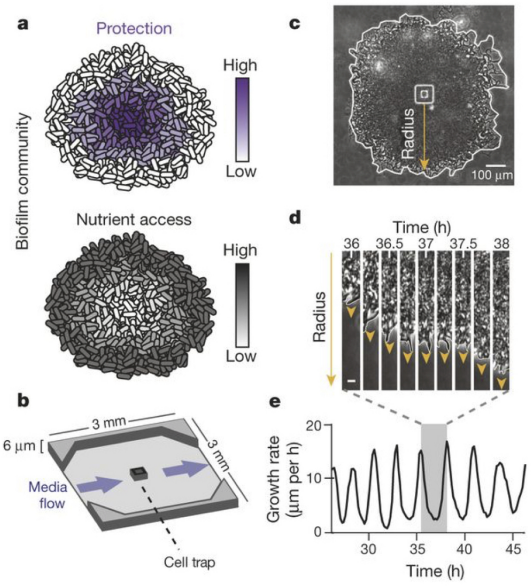

Figure 5.18: Electric communication and coordination of metabolic activity. (A) as a function of location in a cluster (a ball of cells) cells at the core have better physical protection (top, in purple scale) while cells in the outer shell have access to fresh nutrients (bottom, in grey scale). (B)Microfluidic device used where a local population is grown in the patch at the center. As flow is high, only this patch provides cell with protection from advection. (C) Picture of the central area of the device shown in B, where we see the growth of a cell cluster of radius r. (D) We see a radial colection of pictures where we can see the the cluster dynamics indicated by the size of the radiius in time $r(t)$. (E) We can see how the growth rate $\dot{r}(t)$ in time oscillates between grow and not-grow regimes. Images modified from [219].

Heaven and hell

The work of [220] considered a two-patch environment where one side corresponds to heavenly conditions given by a reservoir under constant flow of fresh media and another side corresponds to hell; that is the same media but with the presence of kanamicine antibiotic at 50 MIC concentration. Figure 5.20 shows the 2-patch stems of MHPs which are 8 mm long MHPs 100 μm wide and 10μm deep with nano-slits all over the sides which connect to the other MHP via a 100 μm long 5, μm wide, and 10 μm deep ecological corridor. Figure 5.21A shows the sharp antibiotic gradient which goes from 0 mg/L to 50 mg/L over a distance of 3mm; here distance is measured with respect to the center of the ecological corridor connecting heaven and hell MHPs.

In Figure 5.21B we can observe a kymograph of strain JEK1036 invading *hell* after some meditation living in *heaven*. How is this range expansion accomplished? As initial conditions, the device

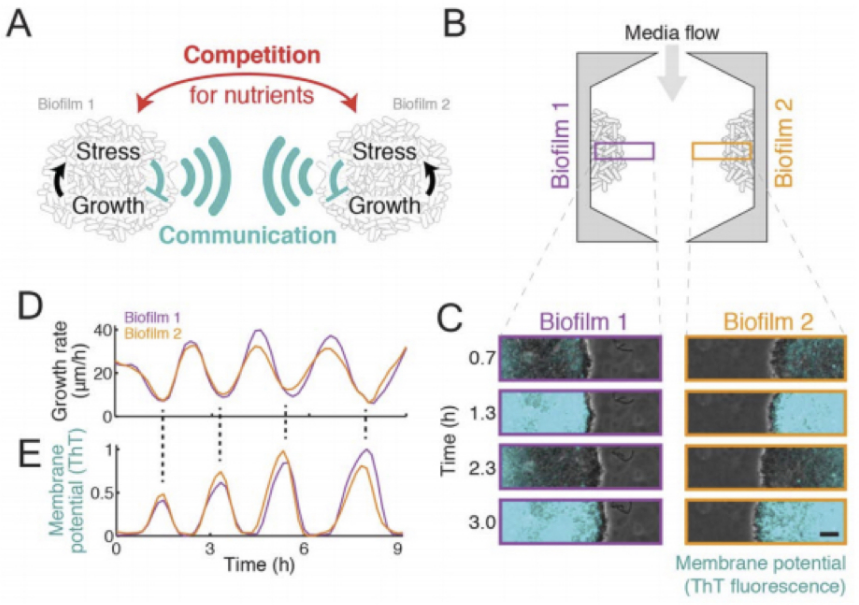

Figure 5.19: Electric long-distance communication (A) two biofilms of *bacillus subtilis* communicating at a long distance via action potentials. (B) Sketch of the micro fluidic set up. A strong (cells cannot swim up stream) flow separates two growing biofilms at each side of a device like in Fig. 5.18B. (C) Two spatial time series from the left and right biofilms. Time series are pictures of thioflavin die indicating changes in membrane potential on the regions indicated by color boxes in B. (D) Biofilm growth rate $\dot{r}_k(t)$ where left and right populations are in phase. (E) Thioflavin signal proxy for membrane potential. Images modified from [219].

is inoculated from the left inlet, from were a founding population establishes itself in heaven. As we can see in the figure, at the beginning from 0 to 2 hours into the expansion, cells coming from the left establish themselves at -4mm at the center of the heaven MHP. From here they keep expanding towards the right approaching the corridor at 4 hours approx. There in region 1 (in red) the motile populations stop progressing through the landscape and localize along the far right of heaven; at this time, in the far left of heaven, at -8.5mm a large population has also been established. At $t = 5$ hours, dense aggregates forming a collection of satellite subpopulations resemble a propagule rain metapopulation [221] with the largest aggregate acting as a main land population. From the border satellite population, at 5-7 hours, we see evanescent waves of motile populations penetrating hell without establishing a local population, that is localized and of high abundance. After 7 hours, however, we see a solid range expansion into the right side of the landscape. After 12 hours the metapopulation system has stabilized, including a large population located at 4mm in hell. When

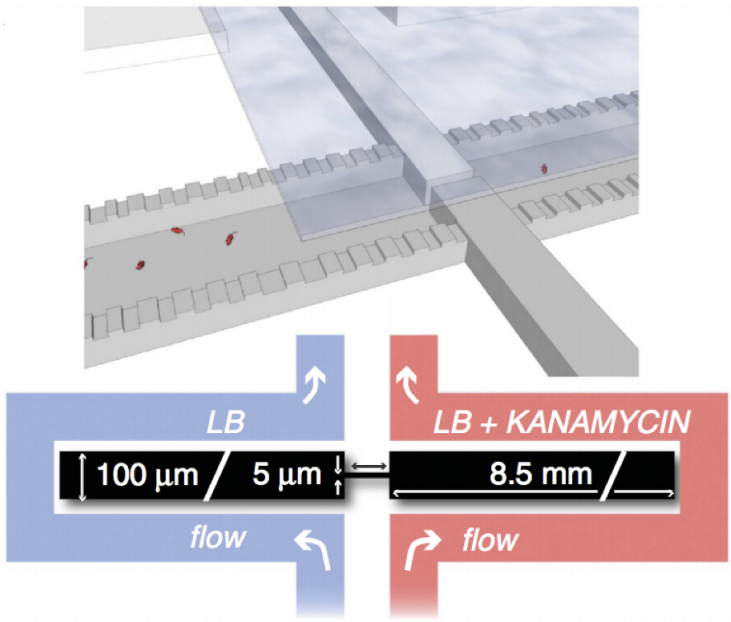

Figure 5.20: heaven and hell landscape consisting of a two-MHP environments where one MHP (heaven) is coupled via nanoslits to a reservoir with constant flow of LB (in blue in bottom panel) while another MHP (hell) is coupled via nanoslits to a reservoir with constant flow of LB + antibiotic. Images modified from [220].

[220] looked into what type of motile population densities allow the foundation of localized sessile settlements in hell, they found that a critical cell density is required. A successful colonization of the antibiotic compartment was observed after a few hours (less than 10) in 4 out of 10 independent experiments where all these motile pelagic populations of high density were observed.

The emergence of adaptation Surprisingly, colonization of the antibiotic compartment is not caused by genetically encoded resistance. When [220] test extracting cells from hell after successful colonization events they do not find changes in the genetic composition of the strains and the cells isolated from the device lose all capacity of living or dividing under the same antibiotics. The phenotype, is only observed on-chip when invading motile populations exceed a critical local density $\tilde{\phi} > \phi_c$ In the four experiments where bacteria successfully conlonized hell [220] isolated cells from the devices after 15, 18, 29, 61 hours after the invasion. Only after 61 hours they could find genetic resistance where a single site mutant emerges for gene cydA. The MIC of this isolated mutant showed a 25-fold increase of the MIC. Contrastingly, the MIC of the bacteria isolated at 15,

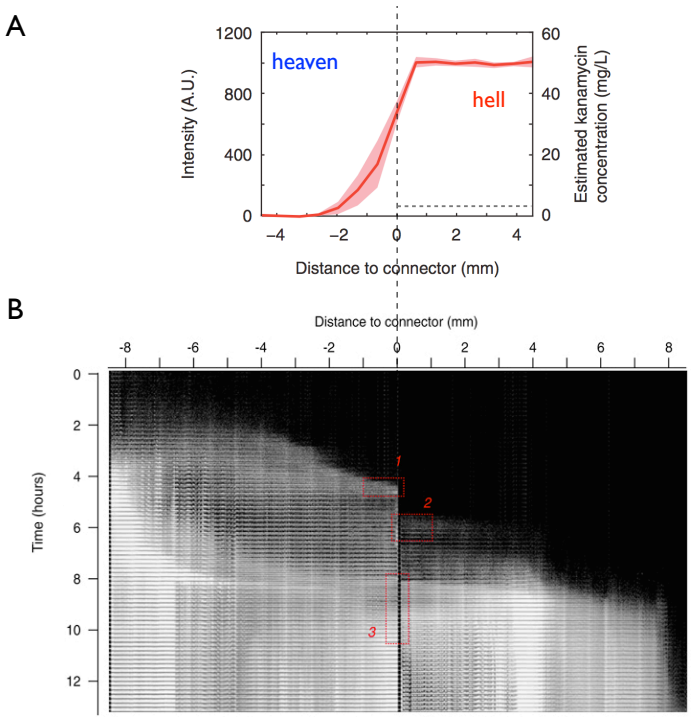

Figure 5.21: Sharp antibiotic gradient and metapopulation dynamics (A) A sharp antibiotic gradient where kanamicin concentration goes from 0 mg/L to 50 mg/L in 3mm distance. (B) Kymograph of JEK1036 strain exhibiting metapopulation dynamics while growing in a heaven and hell device like sketched in Fig. 5.20. Images modified from [220].

18 and 29 hours was identical to that of the ancestral strain! For an adaptively resistant ancestral population successfully colonizing this antibiotic landscape, what role does prolonged exposure play, if any, in the emergence of genetic resistance?

This finding highlights the importance of **adaptive resistance** as a route for bacteria to acquire heritable resistance. The persister phenomena is well documented, and [220] documents the case of a **density-dependent persister** phenomena where a persister phenotype is exhibited only at a population level when local density is above a needed quorum. Microbial persistence is a widespread phenomenon in which a subpopulation of microorganisms is able to survive antimicrobial treatment without acquiring resistance-conferring genetic changes. This local population serves as an evolutionary reservoir from which genotypic mutants may emerge [222]. For the case of kanamicin and a sharp gradient between two MHPs [220] finds that in 10 hours emissions which come from a mother population and which have a local density larger than a critical value can colonize antibiotic

regions without having incorporated mutations into their genome. The emergence of genetic mutants only happens after 61 hours.

Dead galaxy

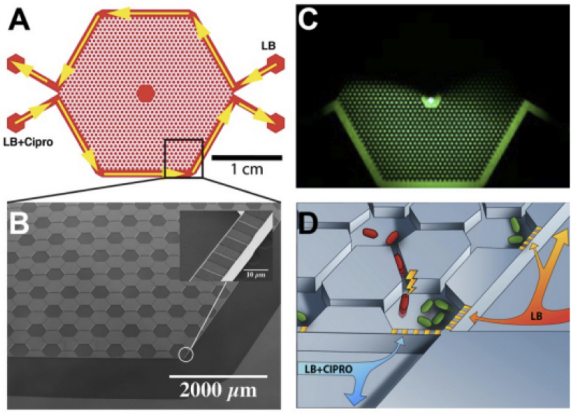

Figure 5.22: Dead galaxy is a landscape consisting of MHPs arranged into an hexagonal lattice which is sandwiched between reservoirs on the edges of the array. Three sides on top (A) contain rich media and the other three sides at the bottom (A) with antibiotic CIPRO. Inset in (B) show how MHPs at the edge of the array are connected to the reservoir via nano-slits. In (C) we see fluorescent marker flowing in the bottom reservoir channel and the gradient it generates over the lower half of the MHP array. (D) Sketch of the device. Images modified from [223].

In a pioneering application of MHP technology (see Section 5.3.2) to the study of adaptation to antibiotic gradients [223] studied a device made of 1200 hexagonal MHPs 10 μm deep each of the MHP's 6 sides are 200 μm long and connected to neighboors via six ecological corridors which are 200 μm long, 10 μm deep, and 10 μm wide. This array of MHPs is sandwiched between reservoirs on the top three and bottom three sides of the hexagonal landscape (see Fig. 5.22). In Figure 5.22C we can see that a gradient (green fluorescent) can be produced by flowing antibiotics along the lower reservoir compartment. This reservoir is connected to the MHPs at the three lower sides of the hexagonal landscape as shown here in Figures 5.22B and 5.22D. Although the geometry and dimensions of the array of MHPs used are different, there are striking similarities between this and heaven and hell studies. One important chemical difference is the type of antibiotic and another important but ecological difference is the relationship between the scale of patches and the steepness of the antibiotic gradient.

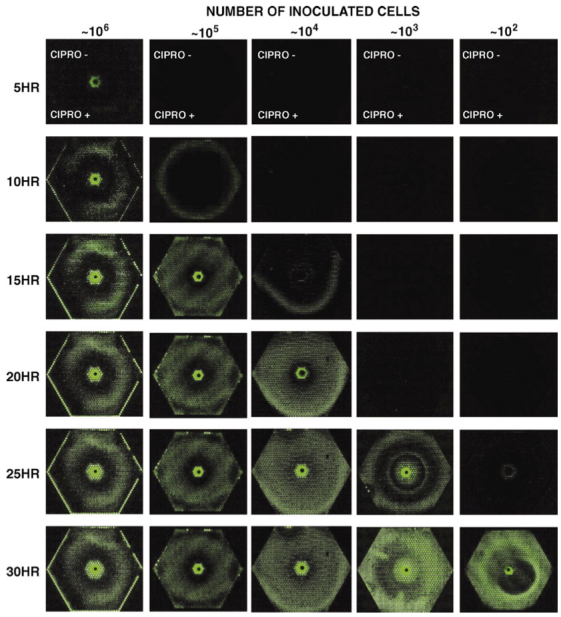

Figure 5.23: Rapid evolution Fluorescent WT strain inoculating at the center of a device as shown in Figure 5.22. Rows correspond to time t in hours after inoculations and Columns correspond to initial density at inoculation. Images modified from [223].

Rapid evolution One difference in the dynamics is the time scale for the emergence of genetic resistance. Unlike [220], who see the emergence of genetic resistance after 61 hour; [223] see the emergence of mutants after 10 hours. This **rapid evolution** is truly impressive and has been the source of inspiration to research further into what is the role of the landscape ecology of microenvironments in allowing us to design novel therapies for understanding resistance in other cell systems [224, 225]. Figure 5.23 shows a typical experiment of [223]. Similar to the results by [220], the successful invasion into the region of antibiotics depends on cell density. This time, the density of the inoculant into the device. If the initial density is $\phi_0 \approx 10^6$ cells/L (left row in Fig. 5.23) then a mother population which establishes at the center of the array, emits a travelling population which radiates outwards and penetrates the antibiotic zone. We also see that as the initial density de-

creases (figure columns towards the right) we see a delay in the emission of the travelling population but when it is emitted it travels into the antibiotic area. The striking result from [223] is that when sequencing cells right after invasion, these already have incorporated beneficial mutations which can be inherited to descendent populations.

5.4 Ecology of communities

Biocenosis [226] is Moebius's idea of thinking on a certain locus in physical space where biological interactions take place among individuals of different sorts, but under otherwise equal physical and chemical conditions; we call this locus a **biotope**. All living systems co-occurring in this place, correspond to an **ecological community**. In such an ideal community, the strength of ecological interactions depends on patterns of co-occurrence among the different organisms under consideration. To refer to these organisms considered together with the physical and chemical conditions, Tansley [227] coined the term **ecosystem** in order to avoid assuming the biological reality of these "communities". From his perspective, organisms belong to ecosystems and not to communities which are abstract concepts. The realism of the concept depends on the scale of spatial and temporal fluctuations defining the biotope and how they compare to the scales of a group of interacting life history strategies. Note that some branches of the tree of life will couple more strongly to certain scales and processes in the landscape. Therefore, when addressing the question about the level of integration and correlation among organisms belonging to a community in a given instant of time, views of ecological communities range from loose to tight associations. Along this spectrum of **symbiosis**, we are always thinking of interactions between individuals living in some place on Earth, observed at some scale of grain and extent in both time and space [228, 208]. Moreover, we think of a "test individual" and its biological context in a given biotope and ask for its fate when co-occurring with others. Physical and chemical conditions are averaged by the life histories at different scales and not necessarily in a congruent fashion. This if the first difficulty which makes us fully understand the resentment of Tansley.

At a geographic scale, we can recognize a pattern in the distribution of **vegetation types**. As plants and the water cycle are related, due to transpiration processes, they are tightly coupled with the climate. Characteristics of a location such as average annual temperature and precipitation are strong determinants structuring plant communities. As plants are macroscopic autotrophs, they are the primary transducers feeding energy into the heterotroph component of the ecosystem. An example of these large scale regularities are the famous Holdrige life zones [229]. At a smaller scale, we can still see tight symbiosis and therefore refer to them as community structures; plants and their communities tend to form characteristic tight associations, *vegetation formation*. Such unity

and stability of structure, lead to the notion of the **climax community** which was introduced by Clements [230] within the context of plant communities.

5.4.1 Climax community

Under the view of a **climax community**, a group of interacting types (species), which would eventually after some transient dynamics reach a stable equilibrium composition know as the climax. This developmental process of the community parallels concepts from TIB discussed in 5.3.3, where the composition of biomass changes over time. Upon some local disturbance, a negative physical or chemical fluctuation which destroys the climax state, a process know as **ecological succession** takes the state back to the climax configuration. As long as the physical factors are constant, the community is stable at some dynamical attractor which is characteristic and unique. The climax is thus a global attractor for the local (within biotope) dynamics. After a forest gap is open by disturbance, is returns to its previous state. On its strongest interpretation, the climax concept has been abused [227] to the level of considering communities like pseudo super organisms with their spatial boundaries being co-determined by strong physiological integration of its individual members. On the contrary, we have the view promoted by Gleason, where such boundaries in space and time will be determined by individual species responses to physical factors [231].

Primary and secondary succession

An importance difference is before and after **soil**; a fundamental ecosystem which is created by life after a surface of bare rock is expose to the biosphere. Soil formation involves a sequence of active processes of chemical transformations over the primary surface which culminates with the generation of a soil ecosystem over a long period of time. Such **niche construction** process is very slow. After soils have been constructed they provide the support for vegetation. Different vegetation types will undergo secondary succession after a local perturbation produces a state away from the climax state; this will be transiently dominated by r-selected types and later on by K-selected ones until converging back to the climax state.

Species, local races, functional types and other categories

Although the notions discussed above focused on macroscopic life-forms; at this scale of biological organisation, and after Linneus, we are thinking on many-cell individuals belonging to a clearly defined **species**. As the species concepts do not clearly apply to bacterial cells, we can ask how much can we apply this concept to co-cultures of different strains of bacteria. Macroscopically we could also ask, how about co-cultures of local "races"? A typical attitude among researchers is to take it as homolog to strains of a given "species" of bacteria; for example, let's consider a community composed of two-strains of *E. coli* bacteria in co-culture in an array of MHPs.

5.4.2 Spatial distributions of two-strain bacterial communities

Species, have habitats which distribute in space, as habitat is degraded, nature restores it and sustainability is possible. The temporal scale and spatial extent of ecosystem services for such habitat renewal are of critical importance when considering bacterial communities due to very intense habitat conditioning.

Habitat landscapes and the spatial distribution of ecosystem services

In Figure 5.24 we focus our attention to co-cultures of two strains of *E. coli* living in two types of micro fabricated habitat landscapes. These landscapes are made of the same number and the same type of MHPs but arranged in a different global topology. These type of MHPs correspond to one with no nano-slits which we refer to as nutrient poor (represented in grey) and another with full number of nano-slits (represented in white). In Figures 5.24A-C we alternate these types of MHPs and in Figures 5.24D-G we arrange so to make a landscape with to large-scale regions: half with one type of MHP and the other with with the other.

Growth Advantage in Stationary Phase (GASP) Long after a culture of a **wild type** strain of *E. coli* has reached long-term stationary phase, mutants emerge and take over the cultures [234]. These mutants have a competitive advantage over the wild-type when they find themselves in a background stationary phase wild type population. To achieve this feat, the mutants invest in scavenging for resources and move towards the K side of the $r - K$ spectrum. Although, these two types of *E. coli* strains represent two different physiological strategies, they are currently considered

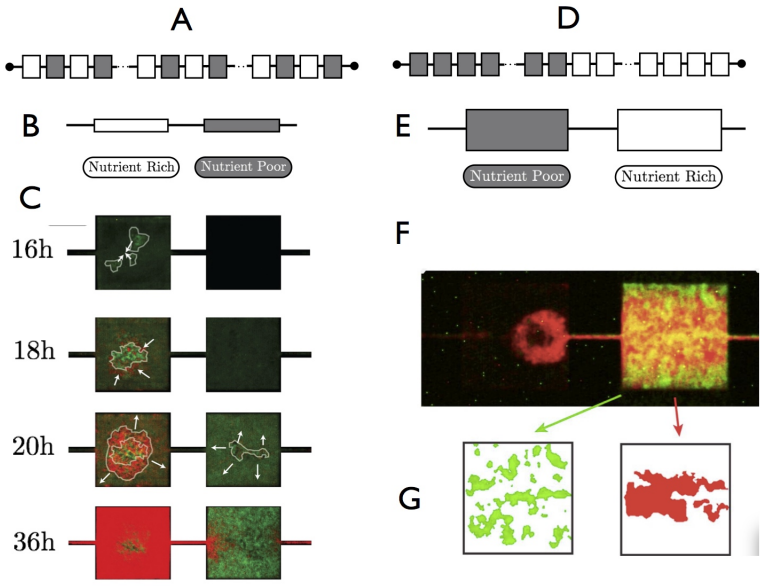

Figure 5.24: Two types of *E. coli* in two types of habitats which are different on their spatial distribution, in (A) we see an **alternating habitat landscape** where habitat renewal services are delivered every other MHP in a canonical 85 MHP array, on the contrary, in (D) we see a **two-region habitat landscape**. Besides the distribution of poor-rich MHPs in the array, these are also different in depth of the devices. The alternating landscape device is shallow (D) and host quasi 2D aggregates while the two-region landscape is fairly deep (E). In (C) a spatial time series of two Rich-Poor MHPs (C) in the alternating landscape; and (F) two MHPs at the only transition between the Rich and Poor regions of the landscape. In the last nutrient rich MHP shown in F right before the poor zone begins, we can see two stains (red and green) adopting two different aggregation strategies (G) giving rise to different patterns of clustering dynamics. Images in A-C are modified from [232], and in D-G, are modified from [233].

as typed instances (strains) of the same species. As demographic regulation in *E. coli* is controlled by partitioning transcription space (ref), mutant in σ-factor σ_s can delay its local density-dependence response and delay its entry into stationary phase. Two strains differing only in which allele (wt or 819) of the σ_s gene (**rpoS**) they carry in their chromosome can be considered two different **life history strategies** and therefore when grown in co-culture we think on communities of two species rather than a population of two randomly labeled individuals. On a given location, a population of these two strains can be considered a two-type community as their demographic strategy is radically different. The **WT** strain enters stationary phase early while the **GASP** strain delays this phenotypic switching.

Neutral markers To track these strains, we paint them with fluorescent proteins (FP) which are expected to act as neutral markers. When using neutral markers on the same genetic background such as wt strain of *E. coli*, we should expect coexistence regardless of the original abundances. Moreover, given enough time, relative abundances should converge to equal partitioning. In Figures 5.24C,F these neutral markers are used to distinguish between WT strain JEK1036 marked with green FP (GPF) from the GASP strain JEK1033 marked with red FP (RFP). Both markers are inserted in the lac operon and induced with IPTG and are expected to have no influence in population performance. All difference in phenotype are therefore attributed to which allele they carry for the rpoS gene.

Initial conditions A **very important consideration** to make when thinking about competition between bacterial strains are the initial conditions used when inoculating the microfluidic devices. The experiments described in Figure 5.24 all start with an mixture of two strains coming from cultures of GASP and WT strains growing separately as monocultures in well-mixed test tubes. After back diluting these cultures, the microfluidic devices containing the habitat landscapes shown in the figure are inoculated with a 1:1 spatially homogeneous mix in low cell number conditions. After inoculation, a **metacommunity** develops at the landscape scale where locally, at each MHP scale, we can think of local communities in a given biotope. After two days (48 hrs), the system converges to a long-term steady state where relative MHP abundances do not change very much; a fact nicely compatible with the notion of a climax community discussed in section 5.4.1.

Biotope: location, location, location

In order to understand how the cultures shown in Figure 5.24 converge to this steady state we think of an MHP as implementing a biotope; that is acting as a **location** where individuals of these strains live and interact with one another. If we want to count individuals we approximate this region to act as a locus for the biological community. Assuming overlapping generations and limited migration rate, we adopt a continuous coarse grained view, and consider the number of individuals of each type writing,

$$\frac{1}{N_i}\frac{d}{dt}N_i = r_i \cdot \left(1 + \sum_j \left[\frac{\alpha_{i,j}}{K_i}\right] \cdot N_j\right), \tag{5.7}$$

to represent local community dynamics; known as the Lotka-Volterra (LV) scenario. Notice, in the dynamics here, we assume a constant biotope compared to the scale of community dynamics. This scenario is the direct generalisation of our population construction, and its notion of density dependence. Thus, now we consider density-dependence at an intra-specific ($i = j$) as well as inter-specific level ($i \neq j$).

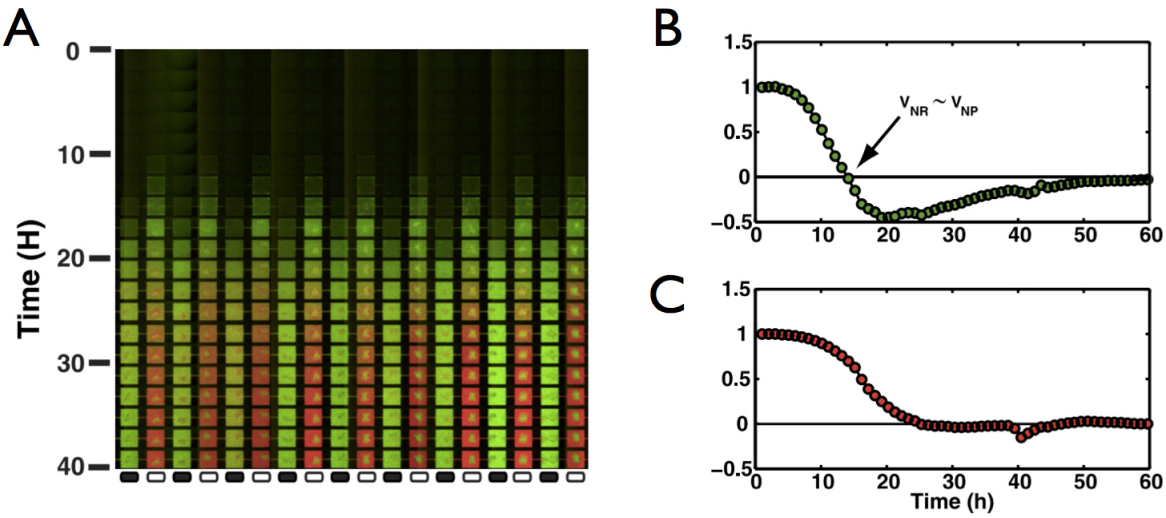

Figure 5.25: Ideal free distributions of bacteria in alternating landscape device of MHPs as shown in Figure 5.24A-C. (A) Landscape meta-community dynamics shown as a kymograph. (B, C) Normalised average per-capita growth rate per MHP in nutrient rich (NR) MHPs, $\frac{1}{r_i}\frac{1}{N_i}\frac{dN_i}{dt}$, estimated from experiments like those in A, for WT (B) and GASP (C) strains. Image modified from [232].

Equilibrium community structure

In Figure 5.25A a stable spatial pattern of fluorescent intensities develops at the landscape scale after around 30 hours of culture. Measuring relative fluorescent intensities we can estimate the normalized average per-capita growth rate, $\frac{1}{r_i}\frac{1}{N_i}\frac{dN_i}{dt}$, per MHP that is nutrient rich (NR, with nano-slits) Figures 5.25 B and C show these estimates for WT and GASP respectively. Notice that after 40 hours their relative per-capita growth rate have reached a steady state. When using a representation of community dynamics like Equation 5.7, we think of its steady state solution, $\hat{N}_i$, as a natural mathematical cartoon for the notion of climax. Long-term community structure is determined by the interaction coefficients $\alpha_{i,j}$ and the carrying capacities K_i while the temporal scales of the

transient response are set by the growth rate r_i. For the long-term scenario of community structure, there are four distinct possibilities: (i) trivial case with both types extinct, (ii) one type dominates (or the other) always independent of initial conditions, (iii) one dominates (or the other) depending on initial conditions, or (iv) both coexist regardless of initial conditions as long as both are initially present. For the strains and habitats discussed here, we are mostly concerned with coexistence.

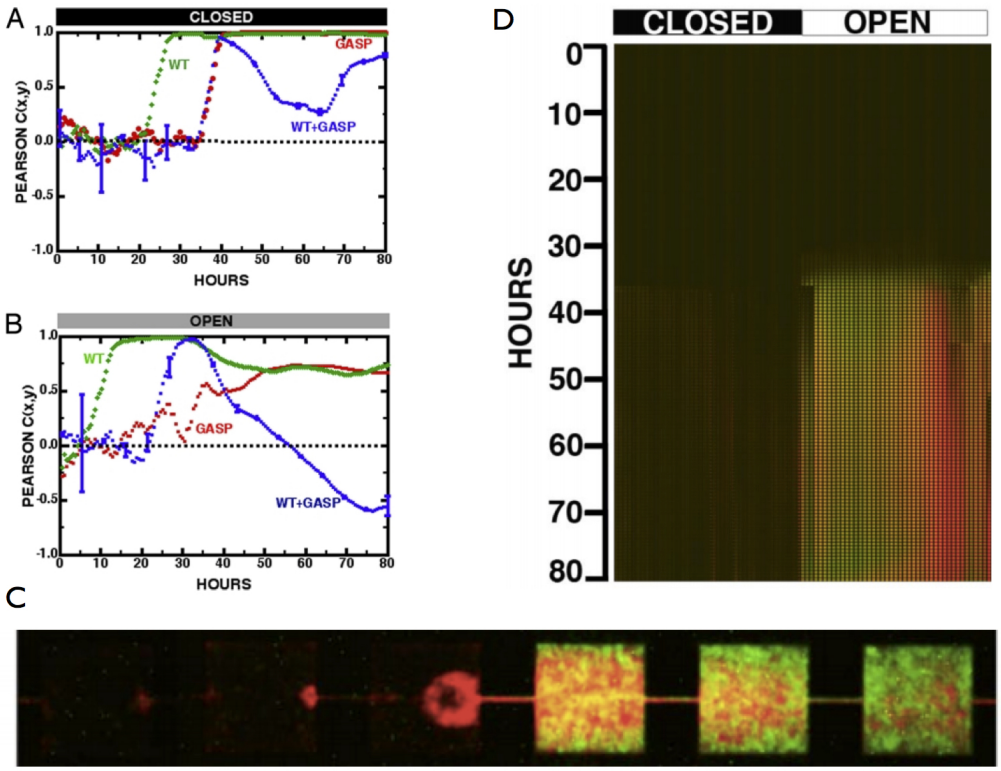

Figure 5.26: Pelagic to sessile transition in a two-region landscape device within MHPs in the te. Bacteria's within MHP aggregation patterns estimated as Pearson correlation coefficient between red and green fluorescent channels averaged within MHPs. In green we see two WT strains one is labeled with GFP (JEK1036) and another marked with RFP (JEK1037). In (A) for the NP and in (B) for NR regions of the landscape. (C) We can see kymograph and in (D) a zoom in transect over 10 MHPs at the transition from NP to NR. Images modified from [233].

Community dynamics

In Figure 5.25A we can see meta-community dynamics between WT (green) and GASP (red) mutant at the whole MHP scale for 40 hours in an MHP array making up a the alternating landscape

shown in Figure 5.24A-C. To explain the transition in dominance, the authors [232] used the ideal free distribution [235]. We can think of the alternating landscape (Fig. 5.24A-C) as a statistical ensemble of many two-MHP system, where one MHP is NP and the other NR. A strategy will freely choose to move between NR and NP MHPs depending on its evaluation of local habitat conditions. After 24 hours of community development, the WT strain (green) stops dominating NR MHPs and begins to give up room to a raising population of the GASP strain (red). After 40 hours of growth, at the bottom of Figure 5.25A GASP (red) dominates in NR (white) and WT (green) dominates in NP (black). In the first 12 hours, WT comes to transiently dominate first both MHPs types although with higher abundance in NR MHPs. Dynamically, WT first prefers NR sites of the landscape but with a small delay it also colonizes NP MHPs. This is consistent with the idea that WT has a higher growth rate $r_{WT} > r_{GASP}$ in both environments types (NP or NR) as it is slightly more r-selected. GASP grow slower but have an enhanced amino acid catabolism [236] and therefore are more K-selected, $K_{WT} < K_{GASP}$.

As WT initially prefers NR MHPs, its cells are mostly in a pelagic state swimming in this type of MHPs at this moment the WT strain's normalized average per-capita growth rate (fitness), $\frac{1}{r_{WT}}\frac{1}{N_{WT}}\frac{dN_{WT}}{dt}$, in the NR and NP MHPs have dropped to zero and begins to dive into negative territory as shown in Figure 5.25B. It is at this moment that WT pelagic cells start to swim away and leave NR patches and migrate into NP regions. Other cells have gone to a pelagic-to-sessile transition and have already clustered within NR MHPs and cannot swim away. This initial clustering is shown in Figure 5.24C (16 hrs). This early aggregation in NR MHPs is consistent with the findings of [233] in two-region landscapes as the ones shown here in Figure 5.24D-G and in Figure 5.26.

During this epoch, NR MHPs undergo a transition in dominance pattern (community structure); they switch from being dominated by WT at the beginning of the epoch ($t = 12$ hrs) to being dominated by GASP by the end of at $t = 24$ hrs (Fig. 5.25A). At this moment WT cells continue to move to NP MHPs. GASP mutant at this moment still enjoy positive normalised average per-capita growth rate (fitness), $\frac{1}{r_{GASP}}\frac{1}{N_{GASP}}\frac{dN_{GASP}}{dt}$, in the NR and stays there. It is also growing in the NP regions and it follows a logistic dynamics. The WT remains in negative fitness and therefore living NR MHPs and start to accumulate in NP regions.

Conditioning growth media, habitat engineering, and niche construction

Nutrient poor (NP) and nutrient rich (NR) are MHP labels that need to be used considering the time-scale at which nano-slits renew the local habitat by passive diffusion from the reservoirs as before inoculation with bacteria, all MHPs hold the same nutrient levels; those present the (LB) growth media. When considering results in two-regions habitat landscapes (Figs. 5.24D-G), In NR regions, densities achieved are higher and WT bacteria aggregates earlier than it does in NP regions as clearly seen here comparing the green curves in Figures 5.25A and 5.25B showing the cases for NP and NR respectively. In NR MHPs WT cells aggregate with one another into clusters after approximate 15 hours after inoculation while it takes double that amount of time (30 hrs) to observe the same in NP regions. Contrary to what happens in NP regions, where WT remains aggregated, in NR regions, we can see that at 35 hours, the Pearson coefficient begins to drop from 1 to a new average value of 0.75. So, in the absence of habitat renewal services (NP) WT bacteria stays aggregated while when renewal is present (NR) it first does it strongly to then do it more loosely.

In Figure 5.8C of Section 5.3 we see how population growth is coupled with conditioning of growth media. Thus, in NP MHPs we expect a higher accumulation of secreted compounds and therefore to see a higher impact of cell-density on the physiology of individuals. Habitat renewal service in NR regions is expected to clean up these compounds by passive diffusion via nano-slits into the reservours. When the habitat modifications have implications at scales larger than survival (τ_0), we talk about niche construction and if the implications are within the life-scape of individual we refer to this conditioning as habitat engineering. In the ecology of metazoa, the scale of these chemical and physical transformations exerted upon the environment are much slower than what is the case in ecologies of microbes. Bacterial cells modify their surrounding environment at a scale larger than it reproduces (τ_+). When this rate is this high, the notion of a stable physical and chemical environment characterising a biotope begins to get compromised. It is this what pose the biggest difficulty when applying ecology to understand cellular assemblages which develop ultra tight interactions which begin to resemble the physiology of tissues.

Notice that in NR regions of the landscape, where habitat renewal services counteract the effects of habitat conditioning, after 50 hours of a dynamic transient in aggregation patterns, when growing separately, both WT and GASP strains achieve similar levels of aggregation in the long-

term. Compare red and green curves in Figure 5.25B. Contrary what it is observed in NP regions, the GASP strain does not aggregate sharply at 35 hours but rather aggregates to similar levels but oscillating between transient aggregation and disaggregation. Compare red curves in Figures 5.26A and B.

When interpreting competition outcomes in experiments we cannot ignore the role of conditioning in determining long-term community patterns of these two strains of *E.coli* we cannot forget the role niche construction by the WT strain plays in the fate of GASP populations. By inspecting the blue curve in Figure 5.26A we see how in NP regions, the WT strains delays aggregation into clusters from what exhibits in isolation (24 hours) to coincide with the timing of aggregation (35 hours) exhibited by the GASP strain in isolation. As soon as such event occurs, we see that the blue curve start decreasing in value to then increase again after 60 hours when the pearson coefficient is about 0.25. On the contrary, in NR regions, the co-culture aggregates at 24 hours to then start monotonically decreasing at 35 hours to reach negative values at 60 hours indicating the strains are avoiding each other at the intra MHP scale.

5.4.3 Games that bacteria play in their social communities

The relationship between the LV equation for one type and the **replicator equation** for two types $i = C, D$.

$$\frac{1}{\phi_i}\frac{d}{dt}\phi_i = \left[f_i(\vec{\phi}) - \bar{f}(\vec{\phi})\right],$$

reveals the deep connection between theoretical ecology and evolutionary game theory [29]. We can think on our local community as a well mixed region where two-player encounters between types of strategies are determined by their relative abundances. Encounters (interactions) are proportional to abundances of each type and therefore to the fraction $\theta = \phi_C/\phi_D$. Thus, comparative distance $f_i - \bar{f}$ to the average fitness $\bar{f} = \theta f_1 + (1-\theta)$ drives community dynamics [237].

Competition vs cooperation

A common scenario invoked is the **two-player game**, a useful caricature of reality, where one follows the trait dynamics between two 'pure' strategies of cooperation and defection. Biologically, this situation is typical where the cost of producing common-pool resources is not distributed equally

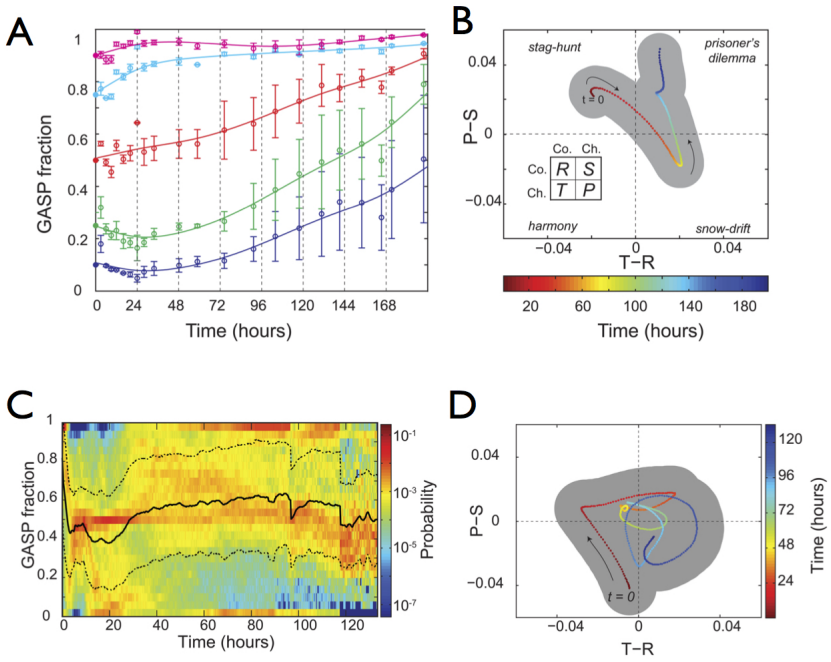

Figure 5.27: Bacterial Games (A) Fraction of defector (GASP mutant) in well-mixed flask over 180 hours, (B) Dynamics of two-player payoff matrix extrapolated from (A). (C) Same as (A) but now in 85-patch micro habitat landscape: GASP fraction (solid line) and ± standard deviation, (dashed line). Color map shows probability density of the GASP fraction of patches with data acquired over 20 independent experiments. (D) same as (B) extrapolated from (C). Image taken from [30].

within a population. Numerous examples can be found studying microbes including, i) budding yeast, *Saccharomyces cerevisiae*, which, in order to metabolize sucrose, secretes a digestive enzyme (invertase) into the environment [70], ii) *Pseudomonas aeruginosa* which, when presented with iron-limited conditions, will begin to excrete an 'iron scavenging' extracellular compound (siderophore) to bind and transport iron across the cell membrane [71] and finally, iii) *E.coli*, where our familiar wild-type and GASP cells differ in their response to diminishing environmental conditions [238]. Cooperative collective action by a wild-type population switching from dividing (exponential) state to arrested growth (stationary) prevents an ecological collapse of the system and ensures a viable long-term stationary population awaiting the renewal of the habitat. In stark contrast to this

approach, GASP mutants discount the future of the long term stationary population and instead continue to exploit the dwindling communal resources.

If we focus on the minimal example, we have a system with numbers of individuals of two types in a given location. For example, as shown here in Figure 5.24, co-cultures of two strains of *E. coli* bacteria which we can characterise by vector $\vec{\phi}_x = (\phi_C, \phi_D)_x$ describing densities (amplitudes) of each strategy at a certain location x. Alternatively, taking the simplest example and neglecting space, as in Figure 5.27A we can track the fraction of the biomass of the GASP type we see that in well mixed scenarios, regardless of initial ratios (different colored lines), the GASP type always wins. In the context of game theory we can consider different types of games. These are defined by the payoff of playing one of the two strategies in any given scenario, i.e. playing against another of the same strategy (Defector & Defector or Cooperator & Cooperator) or different strategy (Defector & Cooperator or Cooperator & Defector). These payoffs make up a payoff matrix which quantifies the fitness incurred when encountering another player.

Mean field, well mixed test-tube cultures For starters we can consider these interactions in the context of the kinetic theory of gases, likening individual ecological strategies as molecules colliding at random with one another. Instead of applying Newtonian mechanics to such collisions we incite a payoff matrix determining the fitness gains and or losses caused by such collisions and follow such ecological dynamics over time.

Fortunately, we can extrapolate these payoffs from the the time-series data of this two player system. In Figure 5.27B we see a an XY plot with labels 'T-R' and 'P-S', respectively. These abbreviate the different payoffs for 'Temptation' and 'Reward' in other words the payoff of being a defector and interacting with a cooperator, and being a cooperator and interacting with another cooperator. For the Y-axis, we consider 'Punishment' and 'Sucker' payoffs which signifies cost of being a defector interacting with another defector or a cooperator interacting with a defector. For scenarios in which $T-R > 0$, i.e. the 'temptation' of defecting outweighs the 'reward' of cooperating and $P-S > 0$ i.e. the 'punishment' of defecting against another defector is not as bad as the cost of being a 'sucker' who cooperates in the presence of a defector, we find that it pays to be a defector. A perceptive reader will notice straight away that the game is dynamic, in fact over the course of 180 hours in a flask this relatively simple system changes qualitatively 3 times! From a 'stag-hunt'

to 'snow-drift' before finally settling to a 'prisoner's dilemma', as described above.

Notice how this many-bodied problem of 10^6 or more microbes interacting with one another has been boiled down into a one-body problem. We have in essence averaged the interactions over all these bacteria into a 'mean field' interaction. Assuming the number of 10^6 cells is approximately correct and a complete graph of interactions generated by a continuously well-mixed flask, a back of an envelope calculation would lead to $\frac{10^6(10^6-1)}{2} \approx 5^{12}$ interactions! It pays to approximate when one can. The question then arises, when does the mean field point of view break down?

Spatial systems: pair approximations and patchy micro habitats Considering spatial structure in such games, muddies the water even further! This is evident when looking at Figure 5.27C-D. One take away, however is that the introduction of space turns this problem from a mean field problem into an altogether more complicated mess. It did not take microbial investigations to discovery this new challenge. Indeed, it could be said that a large part of the applied research in the associated fields of network science and graph theory has to do with understanding the topology of interactions, their dynamics and the ensuing consequences. It is therefore no coincidence that early work to improve the effectiveness of the mean field theory in general were applied to ecological problems. Notably, the formation of the pair approximation, which extended the mean field to consider pairs of interacting types [239].

Returning to Figure 5.27C-D we see that space offers escape for the cooperating, wt, strain and thus leads to coexistence at the level of the landscape, in agreement with results previously discussed.

5.5 Niche theory

5.5.1 Evolution of the niche concept

One of the most fundamental concepts in ecology is the *ecological niche*. The first usage in biology's literature was in Grinnell's beautiful account [240] of the ecology of the California thrasher (*Toxostoma redivivum*), a bird (see Fig. 5.28A) with a very restricted geographic range (see Fig. 5.28D).

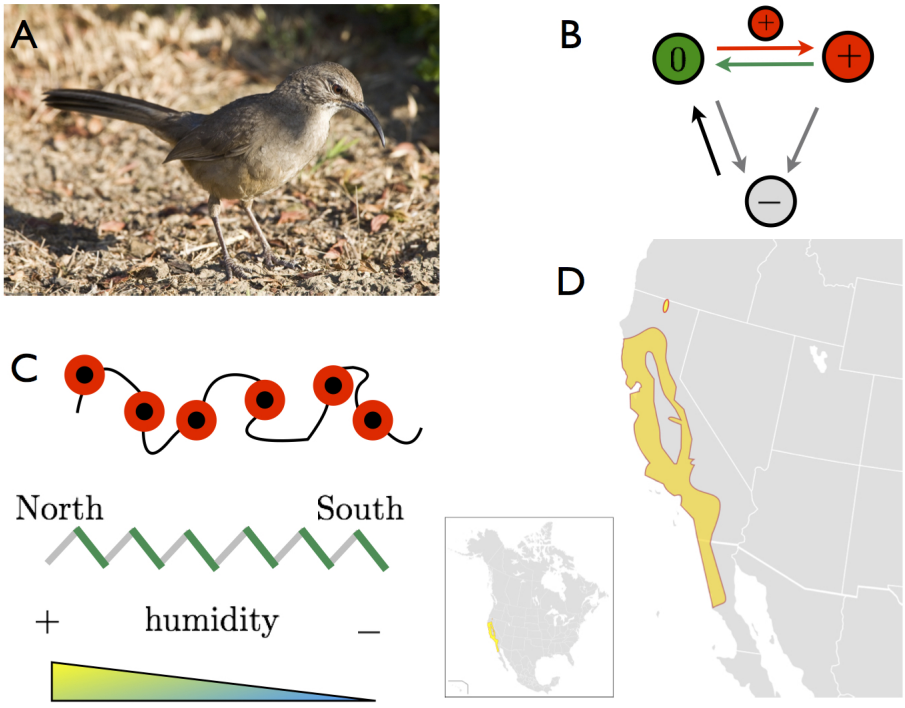

Figure 5.28: The California Trasher (A) *Toxostoma redivivum* (B) Local states: (-) un-suitable, (0) suitable but unoccupied, (+) occupied and active; (C) A Landscape of habitat patches product of patch dynamics regime as well as physical gradients in slope and humidity; (D) Geographic range of *Toxostoma redivivum*.

From the California thrasher to self-reproducing computing automata

The spatial region were the Trasher can be found, its geographic range, is located in the west coast of the USA and Mexico, in the states of California (US) and California del Norte (MX).

The range, shown here in Figure 5.28D is made of local habitat points shown in red at the top panel of Figure 5.28C where we depict such fractal network of habitat patches as an array of discrete locations. These locations are loci where associational requirements are satisfied. The first order association is closely related to temperature and radiation and therefore coverage from sun exposure provides a basic life quality requirement. Sonoran vegetation provides such needed coverage. For the Trasher, such discrete locations of interrupted associational requirements correspond to what we call "sonoran islands".

As shown on Figure 5.28B, these habitat patches can be available but unoccupied (state 0) or be occupied (state 1) by a local population of thrashers.

The dynamics of Sonoran islands fluctuate as a response to vegetation-type metacommunity dynamics which impose these associational requirements. Thrasher populations cannot persist outside this regime (state -).

Along a North-South gradient, which delineates a humidity gradient, the sonoran vegetation type is found only on slopes that face South, Figure 5.28C. Variability among island locations along the gradient give rise to "local races" of thrashers from the north location ($T.r.$ *passadense*) to the south ($T.r.$*sonomae*). These local solutions to the being-Thrasher life-problem are adapted to local differences in secondary associational relationships which are faunal.

5.5.2 The niche, habitat, biotope, and the ecotope

As individuals exist in metapopulations within the context of a metacommunity, niches are written in space. This brings forward all the complexities of multi-scale spatial dynamics which has generated a great deal of confusion between related concepts such as the niche, habitat, ecotope, and the geographic range of a species. Primarily, this has to do with differences between locations in functional space and locations in physical space and the separability of these spaces. A case in point is Hutchinson's continuous view [241] of the niche as: (i) a multidimensional hyper-volume consisting of n environmental variables, (ii) which are considered coordinates in a linear space, and

(iii) which is a snapshot at some point in time t_0 of a hyper volume which is in turn the domain of a population response function (usually population density). In order to organise such ideas and dissolve confusion, [242] suggested the following three concepts: (a) the functional niche, (b) the niche as habitat, and (c) the niche+habitat as ecotope. The authors suggest that the (functional) niche concept should only be applied to the **intracommunity role** of the species (organism) while the broader concept of niche+habitat entailing both **intercommunity** as well as **intracommunity** should be refered to as the ecotope. Finally, the authors suggest the term habitat to be used for the species environment and biotope for the communities environment.

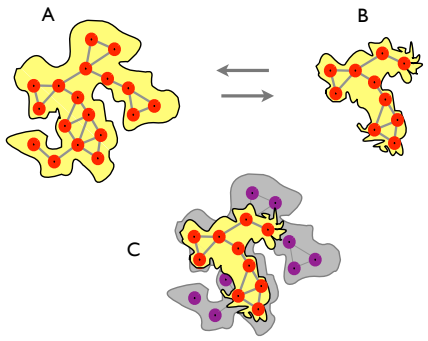

Figure 5.29: Niche and Range (A) fundamental niche; (B) realized niche; (C) difference between fundamental niche and realized niche.

5.5.3 Niche partitioning

At bedrock of the niche+habitat concept lies the **competitive exclusion principle** which dates back to Darwin [243]. The principle asserts the notion that no two species are exactly identical in their abilities, therefore, complete competition for a limited resource leads to either extinction of the inferior competitor or a shift toward another niche [244]. We will soon see how this principle has been challenged in the last 20 years. With competitive exclusion in mind, species competing for similar resources (also known as a **species guild** [245]) must use the environment in ways that permit coexistence. This process, called **niche partitioning**, entered the intellectual landscape with a landmark study by Robert MacArthur who investigated character displacement (differing feeding habits) within a guild of 5 warbler species [246].

This empirical work on character displacement leading to niche partitioning stimulated a surge in theoretical advances helping to resolve open questions regrading the competitive exclusion principle including setting upper bounds on total species related to available resources [247] and other limiting factors [89] as well as limits to similarity within niche space [248, 249].

For microbes, metabolic functional groups represent the microbial equivalent of ecological guilds in macroscopic ecosystems [250]. Here, the functional form of metabolic processes is a defining feature of a microbes ecological niche and thus a building block for understanding larger scale taxanomic distribution, abundance and diversity [111] as well as community level functional redundancy [250] and thus resilience [251]. Within such a functional group we can ask how the metabolic niche is partitioned. The ability to precisely define nutrient gradients within microfluidic devices permits one to study the phenomena of character displacement and niche partitioning at unparalleled levels. By studying the response of wild-type *E.coli* to a gradient of minimal media supplied with only glucose (800μM) as the limiting nutrient, Dal Co et al. were able follow spatial niche partitioning in real time [252].

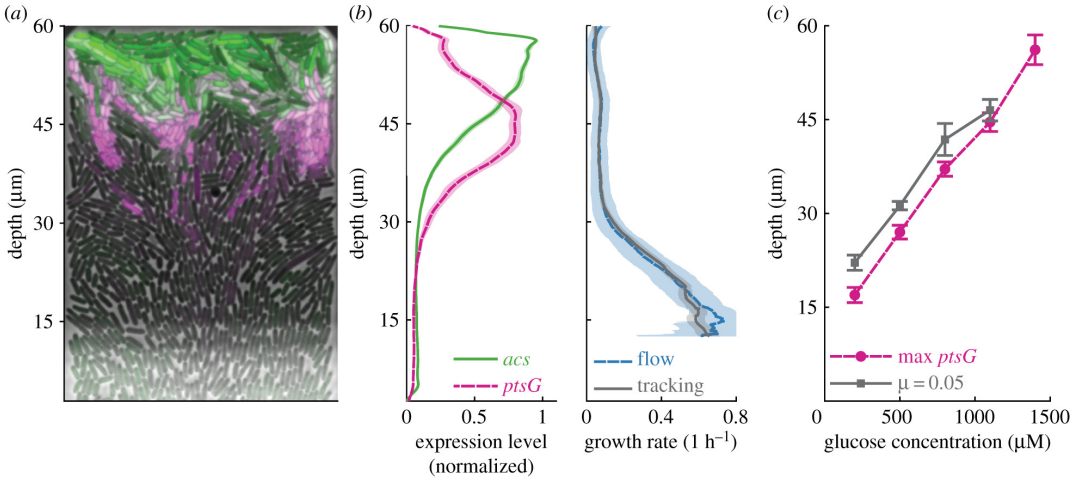

Figure 5.30: Images from [252].

It is well documented that in batch culture glucose and acetate are consumed sequentially. As glucose is fermented, acetate accumulates and only when the former is deplete the later begins to be consumed [253]. To test whether this would hold for spatially distributed populations, the investigators developed a device similar to the mother machine (See Fig5.6B), where a long

(2cm), deep (23μm) main channel constantly flows in nutrients which are able to diffuse into side chambers (40x60x0.76μm), Figure 5.30. Thus the investigators were able to confine and maintain microcolonies ($\sim$ 1000 cells) in these side chambers.

By tracing the expression of genes related to the onset of glucose starvation (Magenta) and acetate growth (Green), they were able to show that nutrient gradients emerged based off the depth within the chamber Fig5.30AB (See [252] for details). Furthermore, by comparing with a mutant strain (Δacs) unable to grow on acetate, the authors were able to show that for the wild-type, this emergent gradient led to a cross-feeding between glucose fermenting cells in the entrance of the chamber where glucose is replete and acetate consuming cells in the back of the chamber where glucose is depleted.

Although wild-type cells in the back of the chamber are able to grow on acetate, their growth rate it diminished compared to their neighbors closer to the entrance. According to the authors and well supported by further experiments, this diversity in resource use and therefore growth rate adds a level of resilience to the within chamber population: When faced with 3h pulses of antibiotics (50μg ml^{-1} streptomycin), such diversified populations were able to persist and continue to grow afterwards. Comparing these results to shallower chambers (30μm), where all cells are fermenting glucose, we see that the more diversified population (deeper chamber) is better able to cope with such perturbations Figure5.31. Furthermore, these results provide an example of niche diversification as a means of optimizing productivity and function. While all cells in the device come from a single isogenic strain, spatial distribution determines their ecological niche for which cell phenotypes quickly adapt to. In the next section we will see how this process of phenotypic adaptation and sorting in space can happen rapidly and lead to predictable outcomes.

5.5.4 r-K & the Competition Colonization trade-off

Species have evolved different life history strategies. This often reflects their competitive ability and the ecological succession within a community where r-selected species are quick to fill vacant gaps after disturbances and K-selected species, while slower, are often competitively superior and thus found in high abundance within climax communities. As the high dimensionality of niche space can be well characterized by limiting factors between competing species [89], we can consider species within a trophic level to fall along a single dimension of niche (aspect) space *sensu* [254].

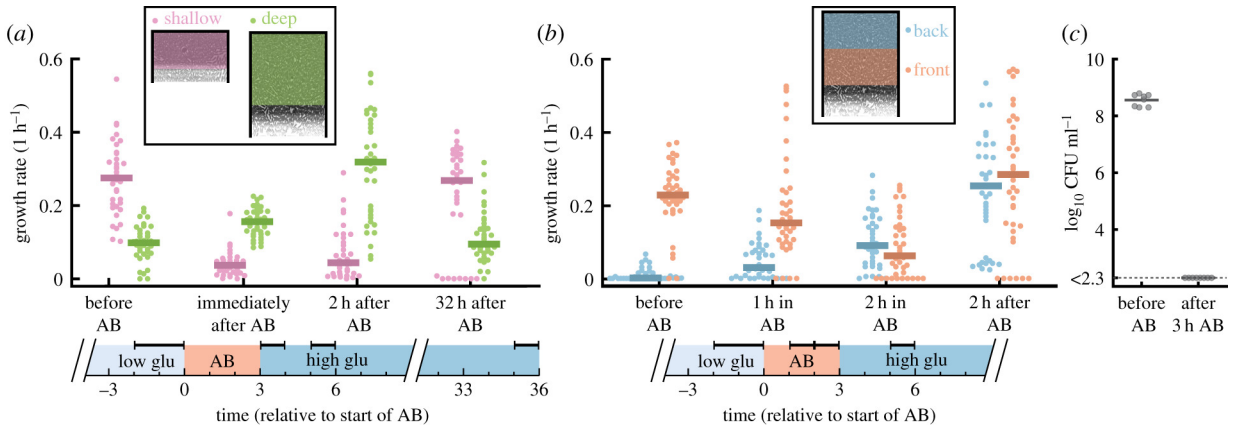

Figure 5.31: Images from [252].

For numerous communities, the limiting resource is space itself [255, 256, 257, 258]. This property applies to bacterial communities as well; Recently, range expansion experiments of *E.coli* growing on semi-solid tryptone broth (TB) agar plates [259] have provided strong evidence for a r-K continuum to emerge in evolved phenotypes during colony formation. Similar to quasi-2D microfluidic experiments, semi-solid agar provides an ecological scenario that hard agar and well-mixed experimental approaches neglect, that is, the choice for individual cells to exploit local resources or explore via run-and-tumble dynamics. For *E.coli*, this choice often comes down to their ability to follow an attractant gradient. Even in isogenic populations we see variability in swimming fitness. This can be characterized by the tumble bias (the average probability to tumble), given a higher tumbling bias relative to other cells in a local populations, cells explore a smaller region of space and are therefore more likely to lose the scent of the attractant gradient [260].

Interestingly, this sets a limit on dissimilarity within a traveling wave allowing one to predict what cell phenotypes (tumble bias) will recruit spatial locations and where, relative to the expanse of the traveling wave [261]. Given this result, [259] developed a simple yet elegant evolution experiment to test predictions regarding range expansion in spatial habitats.

To start, semi-solid agar plates were inoculated at the center with a droplet of culture and then allowed 24 hours to expand and form a colony spanning the entire plate. Following this period, five new plates were inoculated with cells originating at different selection distances from the of center of the 1 day old colony. This way they formed a transect extending from 5mm away (clone X_A) from the center to 25mm away (X_E) in increments of 5mm. They repeated this cycle for 50 days

and periodically tracked expansion speed (u = mm h^{-1}) for the five clones. After this period they found a significant shift in expansion speed relative to the ancestor strain clone X_{Anc} such that: $u_A < u_B < u_{Anc} < u_D < u_E$.

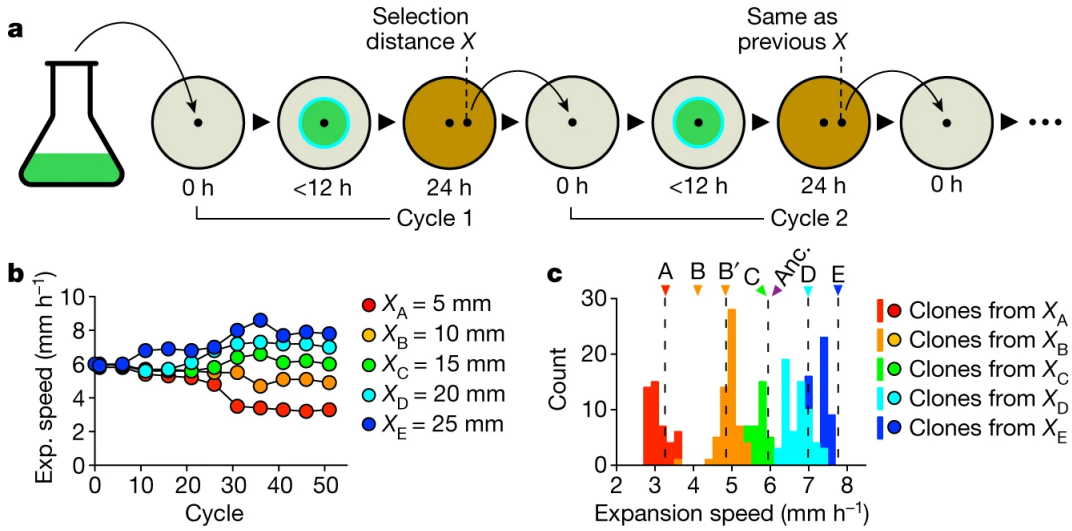

Figure 5.32: Phenotypic adaptive radiation to ecological niche Images from [259].

Strikingly, when multiple clones were inoculated onto a plate after this selection period the investigators found a simple rule predicting which strain would come to dominate some distant d from the center, given the strain whose expansion speed u and growth rate λ satisfied the equation:

$$d^*(u) \propto \frac{u}{\lambda} \tag{5.8}$$

The significance of this work lies in the simplicity of their experimental approach, the generality and clarity of their results by linking the foraging behavior of individual cells to the structuring of communities and most importantly the avenues that it opens for future studies investigating the evolution of niche partitioning in spatial eco-evolutionary settings. For example, if this scenario was implemented for more complex foraging strategies [262] might we see more complex shifts in niche partitioning properties [263]? Or contrastingly if seeded with highly diverse cultures would niche characteristics fade leaving us with neutral processes [21]?

5.6 Neutral-Niche continuum, the meta-community paradigm and beyond...

In the previous section we addressed the theory of the niche, and how the central focus of the competitive exclusion principle has been developed to address foundational questions such as "why are there so many species?". From the perspective of niche theory, the key is the way in which the niche (resources and/or space) is partitioned by different strategies, in the case of the wt and GASP mutant of *E.coli* this was in-part due to the partition of open vs. closed habitat patches in [232]. For glucose fermenting and acetate utilizing strategies, the emergent glucose gradient partitioned the niche [252]. And finally, for the case of range-expansion we saw that one could observe a clear pattern of niche partitioning corresponding to dispersal strategies [259]. Analogous to all three of these scenarios, niche theory addresses species (trait) coexistence from the point of view of necessity. Through competition-colonization trade offs and resource partitioning there are ways in which different life-history strategies cope with the finite nature of space and resources, respectively, and thus competition.

Recently, a counter punch to niche theory has been proposed: Stephen Hubbell, building off of TIB [116] introduced a neutral theory of biodiversity which does not take for granted the concept of the niche, nor fitness differences between individuals of different species. Instead, neutral theory considers all species to live on a flat fitness landscape and therefore the macroscopic properties of biogeography like biodiversity, species distributions, abundance are not the consequence of deterministic (niche based) mechanisms but rather neutral stochastic processes determined by exogenously defined rates of immigration, emigration, local extinction and speciation. In this light, ecological communities are made up of an ensemble of equivalent species whose composition drifts through time. Since its inception almost 20 years ago, the neutral theory of biodiversity has matured from a controversial and often misunderstood framework [264] to an important starting point and an efficient theory [265] which has been capable of generating several testable predictions. For a statistical mechanics perspective of neutral theory see [266]. It is now relatively agreed upon in the field of community ecology that neutral and niche theory define the extremes of a continuum between chance (randomness) and determinism [267, 268, 269]. Most notably, this has been achieved through the meta-community paradigm, which, much like the concept of the metapopulation, con-

siders the regional and local dynamics of a community of communities, see [21]. What remains an open question is the importance of landscape structure and its impact on connectivity and thus the coupling of ecological communities via dispersal. Therefore, the microfluidics platform remains the most ideal test-bed for ecology theory (niche vs neutral) as well as an inspiration for advances in the unification of landscape ecology (the structure of space) and metacommunity ecology (the dynamics of interacting species).

Concluding remarks

It is my hope that through this thesis I have conveyed to the reader the importance of considering spatial structure in the realm of the microscopic world:

At the level of single cells we saw how initial conditions and spatial adjacency determined the outcome of range expansion between competing strains of colicin producing-colicin sensitive E.coli on solid agar landscapes. We discovered connections between the ratio of cell lysis and division rates and concepts from percolation theory which could serve as a useful framework for understanding regimes of strain coexistence, competitive exclusion and extinction in this dynamic landscape.

Next, scaling up to the level of populations, we developed a stochastic spatial toy model with the purpose of exploring the spatial conditions under which microbial common goods games could persist. As a particular system motivating this work, we considered *P. aeruginosa*, which excretes a costly 'iron-scavenging' compound (siderophore) in order to bind and transport iron across the cell membrane. This compound represents a common-pool resource, susceptible to exploitation by nearby bacteria free from producing this metabolically costly resource. Though our model is relatively abstract, our results compared favorably to clinical studies which followed the dynamics of *P. aeruginosa* in the lungs of mechanically ventilated patients. Future microfluidic studies could hone in on the biophysical properties of such systems, notably topology and dimensionality of environment, leakage rate of common-pool resource as well as it's uptake and diffusion rates.

Following this theoretical work, we then began observing 2-species metacommunity dynamics in structured microfabricated landscapes. From these observations we showed how these two bacterial species (*P.aeruginosa* - *E.coli*) enact a competition-colonization tradeoff. An important consideration for such metacommunities was their spatial context. In well-mixed conditions we found the superior competitor, *P.aeruginosa*, always dominated. For our spatial considerations we tested

flat landscapes and patchy landscapes where habitat patches were connected by ecological corridors. While coexistence was observed in both spatial scenarios we found that the confinement of corridors and the earlier arrival of *E.coli* population waves (priority effects) permitted for spatial monopolization of patches. This was facilitated by micro-colony jamming found within corridors, effectively fragmenting the landscape and permitting growth and population development in isolation for the inferior competitor, *E.coli*. To address this phenomena in more detail, we next considered the colonization and long-term metapopulation distribution of *E.coli* in isolation. To our surprise we found that a critical level of induced randomness in the width of ecological corridors could lead to a qualitatively new distribution of the metapopulation reminiscent of a phase transition.

Finally we reviewed this nascent field of research at the interface of microbial ecology and cell biophysics, highlighting ecological theory and landmark experimental discoveries. There is much work to be done with several avenues ripe for pursuit, but time is of the essence.

Oikos or Ecology as it is known today, meaning 'the study of house', entails understanding life's processes, interactions, the flow of energy and materials and the succession of one form to the next. From this framework it becomes clear, understanding the microbial world is equivalent to understanding ourselves, the biosphere and all that makes life on this lonely rock possible and worthwhile.

> For small creatures such as we the vastness is bearable only through love.
>
> - Carl Sagan

Acknowledgments

I am incredibly grateful to numerous people whose support, encouragement, collaborative efforts and good vibes made this thesis possible. I would like to first thank my advisors Juan Keymer and Peter Galajda.

Juan, your joy for teaching and your thirst for an understanding of the natural world is relentless and an inspiration for a young scientist like myself. Even more than your passion for science though, I admire your character as a human being. I have learned countless lessons from you through your actions and I believe my knowing you has made me a better person.

Peter, your kindness, openness and respect for your peers and students was immediately apparent upon my arrival to Szeged. Facilitated by this healthy thinking space, it has been such a pleasure doing science with you over the past 2.5 years, brainstorming about the unknown within the microbial world and thinking of clever microfluidic hacks to tease apart these discovered treasures.

I would like to thank my committee members, María Luisa Cordero and Fernan Federici as well as my committee coordinator, Mauricio Lima, for taking the time and effort to greatly improve my project through our meetings and discussions together. Your inquisitive questions brought a vital perspective to this work.

To my partner, Krisz, thank you for your love and support over the past 2 years. Your smile brings me strength. This past year has been a struggle, given the restrictions on travel and the lack of connection with family and friends, therefore, I am all the more grateful for the connection that we continue to share and the encouragement you provide on those days when I am weak.

To Janneke, your friendship, support and words of encouragement have meant so much to me over the years. I found comfort in our long discussions in the lab, whether it was about the state of science and society, our own unique expat experiences, or the curious creatures we may find under

the microscope in a soil sample. Finally, your resilience in the face of adversity and your strength and perseverance are an inspiration.

Kriszti I am so thankful to have worked with you over the past 2.5yrs. Your energy, day in and day out, was contagious and a constant jolt of energy when I needed it. Your openness to hearing my ideas and sharing in our experimental successes and failures account for some of my fondest memories during this experience.

Laci, thank you for being such a fantastic listener and companion in the cloud when trying to make sense out of our experimental results. I cherish our whiteboard talks we shared together about all subjects under the sun.

To Ági, thank you for your patience as a tour-guide of the micro-fabrication experience. Your wisdom and advice, always delivered calmly, were an often needed reality check for me. I wont forget those times you were able to comfort me during my experimental failures in the lab and assure me that it in fact is not the end of the world.

To Eszter, Saeed, Imre and the rest of the Galajda Lab thank you for sharing this time with me. I enjoyed our talks and the companionship each of you provided in your own unique way. This was a special place for me and I will not forget it.

To Alfredo, Fito, Kevin and Simon in the Keymer lab as well as my companions in Chile, Clara, Derek, Isi, Ellie, I am grateful for the time we shared and the memories we made together. Your support as friends and colleagues meant the world to me.

To my friends in Hungary; including János, Ádám, Csaba, Fruzsi, Zsombor, Raquel, Viktor, Daniel, Noel, Amin and many more, thank you for the frisbee sessions, week night rock climbing, chess matches, Wednesday morning lángos', trips to Maláta, Retyezát Nemzeti Park excursion, swimming in the Tisza, diszno vágás, táncházok, game nights and all the other events that made life in Szeged a treat.

Finally to my family back home, your support and love from afar during this journey has made all the difference. Thank you Mom for your words of encouragement, your love and affection, your strength during this tough time and your unwavering joy and good vibes which emanates from you in our phone calls and rare meetups. Thank you Dad for your constant support, your guidance and the laughter we got to share together. I cherish the send off in Santiago and those few days we had together which are so memorable and a treasure I get to reminisce about. To my siblings

and sibling-in-law Mari, Max and Steph, my heart aches when I think about the time we have been apart. But from those rare moments we could share springs forth pure joy and love; dancing in the street after the concert, a simple walk around the Inner Harbor, or a trip with the dogs to the reservoir. This past 1.5 years has been particularly tough not getting to spend more time with Cora who is already turning into a precious little monkey. Thank you for the constant photos and videos of her, they were always the highlight of my day.

Financial Support

I would like to thank financial support to CONICYT FONDECYT grants 1150430 and 1191893, the national doctoral scholarship CONICYT-PFCHA/2019-21191687, the Hungarian Government and the European Regional Development Fund under the grant numbers GINOP-2.3.2-15-2016-00001 and GINOP- 2.3.2-15-2016-00026, the Hungarian National Research, Development and Innovation Office under grant number K 116516 as well as internal scholarships provided by Pontificia Universidad Catolica de Chile; VRI Assistant Scholarship, VRI Instructor Scholarship and finally the VRI Study Abroad Scholarship.

Bibliography

[1] Xavier Raynaud and Naoise Nunan. "Spatial ecology of bacteria at the microscale in soil". In: *PLoS One* 9.1 (2014), e87217.

[2] Paul G Falkowski, Tom Fenchel, and Edward F Delong. "The microbial engines that drive Earth's biogeochemical cycles". In: *science* 320.5879 (2008), pp. 1034–1039.

[3] David M Raup and J John Sepkoski. "Mass extinctions in the marine fossil record". In: *Science* 215.4539 (1982), pp. 1501–1503.

[4] Sean Nee. "Extinction, slime, and bottoms". In: *PLoS Biol* 2.8 (2004), e272.

[5] Simon A Levin. "Multiple scales and the maintenance of biodiversity". In: *Ecosystems* 3.6 (2000), pp. 498–506.

[6] Simon A Levin. "The problem of pattern and scale in ecology: the Robert H. MacArthur award lecture". In: *Ecology* 73.6 (1992), pp. 1943–1967.

[7] James H Brown et al. *Macroecology*. University of Chicago Press, 1995.

[8] Robert H MacArthur and Edward O Wilson. *The theory of island biogeography*. Vol. 1. Princeton university press, 2001.

[9] L. R. Taylor. "Aggregation, Variance and the Mean". In: *Nature* 189.4766 (1961), pp. 732–735. DOI: 10.1038/189732a0. URL: https://doi.org/10.1038/189732a0.

[10] Esa Ranta et al. "The Moran effect and synchrony in population dynamics". In: *Oikos* (1997), pp. 136–142.

[11] ER PIANKA. "CITATION CLASSIC-ON OPTIMAL USE OF A PATCHY ENVIRONMENT". In: *CURRENT CONTENTS/AGRICULTURE BIOLOGY & ENVIRONMENTAL SCIENCES* 31 (1988), pp. 16–16.

[12] Simon A Levin and Robert T Paine. "Disturbance, patch formation, and community structure". In: *Proceedings of the National Academy of Sciences* 71.7 (1974), pp. 2744–2747.

[13] Eric R Pianka. "On r-and K-selection". In: *The american naturalist* 104.940 (1970), pp. 592–597.

[14] Frank W Preston. "The commonness, and rarity, of species". In: *Ecology* 29.3 (1948), pp. 254–283.

[15] Marten Scheffer. *Critical transitions in nature and society*. Vol. 16. Princeton University Press, 2009.

[16] Rick Durrett. "Stochastic spatial models". In: *SIAM review* 41.4 (1999), pp. 677–718.

[17] Simon A Levin, Thomas M Powell, and John H Steele. *Patch dynamics*. Vol. 96. Springer Science & Business Media, 2012.

[18] J. A. Wiens. "Spatial Scaling in Ecology". In: *Functional Ecology* 3.4 (1989), pp. 385–397. ISSN: 02698463, 13652435. URL: `http://www.jstor.org/stable/2389612`.

[19] Roy J Glauber. "Time-dependent statistics of the Ising model". In: *Journal of mathematical physics* 4.2 (1963), pp. 294–307.

[20] Richard Levins. "Some demographic and genetic consequences of environmental heterogeneity for biological control". In: *American Entomologist* 15.3 (1969), pp. 237–240.

[21] Mathew A Leibold et al. "The metacommunity concept: a framework for multi-scale community ecology". In: *Ecology Letters* 7.7 (2004), pp. 601–613.

[22] Mercedes Pascual and Frédéric Guichard. "Criticality and disturbance in spatial ecological systems". In: *Trends in ecology & evolution* 20.2 (2005), pp. 88–95.

[23] Maureen A O'Malley. "The nineteenth century roots of'everything is everywhere'". In: *Nature Reviews Microbiology* 5.8 (2007), pp. 647–651.

[24] Jennifer B Hughes Martiny et al. "Microbial biogeography: putting microorganisms on the map". In: *Nature Reviews Microbiology* 4.2 (2006), p. 102.

[25] James I Prosser et al. "The role of ecological theory in microbial ecology". In: *Nature Reviews Microbiology* 5.5 (2007), p. 384.

[26] George M Whitesides. "The origins and the future of microfluidics". In: *Nature* 442.7101 (2006), pp. 368–373.

[27] Krisztina Nagy et al. "Application of microfluidics in experimental ecology: the importance of being spatial". In: *Frontiers in microbiology* 9 (2018), p. 496.

[28] Felix JH Hol et al. "Nutrient-responsive regulation determines biodiversity in a colicin-mediated bacterial community". In: *BMC biology* 12.1 (2014), pp. 1–14.

[29] Josef Hofbauer, Karl Sigmund, et al. *Evolutionary games and population dynamics*. Cambridge university press, 1998.

[30] Felix JH Hol et al. "Spatial structure facilitates cooperation in a social dilemma: empirical evidence from a bacterial community". In: *PloS one* 8.10 (2013), e77042.

[31] Juan E Keymer et al. "Computation of mutual fitness by competing bacteria". In: *Proceedings of the National Academy of Sciences* 105.51 (2008), pp. 20269–20273.

[32] Carl Huffaker et al. "Experimental studies on predation: dispersion factors and predator-prey oscillations". In: *Hilgardia* 27.14 (1958), pp. 343–383.

[33] Felix JH Hol et al. "Bacterial predator–prey dynamics in microscale patchy landscapes". In: *Proceedings of the Royal Society B: Biological Sciences* 283.1824 (2016), p. 20152154.

[34] Arthur Prindle et al. "Ion channels enable electrical communication in bacterial communities". In: *nature* 527.7576 (2015), pp. 59–63.

[35] Jintao Liu et al. "Metabolic co-dependence gives rise to collective oscillations within biofilms". In: *nature* 523.7562 (2015), pp. 550–554.

[36] Rosa Martinez-Corral et al. "Metabolic basis of brain-like electrical signalling in bacterial communities". In: *Philosophical Transactions of the Royal Society B* 374.1774 (2019), p. 20180382.

[37] Ashleigh S Griffin, Stuart A West, and Angus Buckling. "Cooperation and competition in pathogenic bacteria". In: *Nature* 430.7003 (2004), pp. 1024–1027.

[38] Thilo Köhler, Angus Buckling, and Christian Van Delden. "Cooperation and virulence of clinical Pseudomonas aeruginosa populations". In: *Proceedings of the National Academy of Sciences* 106.15 (2009), pp. 6339–6344.

[39] Garrett Hardin. "The tragedy of the commons". In: *Journal of Natural Resources Policy Research* 1.3 (2009), pp. 243–253.

[40] Benedikt von Bronk et al. "Effects of stochasticity and division of labor in toxin production on two-strain bacterial competition in Escherichia coli". In: *PLoS biology* 15.5 (2017), e2001457.

[41] Dietrich Stauffer and Ammon Aharony. *Introduction to percolation theory*. CRC press, 1994.

[42] Richard Levins and David Culver. "Regional coexistence of species and competition between rare species". In: *Proceedings of the National Academy of Sciences* 68.6 (1971), pp. 1246–1248.

[43] Alan Hastings. "Disturbance, coexistence, history, and competition for space". In: *Theoretical population biology* 18.3 (1980), pp. 363–373.

[44] AP Kinzig et al. "Limiting similarity, species packing, and system stability for hierarchical competition-colonization models". In: *The American Naturalist* 153.4 (1999), pp. 371–383.

[45] Felix JH Hol et al. "The idiosyncrasy of spatial structure in bacterial competition". In: *BMC research notes* 8.1 (2015), p. 245.

[46] R.D Kronig and WG Penney. "Quantum mechanics of electrons in crystal lattices". In: *Proc. Royal Soc. London* 130 (1931), p. 499.

[47] Martin Ackermann et al. "On the evolutionary origin of aging". In: *Aging cell* 6.2 (2007), pp. 235–244.

[48] Karl August M "o bius. *the oyster and the oyster economy*. Verlag von Wiegandt, Hemple Parey, 1877.

[49] Richard C Lewontin. *The triple helix: Gene, organism, and environment*. Harvard University Press, 2001.

[50] Delphine Legrand et al. "Eco-evolutionary dynamics in fragmented landscapes". In: *Ecography* 40.1 (2017), pp. 9–25.

[51] F John Odling-Smee, Kevin N Laland, and Marcus W Feldman. *Niche construction: the neglected process in evolution*. 37. Princeton university press, 2003.

[52] Clive G Jones, John H Lawton, and Moshe Shachak. "Organisms as ecosystem engineers". In: *Ecosystem management*. Springer, 1994, pp. 130–147.

[53] Robert H Whittaker, Simon A Levin, and Richard B Root. "Niche, habitat, and ecotope". In: *The American Naturalist* 107.955 (1973), pp. 321–338.

[54] James E Byers et al. "Using ecosystem engineers to restore ecological systems". In: *Trends in ecology & evolution* 21.9 (2006), pp. 493–500.

[55] Garry Peterson, Craig R Allen, and Crawford Stanley Holling. "Ecological resilience, biodiversity, and scale". In: *Ecosystems* 1.1 (1998), pp. 6–18.

[56] Sanne de Visser, Elisa Thébault, and Peter C de Ruiter. "Ecosystem engineers, keystone species". In: *Ecological Systems*. Springer, 2013, pp. 59–68.

[57] John C Moore et al. "Detritus, trophic dynamics and biodiversity". In: *Ecology letters* 7.7 (2004), pp. 584–600.

[58] David M Post and Eric P Palkovacs. "Eco-evolutionary feedbacks in community and ecosystem ecology: interactions between the ecological theatre and the evolutionary play". In: *Philosophical Transactions of the Royal Society B: Biological Sciences* 364.1523 (2009), pp. 1629–1640.

[59] Wenying Shou, Sri Ram, and Jose MG Vilar. "Synthetic cooperation in engineered yeast populations". In: *Proceedings of the National Academy of Sciences* 104.6 (2007), pp. 1877–1882.

[60] Zarath M Summers et al. "Direct exchange of electrons within aggregates of an evolved syntrophic coculture of anaerobic bacteria". In: *Science* 330.6009 (2010), pp. 1413–1415.

[61] Souichiro Kato et al. "Stable coexistence of five bacterial strains as a cellulose-degrading community". In: *Appl. Environ. Microbiol.* 71.11 (2005), pp. 7099–7106.

[62] Michael J McInerney, Jessica R Sieber, and Robert P Gunsalus. "Syntrophy in anaerobic global carbon cycles". In: *Current opinion in biotechnology* 20.6 (2009), pp. 623–632.

[63] James T Cronin and John D Reeve. "Host–parasitoid spatial ecology: a plea for a landscape-level synthesis". In: *Proceedings of the Royal Society of London B: Biological Sciences* 272.1578 (2005), pp. 2225–2235.

[64] David C Krakauer, Karen M Page, and Douglas H Erwin. "Diversity, dilemmas, and monopolies of niche construction". In: *The American Naturalist* 173.1 (2008), pp. 26–40.

[65] F John Odling-Smee, Kevin N Laland, and Marcus W Feldman. "Niche construction". In: *The American Naturalist* 147.4 (1996), pp. 641–648.

[66] Kevin N Laland, F John Odling-Smee, and Marcus W Feldman. "Evolutionary consequences of niche construction and their implications for ecology". In: *Proceedings of the National Academy of Sciences* 96.18 (1999), pp. 10242–10247.

[67] August Weismann. *Das Keimplasma: eine theorie der Vererbung*. Fischer, 1892.

[68] Leo W Buss. *The evolution of individuality*. Princeton University Press, 2014.

[69] Gene E Robinson. "Regulation of division of labor in insect societies". In: *Annual review of entomology* 37.1 (1992), pp. 637–665.

[70] R Craig Maclean and C Brandon. "Stable public goods cooperation and dynamic social interactions in yeast". In: *Journal of evolutionary biology* 21.6 (2008), pp. 1836–1843.

[71] JB Neilands. "Siderophores: structure and function of microbial iron transport compounds". In: *Journal of Biological Chemistry* 270.45 (1995), pp. 26723–26726.

[72] Alex McAvoy et al. "Public goods games in populations with fluctuating size". In: *arXiv preprint arXiv:1709.03630* (2017).

[73] Jeff Gore, Hyun Youk, and Alexander Van Oudenaarden. "Snowdrift game dynamics and facultative cheating in yeast". In: *Nature* 459.7244 (2009), pp. 253–256.

[74] John F Bruno, John J Stachowicz, and Mark D Bertness. "Inclusion of facilitation into ecological theory". In: *Trends in Ecology & Evolution* 18.3 (2003), pp. 119–125.

[75] Chi Xu et al. "Local facilitation may cause tipping points on a landscape level preceded by early-warning indicators". In: *The American Naturalist* 186.4 (2015), E81–E90.

[76] Mats Gyllenberg and Kalle Parvinen. "Necessary and sufficient conditions for evolutionary suicide". In: *Bulletin of mathematical biology* 63.5 (2001), pp. 981–993.

[77] Kalle Parvinen. "Evolutionary suicide". In: *Acta biotheoretica* 53.3 (2005), pp. 241–264.

[78] Benjamin Allen, Jeff Gore, and Martin A Nowak. "Spatial dilemmas of diffusible public goods". In: *Elife* 2 (2013), e01169.

[79] Theodore E Harris. "Contact interactions on a lattice". In: *The Annals of Probability* (1974), pp. 969–988.

[80] Thomas Milton Liggett. *Interacting particle systems*. Vol. 276. Springer Science & Business Media, 2012.

[81] Joaqun Marro and Ronald Dickman. *Nonequilibrium phase transitions in lattice models*. Cambridge University Press, 2005.

[82] Roy M Anderson and Robert M May. "Population biology of infectious diseases: Part I". In: *Nature* 280.5721 (1979), p. 361.

[83] Juan E Keymer et al. "Extinction thresholds and metapopulation persistence in dynamic landscapes". In: *The American Naturalist* 156.5 (2000), pp. 478–494.

[84] Jordi Bascompte and Ricard V Solé. "Habitat fragmentation and extinction thresholds in spatially explicit models". In: *Journal of Animal Ecology* (1996), pp. 465–473.

[85] Max Rietkerk et al. "Self-organized patchiness and catastrophic shifts in ecosystems". In: *Science* 305.5692 (2004), pp. 1926–1929.

[86] Michael E Fisher and Michael N Barber. "Scaling theory for finite-size effects in the critical region". In: *Physical Review Letters* 28.23 (1972), p. 1516.

[87] RT Forman. *Land Mosaics: The Ecology of Landscapes and Regions 1995*. Springer, 2014.

[88] RH Whittaker and SA1 Levin. "The role of mosaic phenomena in natural communities". In: *Theoretical population biology* 12.2 (1977), pp. 117–139.

[89] Simon A Levin. "Community equilibria and stability, and an extension of the competitive exclusion principle". In: *The American Naturalist* 104.939 (1970), pp. 413–423.

[90] Claudia Neuhauser. "Ergodic theorems for the multitype contact process". In: *Probability Theory and Related Fields* 91.3-4 (1992), pp. 467–506.

[91] Henry S Horn and Robert H MacArthur. "Competition among fugitive species in a harlequin environment". In: *Ecology* 53.4 (1972), pp. 749–752.

[92] Rick Durrett and Simon Levin. "Spatial aspects of interspecific competition". In: *Theoretical population biology* 53.1 (1998), pp. 30–43.

[93] Joseph H Connell. "Diversity in tropical rain forests and coral reefs". In: *Science* 199.4335 (1978), pp. 1302–1310.

[94] Miles T Wetherington and Juan E Keymer. "What Does Not Kill You Makes You Stronger". In: *Trends in microbiology* 25.8 (2017), pp. 605–607.

[95] Babak Momeni, Adam James Waite, and Wenying Shou. "Spatial self-organization favors heterotypic cooperation over cheating". In: *Elife* 2 (2013), e00960.

[96] Stephen P Diggle et al. "Cooperation and conflict in quorum-sensing bacterial populations". In: *Nature* 450.7168 (2007), pp. 411–414.

[97] Zhenyu Jin et al. "Conditional privatization of a public siderophore enables Pseudomonas aeruginosa to resist cheater invasion". In: *Nature communications* 9.1 (2018), pp. 1–11.

[98] Oskar Hallatschek et al. "Genetic drift at expanding frontiers promotes gene segregation". In: *Proceedings of the National Academy of Sciences* 104.50 (2007), pp. 19926–19930.

[99] Richard Durrett and Simon Levin. "The importance of being discrete (and spatial)". In: *Theoretical population biology* 46.3 (1994), pp. 363–394.

[100] Michael Doebeli and Christoph Hauert. "Models of cooperation based on the Prisoner's Dilemma and the Snowdrift game". In: *Ecology letters* 8.7 (2005), pp. 748–766.

[101] Sebastien Lion and Minus Van Baalen. "Self-structuring in spatial evolutionary ecology". In: *Ecology letters* 11.3 (2008), pp. 277–295.

[102] Sylvie Estrela et al. "Environmentally mediated social dilemmas". In: *Trends in ecology & evolution* (2018).

[103] Christoph Hauert, Camille Saade, and Alex McAvoy. "Asymmetric evolutionary games with environmental feedback". In: *Journal of theoretical biology* 462 (2019), pp. 347–360.

[104] John Maynard Smith and Eors Szathmary. *The major transitions in evolution*. Oxford University Press, 1997.

[105] Francisco G Varela, Humberto R Maturana, and Ricardo Uribe. "Autopoiesis: the organization of living systems, its characterization and a model". In: *Biosystems* 5.4 (1974), pp. 187–196.

[106] Oskar Hallatschek and David R Nelson. "Life at the front of an expanding population". In: *Evolution* 64.1 (2010), pp. 193–206.

[107] Daniel Richardson. "Random growth in a tessellation". In: *Mathematical Proceedings of the Cambridge Philosophical Society*. Vol. 74. 03. Cambridge Univ Press. 1973, pp. 515–528.

[108] Kenneth J Locey and Jay T Lennon. "Scaling laws predict global microbial diversity". In: *Proceedings of the National Academy of Sciences* 113.21 (2016), pp. 5970–5975.

[109] Daniel E Dykhuizen. "Santa Rosalia revisited: why are there so many species of bacteria?" In: *Antonie van Leeuwenhoek* 73.1 (1998), pp. 25–33.

[110] William R Shoemaker, Kenneth J Locey, and Jay T Lennon. "A macroecological theory of microbial biodiversity". In: *Nature Ecology & Evolution* 1.5 (2017), p. 0107.

[111] China A Hanson et al. "Beyond biogeographic patterns: processes shaping the microbial landscape". In: *Nature Reviews Microbiology* 10.7 (2012), pp. 497–506.

[112] Curtis Huttenhower et al. "Structure, function and diversity of the healthy human microbiome". In: *Nature* 486.7402 (2012), p. 207.

[113] Manuel Delgado-Baquerizo et al. "Microbial diversity drives multifunctionality in terrestrial ecosystems". In: *Nature Communications* 7 (2016), p. 10541.

[114] Edmundo Barrios. "Soil biota, ecosystem services and land productivity". In: *Ecological Economics* 64.2 (2007), pp. 269–285.

[115] Peter Chesson. "Mechanisms of maintenance of species diversity". In: *Annual Review of Ecology and Systematics* 31.1 (2000), pp. 343–366.

[116] Stephen P Hubbell. *The Unified Neutral Theory of Biodiversity and Biogeography (MPB-32)*. Princeton University Press, 2001.

[117] Howard V Cornell and Susan P Harrison. "What are species pools and when are they important?" In: *Annual Review of Ecology, Evolution, and Systematics* 45 (2014), pp. 45–67.

[118] Steven D Allison and Jennifer BH Martiny. "Resistance, resilience, and redundancy in microbial communities". In: *Proceedings of the National Academy of Sciences* 105.Supplement 1 (2008), pp. 11512–11519.

[119] Iain M Young and John W Crawford. "Interactions and self-organization in the soil-microbe complex". In: *Science* 304.5677 (2004), pp. 1634–1637.

[120] Tess Nahanni Grainger and Benjamin Gilbert. "Dispersal and diversity in experimental metacommunities: linking theory and practice". In: *Oikos* 125.9 (2016), pp. 1213–1223. DOI: 10.1111/oik.03018. eprint: https://onlinelibrary.wiley.com/doi/pdf/10.1111/oik.03018. URL: https://onlinelibrary.wiley.com/doi/abs/10.1111/oik.03018.

[121] George Livingston et al. "Competition–colonization dynamics in experimental bacterial metacommunities". In: *Nature Communications* 3.1 (2012), p. 1234. DOI: 10.1038/ncomms2239. URL: https://doi.org/10.1038/ncomms2239.

[122] Noah Fierer et al. "Changes through time: integrating microorganisms into the study of succession". In: *Research in Microbiology* 161.8 (2010), pp. 635–642.

[123] Mark C Urban et al. "Evolutionary origins for ecological patterns in space". In: *Proceedings of the National Academy of Sciences* (2020).

[124] George O'Toole, Heidi B Kaplan, and Roberto Kolter. "Biofilm formation as microbial development". In: *Annual Reviews in Microbiology* 54.1 (2000), pp. 49–79.

[125] Jonathan Saragosti et al. "Directional persistence of chemotactic bacteria in a traveling concentration wave". In: *Proceedings of the National Academy of Sciences* 108.39 (2011), pp. 16235–16240.

[126] Joseph H Connell and Ralph O Slatyer. "Mechanisms of succession in natural communities and their role in community stability and organization". In: *The American Naturalist* 111.982 (1977), pp. 1119–1144.

[127] Michelle GJL Habets et al. "The effect of population structure on the adaptive radiation of microbial populations evolving in spatially structured environments". In: *Ecology Letters* 9.9 (2006), pp. 1041–1048.

[128] Tadashi Fukami. "Historical contingency in community assembly: integrating niches, species pools, and priority effects". In: *Annual Review of Ecology, Evolution, and Systematics* 46 (2015), pp. 1–23.

[129] Richard J Telford, Vigdis Vandvik, and Harry John Betteley Birks. "Dispersal limitations matter for microbial morphospecies". In: *Science* 312.5776 (2006), pp. 1015–1015.

[130] Elizabeth K Costello et al. "Bacterial community variation in human body habitats across space and time". In: *Science* 326.5960 (2009), pp. 1694–1697.

[131] Yakov Kuzyakov and Evgenia Blagodatskaya. "Microbial hotspots and hot moments in soil: concept & review". In: *Soil Biology and Biochemistry* 83 (2015), pp. 184–199.

[132] Philippe Hinsinger et al. "Rhizosphere: biophysics, biogeochemistry and ecological relevance". In: *Plant and Soil* 321.1-2 (2009), pp. 117–152.

[133] Juan E Keymer et al. "Bacterial metapopulations in nanofabricated landscapes". In: *Proceedings of the National Academy of Sciences* 103.46 (2006), pp. 17290–17295.

[134] Simon Van Vliet et al. "The effects of chemical interactions and culture history on the colonization of structured habitats by competing bacterial populations". In: *BMC Microbiology* 14.1 (2014), p. 116.

[135] Kristin Aleklett et al. "Build your own soil: exploring microfluidics to create microbial habitat structures". In: *The ISME Journal* 12.2 (2018), pp. 312–319. DOI: 10.1038/ismej.2017.184. URL: https://doi.org/10.1038/ismej.2017.184.

[136] Dong Qin, Younan Xia, and George M Whitesides. "Soft lithography for micro-and nanoscale patterning". In: *Nature Protocols* 5.3 (2010), p. 491.

[137] Julius Adler. "Chemotaxis in Bacteria". In: *Science* 153.3737 (1966), pp. 708–716. ISSN: 0036-8075. DOI: 10.1126/science.153.3737.708. eprint: https://science.sciencemag.org/content/153/3737/708.full.pdf. URL: https://science.sciencemag.org/content/153/3737/708.

[138] Sungsu Park et al. "Influence of topology on bacterial social interaction". In: *Proceedings of the National Academy of Sciences* 100.24 (2003), pp. 13910–13915. ISSN: 0027-8424. DOI: 10.1073/pnas.1935975100. eprint: https://www.pnas.org/content/100/24/13910.full.pdf. URL: https://www.pnas.org/content/100/24/13910.

[139] Sungsu Park et al. "Motion to form a quorum". In: *Science* 301.5630 (2003), pp. 188–188.

[140] Howard C. Berg. *E. coli in Motion*. Springer New York, 2004. ISBN: 9780387216386. DOI: 10.1007/b97370. URL: http://dx.doi.org/10.1007/b97370.

[141] John Gordon Skellam. "Random dispersal in theoretical populations". In: *Biometrika* 38.1/2 (1951), pp. 196–218.

[142] Felix J H Hol et al. "Density-dependent adaptive resistance allows swimming bacteria to colonize an antibiotic gradient". In: *The ISME Journal* 10.1 (2016), pp. 30–38. DOI: 10.1038/ismej.2015.107. URL: https://doi.org/10.1038/ismej.2015.107.

[143] Vincent Calcagno et al. "Coexistence in a metacommunity: the competition–colonization trade-off is not dead". In: *Ecology Letters* 9.8 (2006), pp. 897–907.

[144] Douglas W Yu and Howard B Wilson. "The competition-colonization trade-off is dead; long live the competition-colonization trade-off". In: *The American Naturalist* 158.1 (2001), pp. 49–63.

[145] P. W. Anderson. "Absence of Diffusion in Certain Random Lattices". In: *Phys. Rev.* 109 (5 Mar. 1958), pp. 1492–1505. DOI: 10.1103/PhysRev.109.1492. URL: https://link.aps.org/doi/10.1103/PhysRev.109.1492.

[146] Michael D Abràmoff, Paulo J Magalhães, and Sunanda J Ram. "Image processing with ImageJ". In: *Biophotonics International* 11.7 (2004), pp. 36–42.

[147] Makoto Matsumoto and Takuji Nishimura. "Mersenne Twister: A 623-Dimensionally Equidistributed Uniform Pseudo-Random Number Generator". In: *ACM Trans. Model. Comput. Simul.* 8.1 (Jan. 1998), pp. 3–30. ISSN: 1049-3301. DOI: 10.1145/272991.272995. URL: https://doi.org/10.1145/272991.272995.

[148] R Sunish Kumar et al. "Characterization of antifungal metabolite produced by a new strain Pseudomonas aeruginosa PUPa3 that exhibits broad-spectrum antifungal activity and biofertilizing traits". In: *Journal of applied Microbiology* 98.1 (2005), pp. 145–154.

[149] Kathrin Riedel et al. "N-acylhomoserine-lactone-mediated communication between Pseudomonas aeruginosa and Burkholderia cepacia in mixed biofilms". In: *Microbiology* 147.12 (2001), pp. 3249–3262.

[150] Zoltán Eisler, Imre Bartos, and János Kertész. "Fluctuation scaling in complex systems: Taylor's law and beyond". In: *Advances in Physics* 57.1 (2008), pp. 89–142.

[151] Xiaofeng Xu et al. "Microbial macroecology: In search of mechanisms governing microbial biogeographic patterns". In: *Global Ecology and Biogeography* (2020).

[152] Lionel Roy Taylor. "Aggregation, variance and the mean". In: *Nature* 189.4766 (1961), pp. 732–735.

[153] Ricardo BR Azevedo and Armand M Leroi. "A power law for cells". In: *Proceedings of the National Academy of Sciences* 98.10 (2001), pp. 5699–5704.

[154] Kumiko Tanaka-Ishii and Tatsuru Kobayashi. "Taylor's law for linguistic sequences and random walk models". In: *Journal of Physics Communications* 2.11 (2018), p. 115024.

[155] Meng Xu and Joel E Cohen. "Analyzing and interpreting spatial and temporal variability of the United States county population distributions using Taylor's law". In: *PloS one* 14.12 (2019), e0226096.

[156] Joel E Cohen. "Statistics of primes (and probably twin primes) satisfy Taylor's law from ecology". In: *The American Statistician* 70.4 (2016), pp. 399–404.

[157] Zhanshan Ma. "Power law analysis of the human microbiome". In: *Molecular Ecology* 24.21 (2015), pp. 5428–5445.

[158] Lianwei Li and Zhanshan Ma. "Comparative power law analysis for the spatial heterogeneity scaling of the hot-spring microbiomes". In: *Molecular Ecology* 28.11 (2019), pp. 2932–2943.

[159] Jacopo Grilli. "Macroecological laws describe variation and diversity in microbial communities". In: *Nature Communications* 11.1 (2020), pp. 1–11.

[160] Daniel C Reuman et al. "Synchrony affects Taylor's law in theory and data". In: *Proceedings of the National Academy of Sciences* 114.26 (2017), pp. 6788–6793.

[161] Patrick AP Moran. "The statistical analysis of the Canadian lynx cycle." In: *Australian Journal of Zoology* 1.3 (1953), pp. 291–298.

[162] Agata Fronczak and Piotr Fronczak. "Origins of Taylor's power law for fluctuation scaling in complex systems". In: *Physical Review E* 81.6 (2010), p. 066112.

[163] Wayne S Kendal and Bent Jørgensen. "Tweedie convergence: A mathematical basis for Taylor's power law, 1/f noise, and multifractality". In: *Physical review E* 84.6 (2011), p. 066120.

[164] Joel E Cohen and Meng Xu. "Random sampling of skewed distributions implies Taylor's power law of fluctuation scaling". In: *Proceedings of the National Academy of Sciences* 112.25 (2015), pp. 7749–7754.

[165] John A Wiens. "Metapopulation dynamics and landscape ecology". In: *Metapopulation biology*. Elsevier, 1997, pp. 43–62.

[166] Pablo A Marquet et al. "Scaling and power-laws in ecological systems". In: *Journal of Experimental Biology* 208.9 (2005), pp. 1749–1769.

[167] Silvia Zaoli et al. "Covariations in ecological scaling laws fostered by community dynamics". In: *Proceedings of the National Academy of Sciences* 114.40 (2017), pp. 10672–10677.

[168] John P DeLong et al. "Shifts in metabolic scaling, production, and efficiency across major evolutionary transitions of life". In: *Proceedings of the National Academy of Sciences* 107.29 (2010), pp. 12941–12945.

[169] Sriram Ramaswamy. "Active matter". In: *Journal of Statistical Mechanics: Theory and Experiment* 2017.5 (2017), p. 054002. URL: `http://stacks.iop.org/1742-5468/2017/i=5/a=054002`.

[170] Gabriel Popkin. "The Physics of Life". In: *Nature* 529 (20016), pp. 16–18.

[171] Nikolay Perunov, Robert A. Marsland, and Jeremy L. England. "Statistical Physics of Adaptation". In: *Phys. Rev. X* 6 (2 June 2016), p. 021036. DOI: `10.1103/PhysRevX.6.021036`. URL: `https://link.aps.org/doi/10.1103/PhysRevX.6.021036`.

[172] Eric Smith and Harold J. Morowitz. *The Origin and Nature of Life on Earth: The Emergence of the Fourth Geosphere*. Cambridge University Press, 2016.

[173] Erwin Schrödinger. *What is Life?* Cambridge University Press, 1944.

[174] Humberto Maturana. "Biology of Cognition". In: *BCL Report 9. University of Illinois* (Jan. 1970).

[175] Jonh von Neuman and Arthur Burks. *Theory of self-reproducing automata*. University of Illinois Press, 1966.

[176] Christopher G. Langton. "Self-reproduction in cellular automata". In: *Physica D: Nonlinear Phenomena* 10.1 (1984), pp. 135–144. ISSN: 0167-2789. DOI: https://doi.org/10.1016/0167-2789(84)90256-2. URL: http://www.sciencedirect.com/science/article/pii/0167278984902562.

[177] Bruce Alberts et al. *Molecular Biology of the Cell (6th Ed.)* Garland Science, 2014.

[178] Rob Phillips et al. *The Physical Biology of the Cell*. Garland Science, 2012.

[179] Anuradha Janakiraman and Marcia B. Goldberg. "Recent advances on the development of bacterial poles". In: *Trends in Microbiology* 12.11 (2018), pp. 518–525. DOI: 10.1016/j.tim.2004.09.003. URL: http://dx.doi.org/10.1016/j.tim.2004.09.003.

[180] Humberto Maturana and Francisco Varela. *Demaquinas y seresvivos*. Editorial Universitaria, 1973.

[181] Humberto Maturana-Romesın and Jorge Mpodozis. "The origin of species by means of natural drift". In: *Revista chilena de historia natural* 73.2 (2000), pp. 261–310.

[182] Jeremy L England. "Statistical physics of self-replication". In: *The Journal of chemical physics* 139.12 (2013), 09B623_1.

[183] Michel Godin et al. "Using buoyant mass to measure the growth of single cells". In: *Nature methods* 7.5 (May 2010), pp. 387–390. DOI: 10.1038/nmeth.1452. URL: http://www.ncbi.nlm.nih.gov/pmc/articles/PMC2862099/.

[184] Kleiber. "BODY SIZE AND METABOLIC RATE". In: *Physiological Reviews* 27.4 (1947). PMID: 20267758, pp. 511–541. DOI: 10.1152/physrev.1947.27.4.511. eprint: https://doi.org/10.1152/physrev.1947.27.4.511. URL: https://doi.org/10.1152/physrev.1947.27.4.511.

[185] Martin Ackermann, Stephen C Stearns, and Urs Jenal. "Senescence in a bacterium with asymmetric division". In: *Science* 300.5627 (2003), pp. 1920–1920.

[186] Ariel B Lindner et al. "Asymmetric segregation of protein aggregates is associated with cellular aging and rejuvenation". In: *Proceedings of the National Academy of Sciences* 105.8 (2008), pp. 3076–3081.

[187] Ping Wang et al. "Robust Growth of Escherichia coli". In: *Current Biology* 20.12 (2017/02/19 2017), pp. 1099–1103.

[188] Nathalie Q Balaban. "Szilard's dream". In: *Nat Meth* 2.9 (Sept. 2005), pp. 648–649.

[189] Thomas Malthus. *An Essay on the Principle of Population*. London: St. Paul's Church-Yard, 1798.

[190] Pierre-François Verhulst. "Notice sur la loi que la population poursuit dans son accroissement". In: *Correspondance mathématique et physique* 10 (1838), pp. 113–121.

[191] Aaron Novick and Leo Szilard. "Description of the Chemostat". In: *Science* 112.2920 (1950), pp. 715–716.

[192] Frederick K. Balagaddé et al. "Long-Term Monitoring of Bacteria Undergoing Programmed Population Control in a Microchemostat". In: *Science* 309.5731 (2005), pp. 137–140.

[193] Alex Groisman et al. "A microfluidic chemostat for experiments with bacterial and yeast cells". In: *Nat Meth* 2.9 (Sept. 2005), pp. 685–689.

[194] Martin Ackermann. "A functional perspective on phenotypic heterogeneity in microorganisms". In: *Nat Rev Micro* 13.8 (Aug. 2015), pp. 497–508.

[195] Sungsu Park et al. "Influence of topology on bacterial social interaction". In: *Proceedings of the National Academy of Sciences* 100.24 (2003), pp. 13910–13915.

[196] Gerardo Cárcamo-Oyarce et al. "Quorum sensing triggers the stochastic escape of individual cells from Pseudomonas putida biofilms". In: *Nature Communications* 6 (Jan. 2015), 5945 EP -.

[197] Sungsu Park et al. "Motion to Form a Quorum". In: *Science* 301.5630 (2003), pp. 188–188.

[198] J. Saragosti et al. "Directional persistence of chemotactic bacteria in a traveling concentration wave". In: *Proceedings of the National Academy of Sciences* 108.39 (2011), pp. 16235–16240.

[199] Nikhil Mittal et al. "Motility of Escherichia coli cells in clusters formed by chemotactic aggregation". In: *Proceedings of the National Academy of Sciences* 100.23 (2003), pp. 13259–13263.

[200] James Q. Boedicker, Meghan E. Vincent, and Rustem F. Ismagilov. "Microfluidic Confinement of Single Cells of Bacteria in Small Volumes Initiates High-Density Behavior of Quorum Sensing and Growth and Reveals Its Variability". In: *Angewandte Chemie* 48.32 (2009), pp. 5908–5911.

[201] Juan Keymer et al. "Bacterial metapopulations in nanofabricated landscapes". In: *Proc Natl Acad Sci USA* 103.46 (2006), pp. 17290–17295. ISSN: 0027-8424. DOI: 10.1073/pnas.0607971103.

[202] Richard Levins. "Some Demographic and Genetic Consequences of Environmental Heterogeneity for Biological Control". In: *Bulletin of the Entomological Society of America* 15.3 (1969), p. 237.

[203] Ilkka Hansky. "Metapopulation dynamics". In: *Nature* 396 (1998), pp. 41–49.

[204] Motoo Kimura and George H Weiss. "The stepping stone model of population structure and the decrease of genetic correlation with distance". In: *Genetics* 49.4 (1964), p. 561.

[205] Sewall Wright. "The Roles of Mutation, Inbreeding, Crossbreeding and Selection in Evolution". In: *Proceedings of the Sixth Annual Congress of Genetics* 1 (1932), pp. 356–366.

[206] Dietrich Stauffer and Ammon Aharony. *Introduction to percolation theory*. CRC press, 2018.

[207] MacArthur Robert and Wilson Edward O. *The Theory of Island Biogeography*. Princeton University Press, 1967.

[208] Simon A. Levin. "The Problem of Pattern and Scale in Ecology: The Robert H. MacArthur Award Lecture". In: *Ecology* 73.6 (Dec. 1992), pp. 1943–1967. ISSN: 0012-9658. DOI: 10.2307/1941447. URL: http://dx.doi.org/10.2307/1941447.

[209] Simon A. Levin. "Dispersion and Population Interactions". In: *The American Naturalist* 108.960 (1974), pp. 207–228. ISSN: 00030147, 15375323. URL: http://www.jstor.org/stable/2459851.

[210] S. A. Levin. "Non-Uniform Stable Solutions to Reaction-Diffusion Equations: Applications to Ecological Pattern Formation". In: *Pattern Formation by Dynamic Systems and Pattern Recognition*. Ed. by Hermann Haken. Berlin, Heidelberg: Springer Berlin Heidelberg, 1979, pp. 210–222. ISBN: 978-3-642-67480-8.

[211] Simon van Vliet. "Microbial Population Dynamics in Spatially Structured Environments: Measuring Population Synchrony in Varying Landscape Topologies". MA thesis. TU Delft, 2011.

[212] Hiroshi Matano. "Asymptotic behavior and stability of solutions of semilinear diffusion equations". In: *Publications of the Research Institute for Mathematical Sciences* 15.2 (1979), pp. 401–454. ISSN: 0034-5318. DOI: 10.2977/prims/1195188180. URL: http://dx.doi.org/10.2977/prims/1195188180.

[213] Henry S. Horn and Robert H. Mac Arthur. "Competition among Fugitive Species in a Harlequin Environment". In: *Ecology* 53.4 (1972), pp. 749–752. ISSN: 00129658, 19399170. URL: http://www.jstor.org/stable/1934797.

[214] Richard G. Cutler and John E. Evans. "Synchronization of Bacteria by a Stationary-Phase Method". In: *Journal of Bacteriology* 91.2 (1966), pp. 469–476. ISSN: 0021-9193. eprint: https://jb.asm.org/content/91/2/469.full.pdf. URL: https://jb.asm.org/content/91/2/469.

[215] May Robert. "Simple mathematical models with very complicated dynamics". In: *Nature* 261 (1976), pp. 459–467.

[216] Simon van Vliet et al. "The effects of chemical interactions and culture history on the colonization of structured habitats by competing bacterial populations". In: *BMC Microbiology* 14.1 (2014), p. 116. ISSN: 1471-2180. DOI: 10.1186/1471-2180-14-116. URL: http://www.biomedcentral.com/1471-2180/14/116.

[217] Bonnie Bassler. "Cell-to-Cell Communication in Bacteria". In: *Cell* 109.4 (May 2002), pp. 421–424.

[218] Jintao Liu et al. "Metabolic co-dependence gives rise to collective oscillations within biofilms". In: *Nature* 523 (July 2015), 550 EP -. URL: https://doi.org/10.1038/nature14660.

[219] Jintao Liu et al. "Coupling between distant biofilms and emergence of nutrient time-sharing". In: *Science* (2017). ISSN: 0036-8075. DOI: 10.1126/science.aah4204. eprint: http://science.sciencemag.org/content/early/2017/04/05/science.aah4204.full.pdf. URL: http://science.sciencemag.org/content/early/2017/04/05/science.aah4204.

[220] Felix Hol et al. "Adaptive resistance and growth of Escherichia coli bacteria in an antibiotic gradient". In: *The ISME Journal* 10 (2016), pp. 30–38.

[221] Nicholas J Gotelli. "Metapopulation models: the rescue effect, the propagule rain, and the core-satellite hypothesis". In: *The American Naturalist* 138.3 (1991), pp. 768–776.

[222] Nadia R Cohen, Michael A Lobritz, and James J Collins. "Microbial persistence and the road to drug resistance". In: *Cell host & microbe* 13.6 (June 2013), pp. 632–642. DOI: 10.1016/j.chom.2013.05.009. URL: https://www.ncbi.nlm.nih.gov/pubmed/23768488.

[223] Q Zhang et al. "Acceleration of emergence of bacterial antibiotic resistance in connected microenvironments." In: *Science* 333.6050 (Sept. 2011), pp. 1764–7.

[224] David A. Kessler, Robert H. Austin, and Herbert Levine. "Resistance to Chemotherapy: Patient Variability and Cellular Heterogeneity". In: *Cancer Research* 74.17 (2014), pp. 4663–4670. ISSN: 0008-5472. DOI: 10.1158/0008-5472.CAN-14-0118. eprint: http://cancerres.aacrjournals.org/content/74/17/4663.full.pdf. URL: http://cancerres.aacrjournals.org/content/74/17/4663.

[225] Bos Julia and Bob H Austin. "A bacterial antibiotic resistance accelerator and applications". In: *Methods in Cell Biology*. Vol. 147. Elsevier, 2018. Chap. 3, pp. 41–57.

[226] Karl Moebius. *Die Auster und die Austernwirthschaft*. Verlag von Wiegandt, Hempel and Parey, 1877.

[227] A. G. Tansley. "The Use and Abuse of Vegetational Concepts and Terms". In: *Ecology* 16.3 (July 1935), pp. 284–307. ISSN: 0012-9658. DOI: 10.2307/1930070. URL: http://dx.doi.org/10.2307/1930070.

[228] J. A. Wiens. "Spatial Scaling in Ecology". In: *Functional Ecology* 3.4 (1989), p. 385. ISSN: 0269-8463. DOI: 10.2307/2389612. URL: http://dx.doi.org/10.2307/2389612.

[229] L. R. Holdrige. "Determination of World Plant Formations From Simple Climatic Data". In: *Science* 105.2727 (Apr. 1947), pp. 367–368. ISSN: 1095-9203. DOI: 10.1126/science.105.2727.367. URL: http://dx.doi.org/10.1126/science.105.2727.367.

[230] Frederic E. Clements. "Nature and Structure of the Climax". In: *Journal of Ecology* 24.1 (1936), pp. 252–284. ISSN: 00220477, 13652745. URL: http://www.jstor.org/stable/2256278.

[231] H. A. Gleason. "The Individualistic Concept of the Plant Association". In: *Bulletin of the Torrey Botanical Club* 53.1 (1926), pp. 7–26. ISSN: 00409618, 23258055. URL: http://www.jstor.org/stable/2479933.

[232] Guillaume Lambert et al. "Anomalous Spatial Redistribution of Competing Bacteria under Starvation Conditions". In: *Journal of Bacteriology* 193.8 (2011), pp. 1878–1883.

[233] Juan E Keymer et al. "Computation of mutual fitness by competing bacteria". In: *Proceedings of the National Academy of Sciences* 5.51 (2008), pp. 20269–20273.

[234] Maria Mercedes Zambrano and Roberto Kolter. "GASPing for Life in Stationary Phase". In: *Cell* 86.2 (July 1996), pp. 181–184. ISSN: 0092-8674. DOI: 10.1016/s0092-8674(00)80089-6. URL: http://dx.doi.org/10.1016/S0092-8674(00)80089-6.

[235] Stephen D Fretwell. *Populations in a Seasonal Environment.(MPB-5)*. Vol. 106. Princeton University Press, 2020.

[236] Erik R. Zinser and Roberto Kolter. "Mutations Enhancing Amino Acid Catabolism Confer a Growth Advantage in Stationary Phase". In: *Journal of Bacteriology* 181.18 (1999), pp. 5800–5807. ISSN: 0021-9193. eprint: https://jb.asm.org/content/181/18/5800.full.pdf. URL: https://jb.asm.org/content/181/18/5800.

[237] Peter Schuster and Karl Sigmund. "Replicator dynamics". In: *Journal of theoretical biology* 100.3 (1983), pp. 533–538.

[238] Rv Lange and Regine Hengge-Aronis. "Identification of a central regulator of stationary-phase gene expression in Escherichia coli". In: *Molecular microbiology* 5.1 (1991), pp. 49–59.

[239] Hirotsugu Matsuda et al. "Statistical Mechanics of Population: The Lattice Lotka-Volterra Model". In: *Progress of Theoretical Physics* 88.6 (1992), p. 1035.

[240] Joseph Grinnell. "The niche-relashionships of the california trasher". In: *The Auk* 34 (1917), pp. 427–33.

[241] G. Evelyn Hutchinson. "Concluding Remarks". In: *Cold Spring Harbor Symposia on Quantitative Biology* 22.0 (Jan. 1957), pp. 415–427. ISSN: 1943-4456. DOI: 10.1101/sqb.1957.022.01.039. URL: http://dx.doi.org/10.1101/SQB.1957.022.01.039.

[242] R. H. Whittaker, S. A. Levin, and R. B. Root. "Niche, Habitat, and Ecotope". In: *The American Naturalist* 107.955 (1973), pp. 321–338. ISSN: 00030147, 15375323. URL: http://www.jstor.org/stable/2459534.

[243] Charles Darwin. *The origin of species*. PF Collier & son New York, 1909.

[244] Garrett Hardin. "The competitive exclusion principle". In: *science* 131.3409 (1960), pp. 1292–1297.

[245] Daniel Simberloff and Tamar Dayan. "The guild concept and the structure of ecological communities". In: *Annual review of ecology and systematics* 22 (1991), pp. 115–143.

[246] Robert H MacArthur. "Population ecology of some warblers of northeastern coniferous forests". In: *Ecology* 39.4 (1958), pp. 599–619.

[247] Robert MacArthur and Richard Levins. "Competition, habitat selection, and character displacement in a patchy environment". In: *Proceedings of the National Academy of Sciences of the United States of America* 51.6 (1964), p. 1207.

[248] Robert MacArthur and Richard Levins. "The limiting similarity, convergence, and divergence of coexisting species". In: *The American Naturalist* 101.921 (1967), pp. 377–385.

[249] Robert MacArthur. "Species packing and competitive equilibrium for many species". In: *Theoretical population biology* 1.1 (1970), pp. 1–11.

[250] Stilianos Louca et al. "Function and functional redundancy in microbial systems". In: *Nature ecology & evolution* 2.6 (2018), pp. 936–943.

[251] Ashley Shade et al. "Fundamentals of microbial community resistance and resilience". In: *Frontiers in microbiology* 3 (2012), p. 417.

[252] Alma Dal Co, Simon Van Vliet, and Martin Ackermann. "Emergent microscale gradients give rise to metabolic cross-feeding and antibiotic tolerance in clonal bacterial populations". In: *Philosophical Transactions of the Royal Society B* 374.1786 (2019), p. 20190080.

[253] Alan J Wolfe. "The acetate switch". In: *Microbiology and molecular biology reviews* 69.1 (2005), pp. 12–50.

[254] Jonathan Dushoff et al. "Metapopulations, community assembly, and scale invariance in aspect space". In: *Theoretical Population Biology* 62.4 (2002), pp. 329–338.

[255] Robert T Paine. "Food web complexity and species diversity". In: *The American Naturalist* 100.910 (1966), pp. 65–75.

[256] James W Portfr. "Community structure of coral reefs on opposite sides of the Isthmus of Panama". In: *Science* 186.4163 (1974), pp. 543–545.

[257] Henry S Horn. "Markovian properties of forest succession". In: *Ecology and evolution of communities* (1975), pp. 196–211.

[258] Joseph R McAuliffe. "Competition for space, disturbance, and the structure of a benthic stream community". In: *Ecology* 65.3 (1984), pp. 894–908.

[259] Weirong Liu et al. "An evolutionarily stable strategy to colonize spatially extended habitats". In: *Nature* 575.7784 (2019), pp. 664–668.

[260] Xiongfei Fu et al. "Spatial self-organization resolves conflicts between individuality and collective migration". In: *Nature Communications* 9.1 (2018), pp. 1–12.

[261] Jonas Cremer et al. "Chemotaxis as a navigation strategy to boost range expansion". In: *Nature* 575.7784 (2019), pp. 658–663.

[262] Eshel Ben Jacob et al. "Bacterial linguistic communication and social intelligence". In: *TRENDS in Microbiology* 12.8 (2004), pp. 366–372.

[263] Martin Ackermann and Michael Doebeli. "Evolution of niche width and adaptive diversification". In: *Evolution* 58.12 (2004), pp. 2599–2612.

[264] Peter A Abrams. "A world without competition". In: *Nature* 412.6850 (2001), pp. 858–859.

[265] Pablo A Marquet et al. "On theory in ecology". In: *BioScience* 64.8 (2014), pp. 701–710.

[266] Sandro Azaele et al. "Statistical mechanics of ecological systems: Neutral theory and beyond". In: *Reviews of Modern Physics* 88.3 (2016), p. 035003.

[267] Dominique Gravel et al. "Reconciling niche and neutrality: the continuum hypothesis". In: *Ecology letters* 9.4 (2006), pp. 399–409.

[268] David Tilman. "Niche tradeoffs, neutrality, and community structure: a stochastic theory of resource competition, invasion, and community assembly". In: *Proceedings of the National Academy of Sciences* 101.30 (2004), pp. 10854–10861.

[269] Marten Scheffer and Egbert H van Nes. "Self-organized similarity, the evolutionary emergence of groups of similar species". In: *Proceedings of the National Academy of Sciences* 103.16 (2006), pp. 6230–6235.